Universidade de São Paulo

Instituto de Física

Aspectos de complexidade em holografia

Felipe Soares Sá

Orientador: Prof. Dr. Diego Trancanelli

Dissertação de mestrado apresentada ao Instituto de Física como requisito parcial para a obtenção do título de Mestre em Ciências.

Banca Examinadora:

Prof. Dr. Diego Trancanelli (IF-USP)
Prof. Dr. Horatiu Nastase (IFT-Unesp)
Prof. Dr. Dmitry Melnikov (IIP-UFRN)

São Paulo
2018

FICHA CATALOGRÁFICA
Preparada pelo Serviço de Biblioteca e Informação
do Instituto de Física da Universidade de São Paulo

Sá, Felipe Soares

Aspectos de complexidade em holografia. São Paulo, 2018.

Dissertação (Mestrado) – Universidade de São Paulo. Instituto de Física. Depto. de Física Matemática

Orientador: Prof. Dr. Diego Trancanelli
Área de Concentração: Teoria de cordas.

Unitermos: 1. Complexidade; 2. Entropia de emaranhamento; 3. Holografia.

USP/IF/SBI-030/2018

University of São Paulo

Institute of Physics

Aspects of complexity in holography

Felipe Soares Sá

Supervisor: Prof. Dr. Diego Trancanelli

Dissertation of masters presented to the Institute of Physics as partial requisite to the obtaining of the master of sciences degree.

Examination Committee:

Prof. Dr. Diego Trancanelli (IF-USP)
Prof. Dr. Horatiu Nastase (IFT-Unesp)
Prof. Dr. Dmitry Melnikov (IIP-UFRN)

São Paulo
2018

To my parents and brother that have been supporting me during all these years.

Acknowledgements

I would like to thank Prof. Dr. Diego Trancanelli for advising me during the development of this thesis as well as during the entire master. I also need to thank my friends Alexander Meinke, Carlos Vargas, Marcia Tenser and Leonardo Werneck for the discussions about physics and their friendship. Specially, I thank Gabriel Nagaoka for his participation in the development of my master and Daniel Teixeira that was a kind of second advisor for me. For my girlfriend Lilian, thank you very much to help me in my adaptation to São Paulo and for the entire faith that you deposit in me. For my family, I need to say that I'm here because of you. Lastly, I thank CNPq for the scholarship. This master's thesis would be impossible without such financial support.

Resumo

Recentemente, uma quantidade de informação/computação quântica chamada complexidade computacional tem adquirido mais e mais importância no estudo de buracos negros. Resumidamente, complexidade mede a dificuldade de alguma tarefa. No contexto de mecânica quântica (ou mesmo para estados em uma CFT), qualquer estado tem uma complexidade associada, uma vez que o processo de preparar algum estado, usando operações unitárias, é uma tarefa por sí só. Propostas holográficas para o cálculo de complexidade tem sido desenvolvidas nos anos recentes. Há duas delas que estão mais desenvolvidas: as conjecturas complexidade=volume e complexidade=ação. No contexto da correspondência AdS/CFT é sabido que o buraco negro de Schwarzschild em AdS é dual à um estado térmico que descreve duas CFTs emaranhadas. Para esse caso em específico, a conjectura complexidade=volume iguala a complexidade do estado que descreve esse par de CFTs emaranhadas com o volume da máxima superfície de codimensão um no espaço-tempo dual. Por outro lado, a conjectura complexidade=ação iguala a complexidade da borda com a ação gravitacional calculada sobre uma região do espaço-tempo conhecida como Wheeler-DeWitt patch. O objetivo dessa tese é proporcionar os requisitos necessários para entender as conjecturas relacionadas com complexidade, monstrando alguns resultados importantes proporcionados pelos cálculos holográficos no lado gravitacional.

Palavras-chave: Complexidade. Entropia de Emaranhamento. Holografia.

Abstract

In recent years, a quantity from quantum information/computation called computational complexity has been acquiring more and more importance in the study of black holes. Briefly, complexity measures the hardness of some task. In the context of quantum mechanics (or even for states in a CFT), any state has an associated complexity, once the process of to preparing some state, using unitary operations, is a task by itself. Holographic proposals for the computation of complexity have been developed in recent years. There are two of them that are more developed: the complexity=volume and complexity=action conjectures. In the context of the AdS/CFT correspondence, it is known that the two sided AdS-Schwarzschild black hole is dual to some thermal state that describes two entangled CFTs. For this specific case, the complexity=volume conjecture equates the complexity of the state that describes this pair of entangled CFTs with the volume of the maximal codimension-one surface in the dual space-time. On the other hand, the complexity=action conjecture equates the boundary complexity with the gravitational action evaluated on a region of space-time known as the Wheeler-DeWitt patch. The goal of this thesis is to provide the necessary requisites to understand the conjectures related to complexity, showing some important results provided by holographic computations on the gravitational side.

Key-words: Complexity. Entanglement Entropy. Holography.

List of Figures

List of abbreviations and acronyms

AdS	Anti-de Sitter
CA	Complexity=Action
CV	Complexity=Volume
CFT	Conformal Field Theory
ERB	Einstein-Rosen-Bridge
EE	Entanglement Entropy
QFT	Quantum Field Theory
QIM	Quantum Information Metric
TFD	Thermofield Double
WDW	Wheeler-De Witt

Contents

1 Introduction

The *holographic principle* claims that the entire information content of a *quantum gravity* theory in a given volume can be encoded in a theory at the boundary surface of this volume [1, 2], which means for example that a three-dimensional quantum gravity has a two-dimensional description, requiring one discrete degree of freedom per Planck area. One remarkable result connected with such principle is that the entropy of a black hole is not proportional to its volume, but to the area of the event horizon A_h [3, 4]. The holographic principle is of very general nature and is expected to be found in many examples.

The most complete realization of the holographic principle we have today is the *AdS/CFT correspondence* (or Gauge/Gravity Duality), which was proposed by Juan Maldacena in 1997 [5]. The initials AdS denote *Anti-de Sitter space-time* while CFT means *conformal field theory*. The field and gravity theories involved in the AdS/CFT correspondence display both supersymmetry and conformal symmetry. The AdS/CFT correspondence is characterized by matching computations on the two sides. The best understood example of the AdS/CFT correspondence is the duality between $\mathcal{N} = 4$ *Super Yang–Mills (SYM)* theory, the maximally *superconformal* quantum field theory in $3 + 1$ dimensions with gauge symmetry $SU\,(N)$, and type *IIB superstring* theory on $AdS_5 \times S^5$.

The AdS/CFT correspondence was a significant development in theoretical physics. This precise realization of the holographic principle is also an example of *duality*: the idea of different, but equivalent, formulations of the same physical theory. Two formulations are said to be dual to each other if there is a one-to-one map between obserbables in each of them, as well as for the dynamics of both theories. Dualities are particularly useful for physical processes that are hard to calculate in one formulation, but easy to obtain in another. An example of duality of this type is a map between two equivalent formulations in different coupling constant regimes. For instance, in the large N limit, the AdS/CFT correspondence maps a $\mathcal{N} = 4$ SYM theory, which is strong coupled in this limit, to a weakly coupled type IIB *supergravity*. This way, it is possible to perform explicit calculations.

The success of the AdS/CFT correspondence has inspired theoretical physicists to ask where else the correspondence can be used in order to try to understand open problems in theoretical physics. In special, the existence of the AdS/CFT correspondence provided an easier way to study *entanglement*, which is a property of quantum systems which is not expected from classical systems. The classical world doesn't accom-

modate the fact that it is possible to separate two non-interacting systems in such way that they aren't causally related anymore, but they remain correlated, once knowing one of the parts also implies knowing the other. This "peculiar" feature of the quantum world has been a source of great theoretical interest. The initial debate about the implication of such feature gave rise to the so called Einstein-Podolsky-Rosen (EPR) paradox [6], paving the foundations for more detailed investigation in later years. With John Bell's work [7], the apparent paradox generated by the existence of entanglement was solved, improving the understanding of quantum correlations and their physical implications. Currently, the presence of entanglement as a real feature of quantum systems is natural, mainly for the development of quantum information.

It is easy to see quantum entanglement in simple cases that in general involve a few number of qubits. The standard measure of quantum entanglement between two systems is called *entanglement entropy*. Such quantity can be easily computed for a system of two qubtis (Bell's pair), however, this is not true in the case of continuous systems, for example, the entanglement of the ground state of a QFT. Actually, in order to calculate EE for QFTs, it is necessary to resort to a complex artifice called *replica trick* [8]. This scenario changed after the celebrated proposal by Shinsei Ryu and Tadashi Takayanagi of an holographic alternative to compute entanglement entropy [9, 10]. The so called *holographic entanglement entropy* claims that the entanglement entropy associated with a spatial region in a QFT is given by the area of a particular minimal area surface in the holographic dual geometry. Inspired by the Ryu-Takayanagi proposal, Brian Swingle [11] and Mark Van Raamsdonk [12, 13] argued that the essential building block of the space-time geometry should somehow be related to the entanglement structure of the quantum state in the QFT. This philosophy motivated Juan Maldacena and Leonard Susskind to conjecture "ER = EPR" [14], which refers to a geometric construct, the *Einstein-Rosen bridge* (ERB), being related to the entanglement structure suggested by the Einstein-Podolsky-Rosen experiment.

The fact that entanglement, which is a quantity very useful for *quantum information*, acquired some relevance for the understanding of the structure of the space-time, inspired the idea that other tools from quantum information could be in some way useful to the comprehension of open problems in gravity. One example of such tools is the so called *computational complexity*. In few words, computational complexity is a quantity that measures how hard is to implement a task. Problems or operations in quantum/classical computation can be classified as easy or hard according to the time that they require to be solved or implemented. Complexity is the measure of the hardness of such tasks. With this short definition in mind, it is possible to say that complexity started to obtain some relevance for holography in the context of the discussion about the *AMPS*

firewall paradox [15]. Briefly, the paradox is about the violation of a principle called monogamy of entanglement. Such thing requires that any quantum system cannot be fully entangled with two independent systems at the same time.

In order to try to provide some solution for the AMPS paradox, it was presented in [16] arguments using quantum computational restrictions on the thought experiments used in the formulation of the paradox. This was the first paper to use quantum complexity in black hole physics. Another alternative for the AMPS paradox is the ER=EPR conjecture. Following this prescription, the AMPS is not a paradox by itself. Instead, it proved that there must be a kind of shortcut between the purifier and the interior of the black hole. Purifier in this context means a system entangled to the black hole interior, for example, the *Hawking radiation*. Then you can just say that Alice's disturbance of the purifier sent a signal through this shortcut. The shortcut between the interior of the black hole and the system it's entangled with is the Einstein-Rosen bridge.

Despite the initial motivations that introduced complexity in the study of the information paradox in black holes, it becomes useful to describe the growing of the ERB [17, 18]. Classically, such object grows forever. On the other hand, a black hole comes to thermal equilibrium fast, as well as its dual boundary theory. Apparently, all the evolution stops at a scrambling time t_*. These facts lead us to a question: is there some quantity in the dual theory that can represent the continuing growth of the ERB? The answer is that the quantum state doesn't stop to evolve, which implies that also computational complexity keeps evolving after the scrambling time. Summarizing, computational complexity is the candidate for a dual quantity that describes the growing of ERB. This association gave rise to the *complexity=volume* (CV) conjecture (or *CV duality*) and also provided some insight about a relation between the complexity of the boundary states and volume of objects defined in the bulk theory. Posteriorly, the CV proposal motivated the formulation of a holographic formula for the so-called *subregion complexity* [19, 20], which has a direct parallel with holographic entanglement entropy. Also inspired by CV, it was conjectured in [21, 22] that computational complexity is related to the classical action of the space-time computed over a region called *Wheeler-DeWitt (WDW) patch*. The so called *complexity=action* (CA) conjecture (or *CA duality*) can be considered a improved version of the CV.

The main theme of this thesis is to provide to the reader the necessary requisites to understand the CV and CA conjectures, showing some important results provided by holographic computations in the gravitational side, making possible to compare such results to what is expected from the so called *Hayden-Preskill circuit model* [23, 17]. This thesis is organized in the following way:

- In chapter 2 there is a brief discussion about the role of complexity in quantum information with the most common examples of complexity classes and decision problems, as well as the formalism for two level systems, which is essential to describes qubits. In the last section, we present the concept of *fidelity* and of *quantum information metric* (QIM), which is related to the CV proposal.

- Chapter 3 is dedicated to the requirements from holography necessary to understand the conjectures for complexity. This chapter starts with the main properties of the AdS space-time followed by the description of black holes asymptotically AdS. There is also a section about entanglement entropy, as well as a short section about the AdS/CFT correspondence, where are discussed holographic entanglement entropy and the duality between *eternal black holes* and CFTs at finite temperature.

- The holographic proposals for complexity are presented in chapter 4. This begins with the description of the quantum circuit model for complexity, where there is a specific discussion about the model for the *thermofield double (TFD) state*. Finally, the CV and CA conjectures are formulated, allowing us to perform calculations for some kind of black holes. In particular, for the CA duality, the complexity for uncharged black holes, small charged black holes and the rotating BTZ was computed holographically.

- The last chapter is devoted to the discussion of the results obtained in the previous chapter, as well as comments about future perspectives about the role of complexity in holography.

- There is a series of appendices where it is possible to find interesting results about black holes in Minkowski space-time and the details of the calculations performed in chapter 4.

2 Quantum information and complexity

Quantum information and the notion of complexity are starting to play has an important role holography. The objective of this chapter is to understand what complexity means in the community of quantum information. For this purpose, it is necessary first to understand basic concepts, such as bits, qubits, gates, classical/quantum circuits, etc. A complete course in quantum information can be found in [24], but this chapter will provide the reader with all the necessary requisites to understand what is complexity and its implications for the future topics in this dissertation.

It is not difficult to understand heuristically the meaning of complexity. As is very well discussed in [18], complexity is a quantity that measures how hard is to implement a task. Such explanation seems very ambiguous, but it isn't. In order to compute the complexity of some task, several ingredients are necessary: a system, a space of states, a concept of simple state and a concept of simple operations. Let's take as example a classical computer with n bits. Such system can be represented by a string made of 0 and 1, for example, $(0100...1)$. The space of state is the sum over all the 2^n possible strings made of 0 and 1. For this setup, a good candidate for simple state is $(0000...0)$, however, $(1111...1)$ would be also a good choice. Simple operations are operations that involve a small number of bits at a time. With the role of these ingredients in mind, lastly we need to define a task. Our task could be to take the system from the simple states $(0000...0)$ to a more complex state, for example, $(1010...0)$. The complexity of this process is the minimum number of simple operations needed to implement this task. If our simple operations act on two bits at time, the complexity is no more than $n/2$.

The above explanation illustrates how to compute the complexity of a task for this simple setup. However, we are interested in quantum computers, which in general, are more complex than classical computers. The next step is to study some basic properties of classical information, as well as the main classical complexity classes, and quantum information. After this, we will have in position to understand better the concept of quantum computational complexity.

2.1 Basics of classical information

Given a string of n bits as input, a classical (deterministic) computer evaluates a function $f(x)$ and produces a string with m bits as output, that is uniquely

determined by the input, that is,

$$f : \{0,1\}^n \to \{0,1\}^m \tag{2.1.1}$$

for a given n-bit argument. A function with an m bit value is equivalent to m functions, each with a one-bit value, so we may just as well say that the basic task performed by a computer is the evaluation of

$$f : \{0,1\}^n \to \{0,1\}. \tag{2.1.2}$$

There are 2^n possible inputs, and for each input there are two possible outputs. So there are altogether 2^{2^n} functions taking n bits to one bit. The evaluation of any such function can be reduced to a sequence of elementary logical operations. Let us divide the possible values of some input

$$x = x_1 x_2 ... x_n, \tag{2.1.3}$$

into one set of values for which $f(x) = 1$, and a complementary set for which $f(x) = 0$.

Given a set o inputs $x^{(a)}$, for each one where $f\left(x^{(a)}\right) = 1$, let's consider functions $f^{(a)}$ such that

$$f^{(a)}(x) = \begin{cases} 1 & x = x^{(a)} \\ 0 & x \neq x^{(a)} \end{cases}. \tag{2.1.4}$$

Then, the function

$$f(x) = f^{(1)}(x) \vee f^{(2)}(x) \vee f^{(3)}(x) \vee ... \tag{2.1.5}$$

is the logical OR of all possible $f^{(a)}(x)$. The operation $\vee$ between two bits is represented by

$$x \vee y = x + y - x \cdot y \tag{2.1.6}$$

that is 0 if $x = y = 0$ and 1 otherwise. The function $f^{(a)}$ can be written, in the case where $x^{(a)} = 111...1$, as

$$f^{(a)}(x) = x_1 \wedge x_2 \wedge ... \wedge x_n, \tag{2.1.7}$$

where $\wedge$ is the logical AND of all n bits. For any other $x^{(a)}$, the function $f^{(a)}$ is obtained as the AND of n bits, but it's necessary to apply first the NOT $(\neg)$ operation to each bit $x_i^{(a)} = 0$. For example, consider $x^{(a)} = 0110...01$. The function $f^{(a)}$ in this case is given by

$$f^{(a)}(x) = (\neg x_1) \wedge x_2 \wedge x_3 \wedge (\neg x_4) \wedge ... \wedge (\neg x_{n-1}) \wedge x_n. \tag{2.1.8}$$

The NOT operation is represented as

$$\neg x = 1 - x. \tag{2.1.9}$$

There is another important operation, COPY, that duplicate one bit to two bits. We have now constructed the function $f(x)$ from three elementary logical connectives: NOT, AND, OR. The expression obtained is called the "disjunctive normal form" of $f\,(x)$.

A computer can perform elementary operations on bits or pairs of bits, such as COPY, NOT, AND, OR. A computation is a finite sequence of such operations, a circuit, applied to a specified string of input bits. The result of the computation is the final value of all remaining bits, after all the elementary operations have been executed. It is a fundamental result in the theory of computation that just a few elementary gates suffice to evaluate any function of a finite input [24]. This result means that with very simple hardware components, we can build up arbitrarily complex computations. So far, we have only considered a computation that acts on a particular fixed input, but we may also consider families of circuits that act on inputs of variable size. Circuit families provide a useful scheme for analyzing and classifying the complexity of computations, a scheme that will have a natural generalization when we turn to quantum computation.

2.2 Classical circuits and complexity classes

In the study of complexity, we will often be interested in functions $f\,(x)$ with a one-bit output, as shown in (2.1.2). Such a function may be said to compute a solution to a "decision problem", that is, the function examines the input and produces a YES or NO answer. This is what we can call a decision problem. In order to answer how hard a problem is, we need to quantify the resources needed to solve the problem. For a decision problem, a reasonable measure of hardness is the size of the smallest circuit that computes the corresponding function f. By size we mean the number of elementary gates or components that we must put together to evaluate f. We may also be interested in how much time it takes to do the computation if many gates are permitted to execute in parallel, it means to act with more than one gate at each time. The depth of a circuit is the number of time steps required, assuming that gates acting on distinct bits can operate simultaneously. The width of a circuit is the maximum number of gates that act in any one time step.

The decision problems can be divided into two classes: easy and hard. For this purpose, we consider infinite families of decision problems with variable input size, where the number of bits of input can be any integer n. Then, we can examine how the size of the circuit that solves the problem varies with respect to n. Consider a family of functions $\{f_n\}$ where f_n has n bit as input. There is also a family of circuits $\{C_n\}$ that compute these functions. We say that a circuit family is "polynomial size" if the size of C_n

grows with n no faster than a power of n,

$$size\left(C_n\right) \leq poly\left(n\right), \tag{2.2.1}$$

where $poly$ denotes a polynomial function of n. Then, we can define an important complexity class. Decision problems solved by polynomial size circuits have complexity class P. Decision problems in P are considered easy while decision problems belonging to another complexity classes are considered hard. C_n computes $f_n(x)$ for every possible n bit input, and therefore, if a decision problem is in P we can find the answer even for the "hardest" input using a circuit of size no greater than $poly(n)$. Unfortunately, most of the decision problems are not in P. For a n bit string, there are 2^n possibilities of input and there is no better way to compute $f\left(x\right)$ than to analyze input by input. Such task requires a circuit that has exponential size.

Despite the fact that the decision problems outside of P are considered hard, there are complex decision problems that can be answered by showing an example that is easy to verify. This can be done through a non-deterministic[1] polynomial size circuit known as verifier $V\left(x,y\right)$, associated with the circuit $C\left(x\right)$ belonging to some hard problem, that has the property

$$C\left(x\right)=1 \qquad \text{iff} \qquad V\left(x,y\right)=1 \qquad \text{for some } y, \tag{2.2.2}$$

where x and y are n and m bits strings, respectively. These kind of problems are part of a complexity class called NP and it is considered easy if the solution can be checked by the verifier. The NP problems are also a small subclass of all decision problems. An important example of a problem belonging to NP is the CIRCUIT-SAT. In this case the input is a circuit C with n gates, m input bits, and one output bit. The problem is to determine if any input is accepted by C. The function to be evaluated is

$$f\left(C\right)=\begin{cases}1 & \text{if there exist } x \text{ with } C\left(x\right)=1\\ 0 & \text{otherwise}\end{cases}. \tag{2.2.3}$$

This problem is in NP because if the circuit C has polynomial size, then if we provided an input x accepted by C, it is easy to check that $C(x)=1$.

Until now, we talked about deterministic circuits, however, it is sometimes useful to consider probabilistic circuits that have access to a random number generator. For example, a gate in a probabilistic circuit might act in either one of two ways, and flip a fair coin to decide which action to execute. Such a circuit, for a single fixed input, can

[1] Such terminology is used for historical reasons, maybe generating some confusion since the verifier is actually a deterministic circuit.

sample many possible computational paths. An algorithm performed by a probabilistic circuit is said to be "randomized". If we attack a decision problem using a probabilistic computer, we attain a probability distribution of outputs. Thus, we won't necessarily always get the right answer. But if the probability of getting the right answer is larger than $1/2 + \delta$ for every possible input and $\delta > 0$, then the machine is useful. In fact, we can run the computation many times and use majority voting to achieve an error probability less than ε. Furthermore, the number of times we need to repeat the computation is only polylogarithmic in ε^{-1}. If a problem admits a probabilistic circuit family of polynomial size that always gives the right answer with probability larger than $1/2 + \delta$ (for any input, and for fixed $\delta > 0$), we say the problem is in the class BPP, bounded-error probabilistic polynomial time.

There is more to say about classical complexity theory [25, 24], though, for our proposals, the description of the complexity classes above are sufficient to show what complexity means in the context of classical information. The next step is to understand complexity for quantum computers.

2.3 Basics of quantum information

We have seen that the basic unit of classical information is the bit: an object that can assume the value 0 or 1. The analogue unit in quantum information is the quantum bit or qubit. The qubit is a vector in a two-dimensional Hilbert space. In reference to the classical bit, we can call the elements of the canonical basis in this space of $|0\rangle$ and $|1\rangle$. Then a normalized vector in such space can be represented as

$$|\psi\rangle = a\,|0\rangle + b\,|1\rangle\,, \qquad |a|^2 + |b|^2 = 1, \tag{2.3.1}$$

where $a, b \in \mathbb{C}$. We can perform a measurement that projects $|\psi\rangle$ onto the basis $\{|0\rangle\,, |1\rangle\}$. The outcome of the measurement is not deterministic. The probability that we obtain the result $|0\rangle$ is $|a|^2$ and the probability that we obtain the result $|\psi\rangle$ is $|b|^2$. It's useful for finite-dimensional Hilbert spaces, specially in two dimensions, to make use of the matrix formalism. In this context, states are column matrices, for example

$$|0\rangle = \begin{pmatrix} 1 \\ 0 \end{pmatrix}, \qquad |1\rangle = \begin{pmatrix} 0 \\ 1 \end{pmatrix}, \tag{2.3.2}$$

while operators are 2x2 hermitian matrices. A useful example of such matrices are the well known Pauli matrices

$$X = \begin{pmatrix} 0 & 1 \\ 1 & 0 \end{pmatrix}, \qquad Y = \begin{pmatrix} 0 & -i \\ i & 0 \end{pmatrix}, \qquad Z = \begin{pmatrix} 1 & 0 \\ 0 & -1 \end{pmatrix}. \tag{2.3.3}$$

Given the states $|\psi\rangle = \begin{pmatrix} \alpha \\ \beta \end{pmatrix}$ and $|\phi\rangle = \begin{pmatrix} \gamma \\ \lambda \end{pmatrix}$, the inner product between these states is the matrix multiplication

$$\langle\psi|\,\phi\rangle = \langle\phi|\,\psi\rangle^* = \begin{pmatrix} \alpha^* & \beta^* \end{pmatrix} \begin{pmatrix} \gamma \\ \lambda \end{pmatrix} = \alpha^*\gamma + \beta^*\lambda, \tag{2.3.4}$$

where $\langle\psi| = \begin{pmatrix} \bar{\alpha} & \bar{\beta} \end{pmatrix}$ is the dual vector of $|\psi\rangle$ and α^* is the complex conjugate of α. The action of operators on states becomes simple. For example, the state $|1\rangle$ can be obtained by the action of X on $|0\rangle$. Two examples of physical systems that are described by two dimensional Hilbert space are spin-1/2 particles and polarization states of photons.[2]

As for the classical case, it's common in quantum information to work with a string of n qubits. This one is given by a vector in a 2^n dimensional Hilbert space, that is in fact a tensor product between the n two-dimensional Hilbert spaces $\mathcal{H} = \mathcal{H}_1 \otimes \mathcal{H}_2 \otimes ... \otimes \mathcal{H}_n$, while the basis of this space has elements of the form $|101011...100\rangle$. A general normalized vector can be expanded in this basis as

$$|\psi\rangle = \sum_{i=1}^{2^n} a_i\,|i\rangle\,, \qquad \sum_{i=1}^{2^n} |a_i|^2 = 1. \tag{2.3.5}$$

If we measure all the n qubits by projecting each onto the $\{|0\rangle\,, |1\rangle\}$ basis, the probability of obtaining the outcome $|i\rangle$ is $|a_i|^2$.

We can describe a quantum computation in the following way. Given a string of n qubits, our standard initial can be defined as $|0000...0\rangle$. We then apply a unitary transformation U to the n qubits. The transformation U is constructed as a product of standard quantum gates, unitary transformations that act on just a few qubits at a time. After U is applied, we measure all of the qubits by projecting onto the $\{|0\rangle\,, |1\rangle\}$ basis. The measurement outcome is the output of the computation.

2.4 Quantum circuits

Analogously to the classical case, a quantum circuit is a sequence of quantum gates connected by wires. The quantum gates represent general quantum operations, involving some constant number of qubits, while the wires represent the qubits on which the gates act. In general a quantum circuit may have n input qubits and m output qubits for any choice of integers $n, m \geq 0$. Such circuit induces some quantum operation from n qubits to m qubits, determined by composing the actions of the individual gates

[2] For more details about these two examples, see Chapter 2 of [24]

in the appropriate way. The size of a quantum circuit is the total number of gates, which is a good candidate to quantify the hardness of the circuit. For example if our quantum computer runs in serial, which means that one gate is allowed to act on the qubits at each time interval, then the computing time will be directly proportional to the size of the circuit. On the other hand, if our computer is able to run in parallel, meaning that it can simultaneously apply any number of gates which act on the qubits, then the running time will instead be proportional to what is called the depth of the circuit. This is the number such simultaneous actions that are needed to implement the circuit. The circuit complexity $\mathcal{C}$ of a unitary transformation is then defined as the size (or sometimes depth) of the smallest circuit that implements it to within accuracy ε.

A unitary quantum circuit is a quantum circuit in which all of the gates correspond to unitary quantum operations. Naturally this requires that every gate, and hence the circuit itself, has an equal number of input and output qubits. It is common in the study of quantum computing that one works entirely with unitary quantum circuits.

Figure 1 – Quantum circuit representation of the gates.

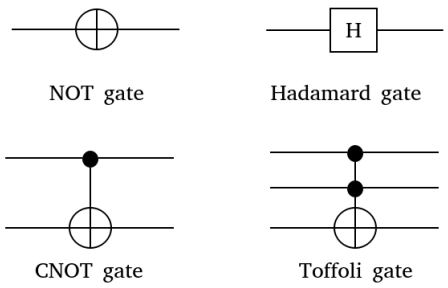

It is useful to show some important gates that are frequently used in problems of quantum information. They quantum circuit representation is shown in the Figure 1:

1. The NOT gate is a single qubit unitary gate that maps $|0\rangle$ to $|1\rangle$ and $|1\rangle$ to $|0\rangle$. It is represented by the Pauli matrix

$$X = \begin{pmatrix} 0 & 1 \\ 1 & 0 \end{pmatrix}. \tag{2.4.1}$$

2. The Hadamard gate is a single qubit unitary gate that creates a superposition acting on the elements of the basis

$$H|a\rangle = \frac{1}{\sqrt{2}}\left[|0\rangle + (-1)^a|1\rangle\right], \qquad H = \frac{1}{\sqrt{2}}\begin{pmatrix} 1 & 1 \\ 1 & -1 \end{pmatrix}, \tag{2.4.2}$$

where a can assume the value 0 or 1.

3. The Phase Shift gate is a single qubit unitary gate that maps the state $|1\rangle$ to $e^{i\phi}|1\rangle$ while leaving the state $|0\rangle$ unchanged. Its matrix representation is given by

$$R_\phi = \begin{pmatrix} 1 & 0 \\ 0 & e^{i\phi} \end{pmatrix}. \tag{2.4.3}$$

4. The controlled NOT gate (CNOT) is a two-qubit unitary gate that performs the NOT operation on the second qubit if the first qubit is $|1\rangle$. Otherwise, nothing change. It is represented by the matrix

$$CNOT = \begin{pmatrix} 1 & 0 & 0 & 0 \\ 0 & 1 & 0 & 0 \\ 0 & 0 & 0 & 1 \\ 0 & 0 & 1 & 0 \end{pmatrix}. \tag{2.4.4}$$

The gate maps the state $|a, b\rangle$ to $|a, a \oplus b\rangle$, where

$$a \oplus b = \begin{cases} 0 & a = b \\ 1 & a \neq b \end{cases}. \tag{2.4.5}$$

The CNOT gate is used to produce entangled states. For example, consider an input state $|00\rangle$ and then apply the Hadamard gate on the first qubit and after the CNOT gate. Such circuit is given by

$$\begin{aligned} (CNOT)H|00\rangle &= (CNOT)\frac{1}{\sqrt{2}}(|0\rangle + |1\rangle) \otimes |0\rangle \\ &= \frac{1}{\sqrt{2}}(|00\rangle + |11\rangle). \end{aligned} \tag{2.4.6}$$

Figure 2 shows the quantum circuit scheme for the above operations.

Figure 2 – Quantum circuit producing entanglement.

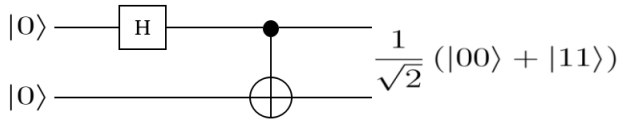

The resulting state is entangled, which means that the qubits are correlated. It is impossible to implement a measurement of the qubits independently. Entangled states will be crucial for future purposes.

5. The Toffoli gate (or CCNOT gate) is a three qubit unitary gate that performs the NOT operation on the third qubit if the first two qubit are $|1\rangle$. Otherwise, nothing changes . It is represented by the matrix form

$$\begin{pmatrix} 1 & 0 & 0 & 0 & 0 & 0 & 0 & 0 \\ 0 & 1 & 0 & 0 & 0 & 0 & 0 & 0 \\ 0 & 0 & 1 & 0 & 0 & 0 & 0 & 0 \\ 0 & 0 & 0 & 1 & 0 & 0 & 0 & 0 \\ 0 & 0 & 0 & 0 & 1 & 0 & 0 & 0 \\ 0 & 0 & 0 & 0 & 0 & 1 & 0 & 0 \\ 0 & 0 & 0 & 0 & 0 & 0 & 0 & 1 \\ 0 & 0 & 0 & 0 & 0 & 0 & 1 & 0 \end{pmatrix}.$$

   The gate maps the state $|a, b, c\rangle$ to $|a, b, c \oplus ab\rangle$.

The gates showed above are universal gates in the sense that every quantum operation can be approximated to within any desired degree of accuracy by some quantum circuit [25].

For a particular case, the circuit complexity will be some number, but more interesting than such number is to look for families of circuits that are defined for arbitrary values of n. The result will be circuits represented by unitary operations U_n which solve some problem of interest for different inputs of size n, using the same algorithm. Summarizing, we want an expression for the circuit complexity that scales with n and has small accuracy ε as n gets large. Typically, a family U_n is called efficient if the circuit complexity is asymptotically bounded by some low order power of n and $1/\varepsilon$. Such upper bound, that is not simple to obtain and involves what is called the Solovay-Kitaev theorem [26], is given by

$$\mathcal{C} \lesssim 2^{2n} \left(\log \frac{1}{\varepsilon}\right)^c$$

where c is some unknown number that must be greater than 1 and less than 2 [16]. Unfortunately, the vast majority of unitary transformations require circuits of exponential size in n. The main goal of quantum complexity theory is to find cases where unitary transformations of interest can be implemented efficiently and sometimes understand why some problems can't be implemented efficiently.

2.5 Fidelity and quantum information metric

Consider two quantum states $|\psi_A\rangle$ and $|\psi_B\rangle$ described by density matrices ρ_A and ρ_B. Then, we can define a quantity called fidelity $F(\rho_A, \rho_B)$ as

$$F(\rho_A, \rho_B) = tr\sqrt{\sqrt{\rho_A}\rho_B\sqrt{\rho_A}}, \tag{2.5.1}$$

where the trace is taken over the Hilbert space of all quantum states of the system. Fidelity measures how close two quantum states are. If these states are pure, i.e., $\rho_A = |\psi_A\rangle \langle\psi_A|$ and $\rho_B = |\psi_B\rangle \langle\psi_B|$, the fidelity reduces to the absolute value of the overlap between these states

$$F(\rho_A, \rho_B) = |\langle\psi_A|\, \psi_B\rangle|\,, \tag{2.5.2}$$

where we considered the fact that for pure states $\rho^2 = \rho$. Now, we can consider a family of states parametrized by a variable λ. The states have a corresponding density matrix ρ_λ. Let's consider two states very close to each other: $|\psi(\lambda)\rangle$ and $|\psi(\lambda + \delta\lambda)\rangle$. The QIM is defined from the Fidelity between these two infinitesimally close states. As a result, we expect a power series in $\delta\lambda$ of the form

$$F(\rho_\lambda, \rho_{\lambda+\delta\lambda}) = 1 - G_{\lambda\lambda}\delta\lambda^2 + \mathcal{O}\left(\delta\lambda^3\right), \tag{2.5.3}$$

where $G_{\lambda\lambda}$ is the QIM. The natural generalization for a multi dimensional parameters space with λ^a is

$$F(\rho_\lambda, \rho_{\lambda+\delta\lambda}) = 1 - G_{ab}\delta\lambda^a\delta\lambda^b + \mathcal{O}\left(\delta\lambda^3\right). \tag{2.5.4}$$

We are going to see in Chapter 4 that the QIM has an holographic dual, similarly what we have in holographic entanglement entropy. In special, there will be a connection between this holographic formulation for the QIM and CV proposal.

3 Holography

The next step is to take a look at three other topics: holography, black holes and entanglement. These subjects are very deep and to learn everything about them is a tall order. We need to study how they are correlated. The correspondence was a breakthrough in theoretical physics, becoming a background for future developments, where two of them are specially interesting for us: the proposal of a holographic formula for entanglement entropy [9, 10] and the relation between black holes in AdS and thermal CFTs [27, 28].

3.1 Black holes in AdS space-time

Black holes are an interesting class of solutions of Einstein's equations of motion which have at least one event horizon. An event horizon is a boundary in space-time beyond which events cannot influence an outside observer. The AdS/CFT correspondence provides a dictionary between black holes in AdS and thermal CFTs. In particular, the two-sided AdS black hole is dual to a thermofield double state. However, before we study black holes in AdS, we need first to understand the main concepts of AdS space-times and black holes in Minkowski space-time. Large part of the discussion of this chapter follows [29].

3.1.1 AdS space-time

Consider Einstein gravity with cosmological constant Λ that is given by the Einstein-Hilbert action

$$\mathcal{A}_{EH} = \frac{1}{16\pi G}\int_{\mathcal{M}} d^{d+1}x\sqrt{-g}\,(R-2\Lambda) + \frac{1}{8\pi G}\int_{\partial\mathcal{M}} d^{d}x\sqrt{-h}K, \tag{3.1.1}$$

where g is the determinant of the metric, R is the Ricci scalar and G is Newton's constant. The integral in the first term is defined over a manifold $\mathcal{M}$. The second term is known as Gibbons-Hawking-York term. It is required in order to have a consistent variational principle in the cases where the manifold $\mathcal{M}$ has a boundary. The quantity h is the determinant of the induced metric on the manifold boundary ∂M and K is the extrinsic curvature of the boundary. The variation with respect to the metric $g_{\mu\nu}$ results in Einstein's field equations

$$R_{\mu\nu} - \frac{1}{2}Rg_{\mu\nu} + \Lambda g_{\mu\nu} = 8\pi G T_{\mu\nu}, \tag{3.1.2}$$

where the energy-momentum tensor $T_{\mu\nu}$ arises from the contribution of a matter action $\mathcal{A}_{matter}$ such that

$$T_{\mu\nu} = -\frac{2}{\sqrt{-g}}\frac{\delta \mathcal{A}_{matter}}{\delta g^{\mu\nu}}. \tag{3.1.3}$$

There are vacuum solutions of (3.1.2), i.e $T_{\mu\nu} = 0$, that have maximal symmetries. The isometries of the manifold $\mathcal{M}$ are given by Killing vectors ξ^{μ} that satisfy the condition for the Lie derivative of the metric $\mathscr{L}_{\xi} g_{\mu\nu} = 0$. A manifold of dimension $d+1$ can have at most $d\left(d+1\right)/2$ independent Killing vectors, which means a maximum number of isometries. Space-times that saturate such quantity are known as maximally symmetric space-times. There are three of them, depending on the sign of the Ricci scalar R: Minkowski space-time for $R = 0$, Anti-de Sitter space for $R < 0$, de Sitter for $R > 0$.

Let's focus our attention to the case $R < 0$. The $d+1$ dimensional Anti-de Sitter space-time is a solution of the Einstein's equations with negative cosmological constant Λ. It can be seen by contracting equation (3.1.2) with the metric $g_{\mu\nu}$, getting then

$$\Lambda = \frac{R\left(d-1\right)}{2\left(d+1\right)}, \tag{3.1.4}$$

remembering that we are considering $T_{\mu\nu} = 0$. The sign of Λ is the same of R. The AdS_{d+1} space-time can be understood as a $d+1$ dimensional manifold embedded in a $d+2$ Minkowski space $\mathbb{R}^{2,d}$ with metric signature $\eta_{\mu\nu} = (-1, 1..., 1, -1)$, which respect the constraint

$$-\left(X^{0}\right)^{2} + \sum_{i=1}^{d}\left(X^{i}\right)^{2} - \left(X^{d+1}\right)^{2} = -L^{2}, \tag{3.1.5}$$

where L is the radius of curvature of the AdS space-time.

The isometry group for AdS is $SO\left(d,2\right)$. A maximally symmetric space-time may be represented as a coset space. The coset is obtained by modifying the isometry group of the manifold $\mathcal{M}$ by the stabiliser group for each point $p \in \mathcal{M}$. The stabiliser group contains those isometries which leave p invariant. For example, for S^2, the isometry group is $SO(3)$. Each point p on S^2 is invariant under the rotations around the axis connecting the center of the sphere to p. Thus S^2 is given by the coset space $SO(3)/SO(2)$. Similarly, in d dimensions, S^d corresponds to $SO(d+1)/SO(d)$. A further example is Minkowski space which is given by the Poincaré group modified by the Lorentz group, $ISO(d,1)/SO(d,1)$. Since AdS_{d+1} is also a maximally symmetric space-time, it is the coset manifold $SO\left(d,2\right)/SO\left(d-1,2\right)$.

Let's first study the specific case of AdS_3 that will be useful for future

purposes. The embedded metric[1] is given by

$$ds^2 = -dT^2 + dX^2 + dY^2 - dW^2. \tag{3.1.6}$$

It won't be difficult to generalize such coordinates for AdS_{d+1}. Implementing the coordinate transformation

$$\begin{aligned} T &= R\cos\tau, \qquad W = R\sin\tau, \\ X &= r\cos\phi, \qquad Y = r\sin\phi, \end{aligned} \tag{3.1.7}$$

where $\tau \in [0, 2\pi)^2$ and $\phi \in [0, 2\pi]$. The metric and the constraint (3.1.5) become

$$\begin{aligned} ds^2 &= -\left(dR^2 + R^2 d\tau^2\right) + dr^2 + r^2 d\phi^2, \\ L^2 &= R^2 - r^2. \end{aligned} \tag{3.1.8}$$

The variables r and R aren't independent. This way, we can eliminate the redundant coordinate R of the metric (3.1.8), which becomes

$$ds^2 = -L^2\left(1 + \frac{r^2}{L^2}\right)dt^2 + \frac{dr^2}{1 + \frac{r^2}{L^2}} + r^2 d\phi^2. \tag{3.1.9}$$

Another similar coordinate system can be obtained by parameterizing $R = L\cosh\rho$ and $r = L\sinh\rho$ with $\rho \in \mathbb{R}^+$. The full coordinate change is

$$\begin{aligned} T &= L\cosh\rho\cos\tau, \qquad W = L\cosh\rho\sin\tau, \\ X &= L\sinh\rho\cos\phi, \qquad Y = L\sinh\rho\sin\phi, \end{aligned} \tag{3.1.10}$$

where the metric becomes

$$ds^2 = L^2\left(-\cosh^2\rho d\tau^2 + d\rho^2 + \sinh^2\rho d\phi^2\right). \tag{3.1.11}$$

Both coordinates (τ, r, ϕ) and (τ, ρ, ϕ) are global coordinates for AdS_3 since they cover all the surface defined by the constraint (3.1.5). The generalization for the metric (3.1.11) for AdS_{d+1} is

$$ds^2 = L^2\left(-\cosh^2\rho d\tau^2 + d\rho^2 + \sinh^2\rho d\Omega_{d-1}^2\right). \tag{3.1.12}$$

It can be done by replacing $dX^2 + dY^2$ by $\sum_i \left(dX^i\right)^2$, which is equivalent to trade $d\phi^2$ for $d\Omega_{d-1}^2$. Figure 3 shows AdS_2 space-time embedded into a three-dimensional Minkowski space-time with coordinates X^0, X^1 and X^2.

[1] Refer to the line element ds^2 as "metric" is a clear abuse of language. The relation between ds^2 and $g_{\mu\nu}$ is given by $ds^2 = g_{\mu\nu}dx^\mu dx^\nu$.

[2] If the fact that the coordinate τ is periodic in 2π bothers you, we can consider the universal covering $\widetilde{AdS}_d$ by unwrapping the timelike circle. This is done by taking $\tau \in \mathbb{R}$ without identifying points.

Figure 3 – Schematic illustration of the AdS_2 space-time embedded in three dimensional Minkowski space-time.

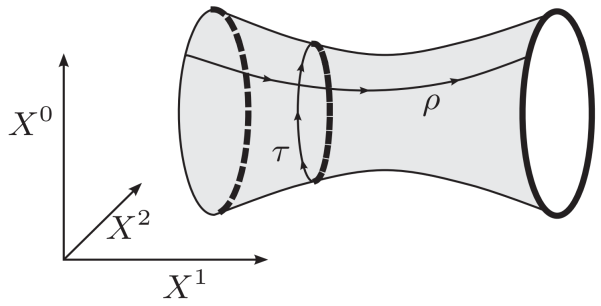

Source: [29]

The AdS$_{d+1}$ space-time has a boundary that is $\mathbb{R} \times S^{d-1}$. In order to see this, consider the global coordinates (3.1.10). Considering a new change of coordinates

$$\tan\theta = \sinh\rho, \qquad 0 \leqslant \theta < \frac{\pi}{2}, \tag{3.1.13}$$

the metric (3.1.12) becomes

$$ds^2 = \frac{L^2}{\cos^2\theta}\left(-d\tau^2 + d\theta^2 + \sin^2\theta d\Omega_{d-1}^2\right), \tag{3.1.14}$$

that is the d-dimensional $\mathbb{R} \times S^d$ space-time[3]. One direct consequence of the range of the θ coordinate is that the above metric covers half of a sphere S^d. Adding the point $\theta = \pi/2$ corresponding to the spatial infinity, the compactified spacefime is given by the metric

$$ds^2 = -d\tau^2 + d\theta^2 + \sin^2\theta d\Omega_{d-1}^2, \qquad 0 \leqslant \theta \leq \frac{\pi}{2}, \qquad 0 \leqslant \theta < 2\pi. \tag{3.1.15}$$

Another useful coordinate is system is the Poincaré patch coordinates $(t, r, \vec{x})$, that are related with the embedded coordinates $\left(X^0, ..., X^d\right)$ of $\mathbb{R}^{2,d}$ by

$$\begin{aligned}
X^0 &= \frac{L^2}{2r}\left(1 + \frac{r^2}{L^4}\left(\vec{x}^2 - t^2 + L^2\right)\right), \\
X^i &= \frac{rx^i}{L} \qquad \text{for } i \in \{1, ..., d-1\}, \\
X^d &= \frac{L^2}{2r}\left(1 + \frac{r^2}{L^4}\left(\vec{x}^2 - t^2 + L^2\right)\right), \\
X^{d+1} &= \frac{rt}{L},
\end{aligned} \tag{3.1.16}$$

where $t \in \mathbb{R}$, $\vec{x} = \left(x^1, ..., x^{d-1}\right) \in \mathbb{R}^{d-1}$ and $r \in \mathbb{R}^+$. The metric for the Poincaré path coordinate is

$$ds^2 = \frac{L^2}{r^2}dr^2 + \frac{r^2}{L^2}\left(-dt^2 + d\vec{x}^2\right). \tag{3.1.17}$$

[3] The global factor in the metric (3.1.14) doesn't change the causal structure of the space-time.

The AdS_{d+1} space-time in the Poincaré can be seen as a flat space-time given by the coordinates $(t, \vec{x})$ plus an warped direction r. Figure 4 shows a sketch of the AdS_{d+1} in these coordinates. There are two singularities. First, for $r \to 0$ we have the Poincaré horizon, that is a singularity of the coordinate system. On the other side of the horizon, i.e. for $r < 0$, there is another Poincaré patch, which is needed to cover the whole of AdS space-time. For $r \to \infty$ the flat part of the metric diverges. However, the dr^2 term of the metric (3.1.17) disappear. It can be interpreted as there is a conformal boundary[4] located at $r \to \infty$.

Figure 4 – AdS_d space-time in Poincaré patch coordinates.

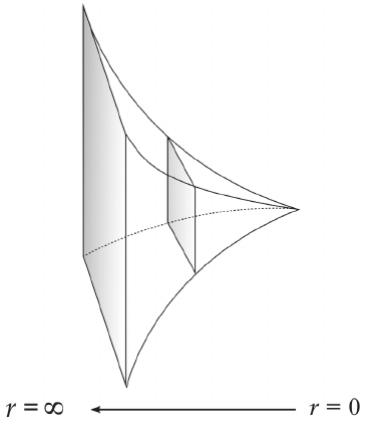

Source: [29]

Just as a commentary, sometimes it is more convenient to invert the coordinate r by defining $z = L^2/r$. In the (z, t, x), the conformal boundary is located at $z = 0$. It is possible to verify by a direct change of coordinates that the metric with the z coordinates has the form

$$ds^2 = \frac{L^2}{z^2}\left(dz^2 - dt^2 + d\vec{x}^2\right) = \frac{L^2}{z^2}\left(dz^2 - dt^2 + d\vec{x}^2\right), \tag{3.1.18}$$

where the coordinates (t, x) keep being the boundary coordinates.

We can define an Euclidean AdS_{d+1} performing a Wick rotation on the time coordinate. For example, considering the metric (3.1.11) and defining $\tau_E = i\tau$, we obtain

$$ds^2 = L^2\left(\cosh^2\rho d\tau_E^2 + d\rho^2 + \sinh^2\rho d\Omega_{d-1}^2\right) \tag{3.1.19}$$

that has Euclidean signature. The same thing can be done for the Poincaré path metric (3.1.17) by defining $t_E = it$. The isometry group of Euclidean AdS_{d+1} is given by $SO(d+1, 1)$ instead of $SO(d, 2)$. Such procedure is necessary to study quantum field theories at finite temperature.

[4] There is a discussion about this name conformal boundary coordinates on pag. 74 of [29].

Lastly, a relevant comment. We can calculate the Christoffel symbols $\Gamma^{\mu}_{\nu\rho}$ of the metric (3.1.17) and also the Riemann tensor $R_{\mu\nu\rho\sigma}$. The result is the Ricci scalar R is given by

$$R = -\frac{d\,(d+1)}{L^2}. \tag{3.1.20}$$

We know of a direct relation between the Ricci scalar and the cosmological constant, see (3.1.4). Then,

$$\Lambda = -\frac{d\,(d-1)}{2L^2}. \tag{3.1.21}$$

The cosmological constant Λ has a direct relation with the radius of the AdS_{d+1} space-time.

3.1.1.1 Penrose diagram

The change of coordinates in (3.1.13) can be thought of as a compactification of the coordinate ρ. Originally, its range covered all the $\mathbb{R}^+$, however, after the coordinate change, we have the variable θ which is bounded by the interval $[0, \pi/2]$. The metric (3.1.14) has a divergence for $\theta = \pi/2$. It is not a problem once we can eliminate such divergence, without changing the causal structure of the space-time, implementing an adequate conformal compactification

$$ds^2 \to d\widetilde{s}^2 = \Lambda^2\,(x)\,ds^2, \qquad \Lambda \neq 0, \tag{3.1.22}$$

where x refers to the coordinates of interest and $\Lambda \to 0$ on the divergent point. For the metric (3.1.14), the function is $\Lambda = \cos^2\theta/L^2$, which goes to zero when $\theta = \pi/2$. The compactified metric is shown in (3.1.15). The Penrose diagram (or Conformal diagram) for AdS_2 is shown in the Figure 5. It is useful to study the causal structure of the space-time.

Figure 5 – Penrose diagram for AdS_2.

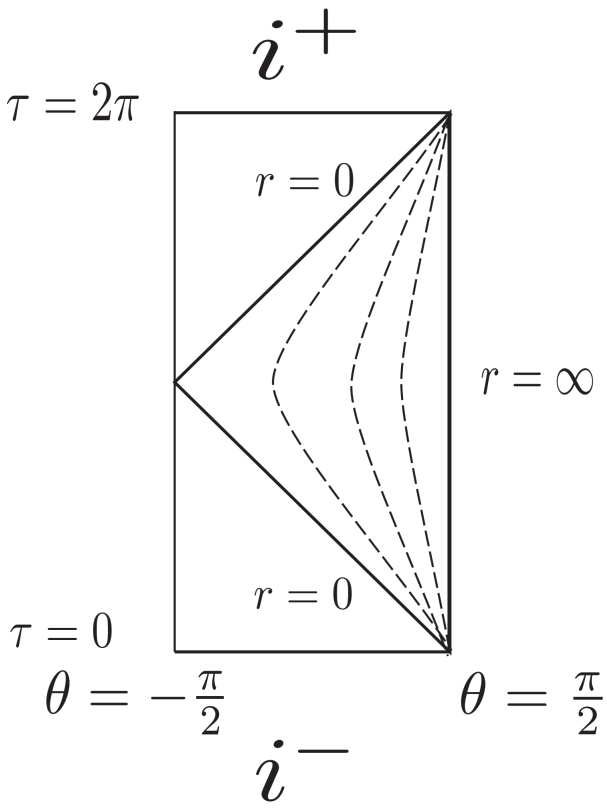

Source: [29]

The Poincaré coordinates cover the triangular region shown. Timelike geodesics begin at i^- and end at i^+.

A second example is the Penrose diagram for the Minkowski space-time. Consider the d dimensional case where the metric is given by

$$ds^2 = -dt^2 + dr^2 + r^2 d\Omega_{d-2}^2. \tag{3.1.23}$$

Defining light-cone coordinates

$$\begin{aligned} u &= t - r, \qquad -\infty < u < \infty, \\ v &= t + r, \qquad -\infty < v < \infty, \end{aligned} \tag{3.1.24}$$

in such way that ds^2 becomes

$$ds^2 = -dudv + \frac{(u-v)^2}{4} d\Omega_{d-2}^2. \tag{3.1.25}$$

In order to compactify u and v, consider a second coordinate transformation

$$\begin{aligned} u &= \tan \widetilde{U}, \qquad -\pi/2 < \widetilde{U} < \pi/2, \\ v &= \tan \widetilde{V}, \qquad -\pi/2 < \widetilde{V} < \pi/2, \end{aligned} \tag{3.1.26}$$

where $V \geq \widetilde{U}$ once $r \geq 0$. As a consequence,

$$ds^2 = \frac{1}{4\cos^2\widetilde{U}\cos^2\widetilde{V}}\left(-4d\widetilde{U}d\widetilde{V} + \sin^2\left(\widetilde{V}-\widetilde{U}\right)d\Omega_{d-2}^2\right). \tag{3.1.27}$$

For the above metric, the divergences are located at $\widetilde{U},\widetilde{V} = \pm\pi/2$. Fortunately, they can be eliminated choosing $\Lambda\left(\widetilde{U},\widetilde{V}\right) = 2\cos\widetilde{U}\cos\widetilde{V}$. Finally, we can come back to some regular coordinates

$$\begin{aligned} \widetilde{T} &= \widetilde{V}+\widetilde{U}, \qquad -\pi < \widetilde{T} < \pi, \\ \widetilde{R} &= \widetilde{V}-\widetilde{U}, \qquad 0 < \widetilde{R} < \pi. \end{aligned} \tag{3.1.28}$$

The result is the compactified metric

$$d\widetilde{s}^2 = -d\widetilde{T}^2 + d\widetilde{R}^2 + \sin^2\widetilde{R}d\Omega_{d-2}^2. \tag{3.1.29}$$

The Penrose diagram for the d dimensional Minkowski space-time is shown in Figure 6.

Figure 6 – Penrose diagram for Minkowski space-time.

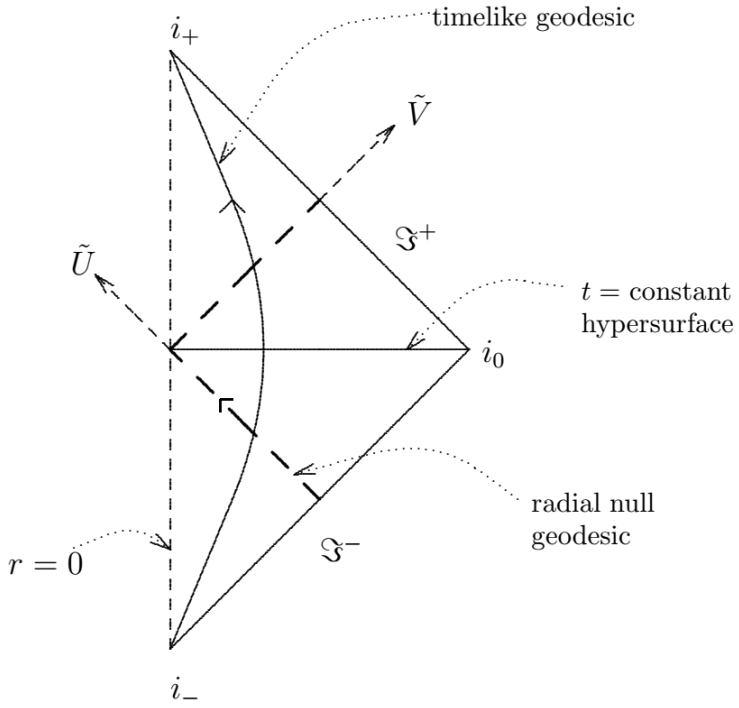

Source: [30]

Each point on the diagram represents a sphere S^{d-2} with radius $\sin^2\widetilde{R}$, except at $r = 0$ and i_0,$i_\pm$. Light rays travel at 45^o from $\mathfrak{J}^-$ through $r = 0$ and then out to $\mathfrak{J}^+$, where $\mathfrak{J}^\pm$ are null hypersurfaces.

3.1.2 AdS-Schwarzschild Black Hole

In Appendix A there is a discussion about the main properties of the asymptoticly flat Schwarzschild black hole, which means that a observer far from of the black hole lives in a Minkowski space-time. Despite of the importance of such geometry, our main interest is about black holes in Anti-de Sitter. However, many of the computations in that appendix could be used in the case of the AdS black holes.

The most direct way to place a black inside of the AdS_{d+1} space-time is modifying the metric (A.1.2) to

$$ds^2 = -f\left(r\right)dt^2 + \frac{dr^2}{f\left(r\right)} + r^2 d\Omega_{d-1}^2, \qquad f\left(r\right) = 1 - \frac{2\mu}{r^{d-2}} + \frac{r^2}{L^2}, \tag{3.1.30}$$

where

$$\mu = \frac{8\pi GM}{\left(d-1\right)\Omega_{d-1}}, \qquad \Omega_{d-1} = \frac{2\pi^{d/2}}{\Gamma\left(\frac{d}{2}\right)}. \tag{3.1.31}$$

Asymptotically, the metric (3.1.30) becomes the AdS metric (3.1.9) once r^2/L^2 is the relevant term of $f\left(r\right)$ in this limit $r \to \infty$. The AdS-Schwarzschild black hole, as well as the flat case, has an event horizon at $r = r_h$, where r_h is the largest root of $f\left(r_h\right) = 0$. The Hawking temperature can be calculated using (A.1.41), as result

$$T = \frac{\left(d-2\right)L^2 + dr_h^2}{4\pi L^2 r_h}. \tag{3.1.32}$$

There are two possible classifications for black holes according to the radius of the horizon. Black holes with $r_h \ll L$ are classified as small black holes. For these cases, we can ignore the r_h^2 contribution in (3.1.32), resulting then in

$$T = \frac{\left(d-2\right)}{4\pi r_h}. \tag{3.1.33}$$

On the other hand, black holes with $r_h \gg L$ are referred to as large black holes. For them, we can neglect the L^2 in (3.1.32). Thus, the Hawking temperature for large black hole is given by

$$T = \frac{dr_h}{4\pi L^2}. \tag{3.1.34}$$

As an interesting remark, the Hawking temperature has a minimum at $r_h = \sqrt{\frac{(d-2)}{d}}L$. Then, the minimum temperature for a black hole in AdS is

$$T_{min} = \frac{\sqrt{d\left(d-2\right)}}{2\pi L}, \tag{3.1.35}$$

which implies that black holes exist only for temperatures larger than T_{min}.

We can repeat the same steps done for the black hole in Minkowski in order to get the Kruskal extension of the AdS space-time. First, we introduce the light-cone tortoise coordinates

$$v = t + r^*, \qquad u = t - r^*, \qquad dr^* = \frac{dr}{f(r)}, \tag{3.1.36}$$

in such way that

$$ds^2 = -f(r)\, dudv + r^2 d\Omega_{d-1}^2.$$

Then, we introduce the Kruskal coordinates (U, V) for the AdS case as

$$\begin{aligned} U &= -\exp\left(-\frac{f'(r_h)\, u}{2}\right), \qquad V = \exp\left(\frac{f'(r_h)\, v}{2}\right), \\ UV &= -\exp\left(f'(r_h)\, r^*\right), \qquad \frac{U}{V} = -\exp\left(-f'(r_h)\, t\right), \end{aligned} \tag{3.1.37}$$

which allow us to write the Kruskal extension for the AdS-Schwazschild black hole as

$$ds^2 = -\frac{4f(r)}{f'(r_h)^2} \exp\left(-f'(r_h)\, r^*\right) dUdV + r^2 d\Omega_{d-1}^2. \tag{3.1.38}$$

This is the two-sided AdS black hole. It has the same interpretation as the two-sided case in Minkowski: this geometry describes a ERB connecting two asymptotically AdS space-times. Figure 7 shows the conformal diagram for the two-sided AdS black hole.

Figure 7 – Conformal diagram for Kruskal-Szekeres coordinates in AdS_{d+1}.

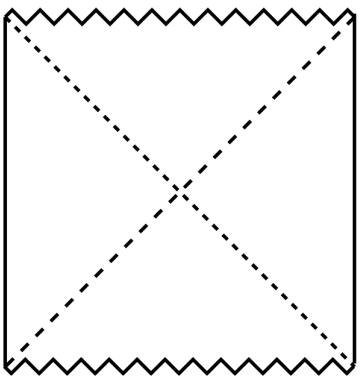

Source: [31]

Lines of constant r are the same if we compare to the two-sided case in Minkowski (see Figure 22).

It is possible to generalize the AdS–Schwarzschild metric to non-spherical event horizons. Namely,

$$ds^2 = -f(r)\, dt^2 + \frac{dr^2}{f(r)} + r^2 d\Sigma_{k,d-1}^2, \qquad f(r) = k - \frac{2\mu}{r^{d-2}} + \frac{r^2}{L^2}, \tag{3.1.39}$$

where k indicates the curvature of the $(d-1)$-dimensional line element $d\Sigma^2_{k,d-1}$, which is

$$d\Sigma^2_{k,d-1} = \begin{cases} d\Omega^2_{d-1} = d\theta^2 + \sin^2\theta d\Omega^2_{d-2} & \text{for } k=1 \\ dl^2_{d-1} = \sum_{i=1}^{d-1} dx_i^2/L^2 & \text{for } k=0 \\ d\Xi^2_{d-1} = d\theta^2 + \sinh^2\theta d\Omega^2_{d-2} & \text{for } k=-1 \end{cases} \tag{3.1.40}$$

In this generalization, we will use $\Sigma_{k,d-1}$ to denote the dimensionless volume of the relevant spatial geometry. It will appears inside the expression for the mass parameter μ and the entropy S of the black hole as

$$\mu = \frac{8\pi GM}{(d-1)\,\Sigma_{k,d-1}}, \qquad S = \frac{A_h}{4G} = \frac{\Sigma_{k,d-1} r^{d-1}}{4G} \tag{3.1.41}$$

The parameter k can assume the values $1, 0, -1$. The case $k = 1$ corresponds to the spherical geometry, which recovers the AdS-Schwarzschild metric (3.1.30). For $k = 0$, namely planar geometry, the metric is asymptotically AdS, described by Poincaré coordinates, which only cover a portion of the full AdS geometry. Lastly, for $k = -1$, the hyperbolic geometry. Asymptotically, the vacuum bulk metric is AdS space in the so-called AdS-Rindler coordinates.

3.1.3 Charged AdS black hole

Let's consider the Einstein-Maxwell theory given by the action

$$\begin{aligned} \mathcal{A}_{EM} = &\frac{1}{16\pi G}\int_{\mathcal{M}} d^{d+1}x\sqrt{-g}\,(R - 2\Lambda) \\ &+ \frac{1}{8\pi G}\int_{\partial\mathcal{M}} d^d x\sqrt{-h}K - \frac{1}{16\pi}\int_{\mathcal{M}} d^{d+1}x\sqrt{-g}F_{\mu\nu}F^{\mu\nu}. \end{aligned} \tag{3.1.42}$$

The equations of motion are

$$\begin{aligned} R_{\mu\nu} - \frac{1}{2}g_{\mu\nu}R + \Lambda g_{\mu\nu} &= 8\pi G T_{\mu\nu}, \\ \partial_\mu\left(\sqrt{-g}F^{\mu\nu}\right) &= 0 \end{aligned} \tag{3.1.43}$$

where

$$T_{\mu\nu} = \frac{1}{8\pi}\left[F_{\mu\rho}F^{\rho}_{\nu} - \frac{1}{4}F_{\rho\sigma}F^{\rho\sigma}g_{\mu\nu}\right]. \tag{3.1.44}$$

The solution of the above equations is the so called Reissner-Nordstrom-AdS black hole, which has metric

$$\begin{aligned} ds^2 &= -f(r)\,dt^2 + \frac{dr^2}{f(r)} + r^2 d\Omega^2_{d-1}, \\ f(r) &= 1 - \frac{2\mu}{r^{d-2}} + \frac{\alpha^2}{r^{2(d-2)}} + \frac{r^2}{L^2}, \end{aligned} \tag{3.1.45}$$

where α is related to the charge of the black hole Q by

$$\alpha^2 = \frac{8\pi G}{(d-1)\,\Omega_{d-1}} Q^2. \tag{3.1.46}$$

Horizons occur where $f(r) = 0$. The charged black hole has two horizons: the inner horizon r_- and the outer horizon r_+. As a consequence, the Hawking temperature can be computed from (A.1.41) considering the outer horizon, while the entropy is the area of the sphere at r_+.

For future purposes, let's take the trace of the equation (3.1.43),

$$R = 2\frac{(d+1)}{(d-1)}\Lambda + \frac{d-3}{2\,(d-1)} G F_{\rho\sigma} F^{\rho\sigma}, \tag{3.1.47}$$

which provides with us a relation for the Ricci scalar in terms of Λ and the field strength $F_{\mu\nu}$. Additionally, for the case $d = 3$, where the trace of $T_{\mu\nu}$ is zero, the relation between R and Λ is the same as for uncharged black holes and pure AdS space-time.

3.2 Entanglement entropy

Entanglement entropy is a key concept for the understanding of complexity. Direct similarities will appear in the holographic computations of both quantities. In this section, we are going to study the main concepts of entanglement entropy. For a complete review about holographic entanglement entropy, see [32]. The entanglement entropy S_A in quantum field theories or quantum many body systems is a non-local quantity as opposed to correlation functions. It is defined as the von Neumann entropy

$$S_A = -tr\rho_A \log \rho_A \tag{3.2.1}$$

of the reduced density matrix ρ_A when we trace out degrees of freedom inside a $(d-1)$-dimensional space-like submanifold B in a given d-dimensional QFT, which is a complement of A. The quantity S_A measures how the subsystems A and B are correlated with each other. The historical motivation to consider the entanglement entropy in quantum field theories is due to the fact that S_A looks analogous to the black hole entropy. Interestingly, the leading divergence of S_A is proportional to the area of the subsystem A, called the area law.

Firstly, let's consider a quantum mechanical system with many degrees of freedom, like a spin chains (a string of qubits), for example. We can also extend the formalism for quantum field theories. Assuming that our system is at zero temperature, the total quantum system is described by the pure ground state $|\Omega\rangle$. We are also assuming no degeneracy of the ground state. Given this, the density matrix is that of the pure state

$$\rho_{tot} = |\Omega\rangle \langle\Omega| . \tag{3.2.2}$$

We can compute that the von Neumann entropy of the total system is

$$S_{tot} = -tr\rho_{tot}\log\rho_{tot} = -tr\rho_{tot}\log\rho_{tot}^2 = 2S_{tot}$$
$$S_{tot} = 0, \tag{3.2.3}$$

where we used that for pure states $\rho^2 = \rho$. However, if we divide the total system into two subsystems A and B, how is shown in Figure 8, the total Hilbert space $\mathcal{H}_{tot}$ can be written as a direct product of two spaces $\mathcal{H}_{tot} = \mathcal{H}_A \otimes \mathcal{H}_B$ corresponding to those of subsystems A and B.

Figure 8 – Schematic choice of the subsystems A and B for a spin chain and a quantum field theory.

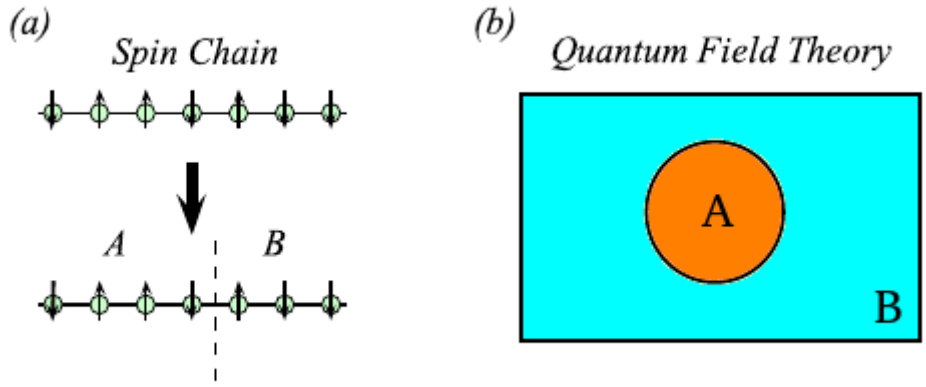

Source: [32]

Then, the subsystem A is described by the reduced density matrix

$$\rho_A = tr_B\rho_{tot}, \tag{3.2.4}$$

where we trace out the contributions that come from the Hilbert space $\mathcal{H}_B$. So, the entanglement entropy of the subsystem A as the von Neumann entropy of the reduced density matrix ρ_A, namely

$$S_A = -tr\rho_A\log\rho_A. \tag{3.2.5}$$

This quantity provides us with a convenient way to measure how closely entangled a given state $|\Omega\rangle$ is. The exact same thing can be done for the region B, defining a reduced density matrix ρ_B tracing out degrees of freedom of the region A. As a comment, it is possible to compute von Neumann entropy of a thermal state with temperature $T = \beta^{-1}$. This can be done by replacing ρ_A with the thermal density matrix in (3.2.1), namely

$$\rho_{thermal} = \frac{e^{-\beta H}}{Z(\beta)}, \tag{3.2.6}$$

where H is the total Hamiltonian and $Z(\beta) = tre^{-\beta H}$ is the partition function. For the total system

$$S_{thermal} = -tr\rho_{thermal}\log\rho_{thermal} = -\frac{1}{Z(\beta)}tre^{-\beta H}\log\frac{e^{-\beta H}}{Z(\beta)}$$
$$S_{thermal} = \left(1-\beta\frac{\partial}{\partial\beta}\right)\log Z(\beta), \tag{3.2.7}$$

which means that the above quantity is the thermal entropy, as expected.

There are useful properties which the entanglement entropy respects generally. We are going to show the most important of them [33, 32]:

- If the density matrix ρ_{tot} represents a pure state, such as in the zero temperature system, then we find the following relation, assuming B is the complement of A,

$$S_A = S_B. \tag{3.2.8}$$

  Such property means that the entanglement entropy is not an extensive quantity. The above equality is violated at finite temperature.

- For any three subsystems A, B and C that do not intersect each other, we have the following inequalities

$$S_{A+B+C} + S_B \leq S_{A+B} + S_{B+C},$$
$$S_A + S_C \leq S_{A+B} + S_{B+C}, \tag{3.2.9}$$

  that are called strong subadditivity [34, 35], which is a very powerful inequality obtained so far with respect to the entanglement entropy. For example, in [36, 37] the authors presented an entropic proof of the c-theorem by applying the strong subadditivity to $2d$ quantum field theories.

- By setting B empty in (3.2.9), we can find the subadditivity relation

$$S_{A+B} \leq S_A + S_B. \tag{3.2.10}$$

  The subadditivity allows us to define an interesting quantity called mutual information $I(A,B)$ by

$$I(A,C) = S_A + S_B - S_{A+B} \geq 0. \tag{3.2.11}$$

A simple example that shows the entanglement between two systems A and B is the Bell's pair given by

$$|\psi\rangle = \frac{1}{\sqrt{2}}\left(|+\rangle_A|-\rangle_B - |-\rangle_A|+\rangle_B\right), \tag{3.2.12}$$

where $+$ and $-$ denote spin up and down, respectively. The reduced density matrix ρ_A is

$$\rho_A = \frac{1}{2}\left(|+\rangle\langle+| + |-\rangle\langle-|\right) = \frac{I_2}{2}, \tag{3.2.13}$$

where I_2 is the 2-dimensional identity matrix. Then, the entanglement entropy is

$$S_A = \log 2. \tag{3.2.14}$$

The Bell's pair (3.2.12) is an example of maximally entangled system. A given state is maximally entangled if the reduced density operator of the system is a multiple of the identity operator.

The Rényi entropy is a one-parameter generalization of entanglement entropy labeled by an integer n, namely

$$S_n(A) = \frac{1}{1-n}\log tr_A \rho_A^n.$$

In the limit of $n \to 1$, the Rényi entropy reduced to entanglement entropy. The Rényi entropy provides us more information about the eigenvalues of the reduced density matrix than entanglement entropy. It is defined for an integer n, but we analytically continue n to a real value when we take the limit $n \to 1$. This analytic continuation will be useful to compute entanglement entropy of a QFT .

3.2.1 Entanglement entropy in QFT

Consider a d-dimensional QFT defined on a manifold $\mathbb{R} \times \mathcal{M}_{d-1}$, where $\mathbb{R}$ and $\mathcal{M}_{d-1}$ denote the time direction and the $(d-1)$-dimensional space-like manifold, respectively. At fixed time $t = t_0$, it is possible to define on this$(d-1)$-dimensional manifold a subregion A. Furthermore, let's denote its complementary region by B. The boundary of A, which is denoted by ∂A, divides the manifold $\mathcal{M}_{d-1}$ into two sub-manifolds A and B. Then, we can compute the entanglement entropy S_A using (3.2.5). It is interesting to note that sometimes this kind of entropy can be dependent of the geometry of the sub-manifold A.

The entanglement entropy has the feature to be always divergent for continuum theories, as QFTs for example. Because this fact, it is necessary to introduce an ultraviolet cut off δ (lattice spacing) in order to perform the computations. The coefficient in front of the divergence turns out to be proportional to the area of the boundary ∂A of the sub-system A,

$$S_A = \gamma \frac{Area\,(\partial A)}{\delta^{d-2}} + \text{subleading terms}, \tag{3.2.15}$$

where γ is a constant which depends on the system. This behavior can be intuitively understood since the entanglement between A and B occurs more between degrees of

freedom close to the boundary ∂A. However, this area law doesn't always describe the scaling behavior of the entanglement entropy in generic situations. For example, the entanglement entropy of $2d$ CFT scales logarithmically with respect to the length l of A,

$$S_A = \frac{c}{3} \log\left(\frac{l}{\delta}\right), \tag{3.2.16}$$

where c is the central charge of the CFT. However, the above result is in accord to the expected UV behavior of S_A, which has the form

$$S_A = \begin{cases} a_{d-2}\left(\frac{l}{\delta}\right)^{d-2} + a_{d-4}\left(\frac{l}{\delta}\right)^{d-4} + \cdots + a_1 \frac{l}{\delta} + (-1)^{(d-1)/2} C_A + \mathcal{O}(\delta) & d \text{ odd} \\ a_{d-2}\left(\frac{l}{\delta}\right)^{d-2} + a_{d-4}\left(\frac{l}{\delta}\right)^{d-4} + \cdots + (-1)^{(d-2)/2} C_A \log\left(\frac{l}{\delta}\right) + \mathcal{O}(\delta) & d \text{ even} \end{cases}, \tag{3.2.17}$$

where l is a typical length scale of ∂A. While most of the coefficients a_i in the above expansion are cut-off dependent, thus, these terms aren't significant. The relevant information is contained in the universal piece denoted by C_A, which is the cut-off independent. This term captures useful information about the conformal anomalies in the theory. For the case $d = 2$, the full expression for S_A reduces to (3.2.16) with $C_A = c/3$.

3.2.1.1 A brief discussion about replica trick

In order to compute entanglement entropy for QFTs, it is necessary to compute the $\log \rho_A$. The problem is that for systems of infinite dimension, this operations isn't well defined. To avoid such problem, we use the replica trick [8]. It is possible to write the von Neumann entropy (3.2.1) as

$$S_A = -\frac{\partial}{\partial n} tr_A \rho_A^n \Big|_{n=1} = -\frac{\partial}{\partial n} \log tr_A \rho_A^n \Big|_{n=1}. \tag{3.2.18}$$

The replica trick consists in evaluating $tr_A \rho_A^n$ for a given QFT. This way, consider the ground state $|\Omega\rangle$. The reduced density matrix ρ_A is given by

$$\rho_A = tr_B |\Omega\rangle \langle\Omega|. \tag{3.2.19}$$

The ground state wave function can be represented in a path integral form as

$$|\Omega\rangle = \frac{1}{\sqrt{Z}} \int_{\phi(-\infty)=\phi_0}^{\phi(0)=\phi_f} D\phi e^{-\mathcal{A}[\phi]}, \tag{3.2.20}$$

where Z is the partition function and $\mathcal{A}$ is the Euclidean action. Similarly,

$$\langle\Omega| = \frac{1}{\sqrt{Z}} \int_{\phi(0)=\phi_f}^{\phi(\infty)=\phi_0} D\phi e^{-\mathcal{A}[\phi]}, \tag{3.2.21}$$

where the field configuration ϕ_f needs to be specified at $t = 0$. In the above representations for the ground state, t is the Euclidean time direction where for each given time we have

a configuration for the field $\phi(\vec{x})$. Figure 9 shows a pictorial representations of this procedure.

Figure 9 – Path integral representations of wave functions.

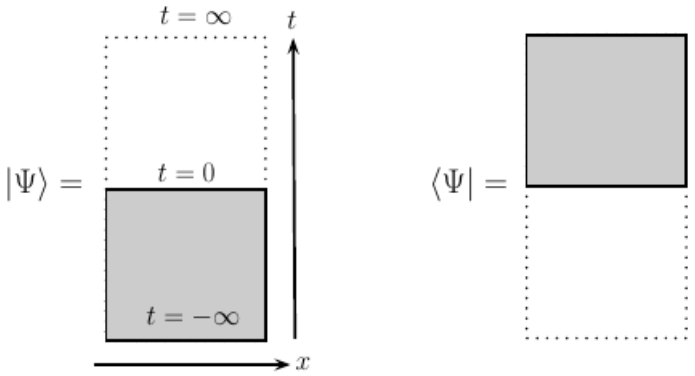

Source: [32]

The Euclidean path integral is useful to prepare states. In the above figure, it is possible to see that the integral is taken over the shaded regions, which are an infinite strip $I_t \times \mathbb{R}^{d-1}$, where I_t denotes the time interval. In this picture, taking the partial trace over the sub-system B is equivalent to gluing the edges of the two sheets $\langle\Omega|$ and $|\Omega\rangle$ along B. Then, the reduced density matrix has two indices $[\rho_A]_{ab} = \langle\phi_a^A| \rho_A |\phi_b^A\rangle$ where ϕ_a^A and ϕ_b^A specify the boundary conditions on the region A at $t = 0^+$ and $t = 0^-$, respectively. On the left side of Figure 10, such glue procedure is illustrated.

Figure 10 – Path integral picture for the reduced density matrix ρ_A.

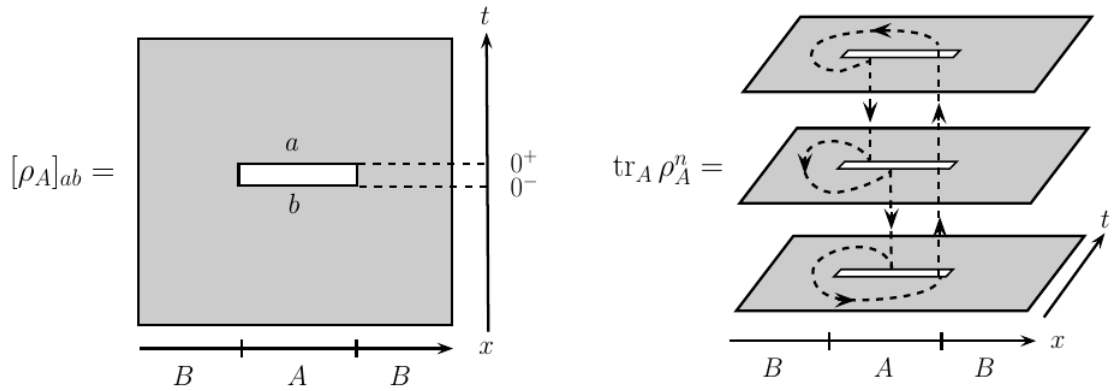

Source: [32]

In this path integral picture, the reduced density matrix ρ_A is represented by a path integral on an Euclidean space with a cut along the subsystem A, which means

that

$$[\rho_A]_{ab} = \frac{1}{Z}\int_{t=-\infty}^{t=\infty} D\phi e^{-\mathcal{A}[\phi]} \prod_{\vec{x}\in A} \delta\left(\phi\left(0^+,\vec{x}\right) - \phi_a^A\left(\vec{x}\right)\right)\delta\left(\phi\left(0^-,\vec{x}\right) - \phi_b^A\left(\vec{x}\right)\right). \tag{3.2.22}$$

In order to find $tr_A\rho_A^n$, we can prepare n copies of $[\rho_A]_{ab}$, namely

$$[\rho_A^n]_{a_1b_n} = [\rho_A]_{a_1a_2}[\rho_A]_{a_2a_3}[\rho_A]_{a_3a_4}\cdots[\rho_A]_{a_nb_n}. \tag{3.2.23}$$

In the path integral formalism, it is possible to take the trace by gluing $\phi_{a_i}^A$ with $\phi_{b_i}^A$, where we have the identification $\phi_{b_i}^A = \phi_{a_{i+1}}^A$, and then integrate over $\phi_{a_i}^A$. This gluing procedure between different copies of the QFT is shown on the right side of Figure 10. In this way, $tr_A\rho_A^n$ is given in terms of the path integral on an n-sheeted Riemann surface $\mathcal{R}_n$

$$tr_A\rho_A^n = \frac{1}{Z^n}\int_{(t,x)\in\mathcal{R}_n} D\phi e^{-\mathcal{A}[\phi]} = \frac{Z_n}{(Z)^n}, \tag{3.2.24}$$

where Z_n is a short notation for the above path integral. Finally, placing the expression for $tr_A\rho_A^n$ inside (3.2.18), we have that

$$S_A = -\lim_{n\to 1}\partial_n\left(\log Z_n - n\log Z\right). \tag{3.2.25}$$

For 2-dimensional CFTs, it is possible to analytically calculate (3.2.24) to find the (3.2.16) [8, 38]. However, in higher dimensions, analytical calculations of S_A become very complicated.

3.3 Holographic proposals

3.3.1 Elements of the AdS/CFT correspondence

The AdS/CFT correspondence proposed by Juan Maldacena in [5] is the key concept behind the holographic computations that we are going to perform below. Furthermore, it provides us with the dual description of the eternal black holes by the so called thermofield double state [28]. A full understanding of AdS/CFT requires some discussion about string theory and supersymmetry [29, 39], but here we limit ourselves to discussing the basic statement of correspondence [40].

Consider a d-dimensional conformal field theory (CFT) is a QFT with a particular space-time symmetry called conformal invariance [41]. In few words, conformal invariance is a symmetry under Poincaré transformation (rotations + translations), local scale transformations and special conformal transformations (SCT). This last one consists in transformations of the form

$$x'^{\mu} = \frac{x^{\mu} - b^{\mu}x^2}{1 - 2b\cdot x + b^2x^2}, \tag{3.3.1}$$

where b^μ is a parameters that describes the transformation. The consequence of conformal symmetry is that the correlation functions behave nicely under coordinate re-scalings $x \to \lambda x$. Correlation functions of primary operators, which are lowest weight states of a conformal representation, obey

$$\left\langle \mathcal{O}_1\left(x_1'\right)\mathcal{O}_2\left(x_2'\right)\cdots\mathcal{O}_n\left(x_n'\right)\right\rangle = \lambda^{\Delta_1+\Delta_2+\cdots+\Delta_n}\left\langle \mathcal{O}_1\left(x_1\right)\mathcal{O}_2\left(x_2\right)\cdots\mathcal{O}_n\left(x_n\right)\right\rangle, \quad (3.3.2)$$

where Δ_i is called scaling dimension of the operator $\mathcal{O}_i$. The above fact together with the other symmetries implies the following form for the 2-point function

$$\left\langle \mathcal{O}\left(x\right)\mathcal{O}\left(y\right)\right\rangle = \frac{1}{\left|x-y\right|^{2\Delta}}. \quad (3.3.3)$$

The simplest example of a CFT is a free massless scalar field,

$$\mathcal{A} = \frac{1}{2}\int d^d x \partial_\mu\phi\partial^\mu\phi, \quad (3.3.4)$$

where for example in $d = 4$, we have that

$$\left\langle \phi\left(x\right)\phi\left(y\right)\right\rangle = \frac{1}{\left|x-y\right|^{2}}. \quad (3.3.5)$$

A massive free field is not a conformal theory, since m appears in the correlation functions and spoils the power behavior (3.3.4). In general, it is true that CFTs don't have any dimensionful parameters, so there can be no mass terms in the Lagrangian.

On the other hand, the AdS_{d+1} space-time in Poincaré coordinates is given by the metric

$$ds^2 = \frac{L^2}{z^2}\left(dz^2 + dt^2 + d\vec{x}^2\right) = \frac{L^2}{z^2}\left(dz^2 + dx^2\right), \quad (3.3.6)$$

where x denotes the coordinates on $\mathbb{R}^d$ and the boundary of the space-time is at $z = 0$. The AdS/CFT correspondence is the exact relationship between a given theory of quantum gravity in asymptotically AdS_{d+1} space-time and a CFT_d without gravity. This relationship is called a duality. It is holographic since the gravitational theory lives in one extra dimension. The theories are believed to be entirely equivalent: any physical quantity that can be computed in one theory can also be computed in the dual. However, the mapping between the two theories can be highly nontrivial. For example, easy calculations on one side often map to strongly coupled quantities on the other side.

The statement of the AdS/CFT correspondence is given by the so called GKPW dictionary [42, 43], namely

$$Z_{grav}\left[\phi_i^0\left(x\right) = \phi_i\left(z,x\right)\big|_{z=0}; \partial\mathcal{M}\right] = \left\langle \exp\left(-\sum_i \int d^d x \phi_i^0\left(x\right)\mathcal{O}_i\left(x\right)\right)\right\rangle_{CFT \text{ on } \partial\mathcal{M}}. \quad (3.3.7)$$

The index i runs over the fields in the bulk effective field theory, which corresponds to sources of local operators in the boundary CFT. The gravitational partition function Z_{grav} is in an asymptotically AdS space-time. Once AdS has a boundary, we must provide boundary conditions to define this path integral. The boundary conditions on bulk scalars are

$$\phi_i(z,x) = z^{d-\Delta}\phi_i^0(x) + \text{subleading terms}, \tag{3.3.8}$$

where the mass of the bulk scalar is related to the scaling dimension of the CFT operator by

$$m^2 = \Delta(d-\Delta). \tag{3.3.9}$$

Similar statements apply to all bulk fields, including the metric. The boundary conditions on the metric involve a choice of topology as well as the actual metric, which is why it was indicated explicitly that Z_{grav} depends on the boundary manifold ∂M. On the other hand side, we have the generating functional of correlators Z_{CFT} of the CFT. In this equation, the $\phi_i^0(x)$ are sources, while $\mathcal{O}_i(x)$ are CFT operators. Denoting the generating functional of the CFT by $Z_{CFT}[\phi_i^0]$, the correlation functions are computed by

$$\langle \mathcal{O}_1(x_1)\mathcal{O}_2(x_2)\cdots\mathcal{O}_n(x_n)\rangle = \frac{\delta^n}{\delta\phi_1^0(x_1)\,\delta\phi_2^0(x_2)\cdots\delta\phi_n^0(x_n)} Z_{CFT}\left[\phi_i^0\right]\Big|_{\phi_i^0=0}. \tag{3.3.10}$$

Each field in gravity corresponds to a local operator in CFT. The spin of the bulk field is equal to the spin of the CFT operator, while the mass of the bulk field fixes the scaling dimension of the CFT operator. Here are some examples:

- Scalar: A bulk scalar field $\phi(z,x)$ is dual to a scalar operator in CFT. The boundary value of ϕ acts as a source in CFT.
- Graviton: Every theory of gravity has a massless spin-2 particle, the graviton $g_{\mu\nu}$. This is dual to the stress tensor $T_{\mu\nu}$ in the CFT. This makes sense once every CFT has a stress tensor. The fact that the graviton is massless corresponds to the fact that the CFT stress tensor is conserved. It also fixes the scaling dimension to ΔT = d.
- Vector: If our theory of gravity has a spin-1 vector field A_μ, then the dual CFT has a spin-1 current J_μ. If A_μ is massless, then $\Delta_J = d-1$ and J_μ is a conserved current. Otherwise, $\Delta_J > d-1$ and the current is not conserved. A general and important feature of AdS/CFT is that gauge symmetries in the bulk correspond to global symmetries in the CFT.

Another important result from AdS/CFT is that thermal states in CFT are dual to black holes in quantum gravity. In fact, this is a special case of the dictionary (3.3.7), where we

impose boundary conditions appropriate to thermal field theory. That is,

$$Z_{grav}\left[\partial\mathcal{M} = M\right] = Z_{CFT}\left[M\right], \tag{3.3.11}$$

where the CFT lives on the manifold

$$M = \mathbb{R}^{d-1} \times S^1_\beta. \tag{3.3.12}$$

Here S^1_β is a circle of size β. As can be seen in Appendix A, the Euclidean path integral on $\mathbb{R}^{d-1} \times S^1_\beta$ defines the finite-temperature state on $\mathbb{R}^{d-1}$. We need to calculate the gravity partition function with boundary condition M on the bulk manifold $\mathcal{M}$. Explicitly, the metric itself obeys the boundary condition that is to become the AdS space-time asymptotically. Since we know the boundary manifold M, the gravity dual is given by the manifold $\mathcal{M}$ such that $\partial\mathcal{M} = M$. This is the main argument to perform a match between gravity and boundary theories.

3.3.2 Holographic entanglement entropy

In this section we are going to present briefly the celebrated proposal by [9, 10] to calculate the entanglement entropy of a d-dimensional CFT using the gravity dual in AdS$_{d+1}$. In order to define the entanglement entropy in the CFT$_d$, it is necessary to divide the time slice manifold $\mathcal{M}_{d-1}$ into two subregions A and B. Using Poincaré coordinate (see (3.1.18)), we set $\mathcal{M}_{d-1} = \mathbb{R}^{d-1}$ and consider that the CFT$_d$ lives on the boundary of AdS$_{d+1}$ at $z = \delta$. To have its dual gravity picture, we need to extend this division $\mathcal{M} = A \cup B$ to the time slice $\mathcal{B}_d$ of the bulk space-time. In the setup (Poincaré coordinates), $\mathcal{B}_d$ is the d-dimensional hyperbolic space-time. We need to extend ∂A to a surface γ_A in the entire $\mathcal{B}$ such that $\partial\gamma_A = \partial A$. The first problem that could arise is that there are infinitely many different choices of γ_A . This problem is avoided by the claim that it is necessary to choose the minimal area surface. This means that we require that the variation of the area functional vanishes. In the case of multiple solutions, we choose the one whose area takes the minimum value. In this setup, the holographic proposal for the entanglement entropy S_A in the CFT$_d$ is given by the formula

$$S_A = \frac{Area\left(\gamma_A\right)}{4G}, \tag{3.3.13}$$

where G is the $(d+1)$-dimensional Newton's constant. The appearance of the formula (3.3.13) looks very similar to the area law of the Bekenstein-Hawking formula of black hole entropy. Indeed, the formula (3.3.13) can be seen as a generalization of the BH formula because in the presence of an event horizon, such as the AdS-Schwarzschild black hole, the minimal surface tends to wrap the horizon. Figure 11 shows the minimal surfaces in the presence of the BTZ black hole.

Figure 11 – Minimal surfaces in the of the BTZ black hole.

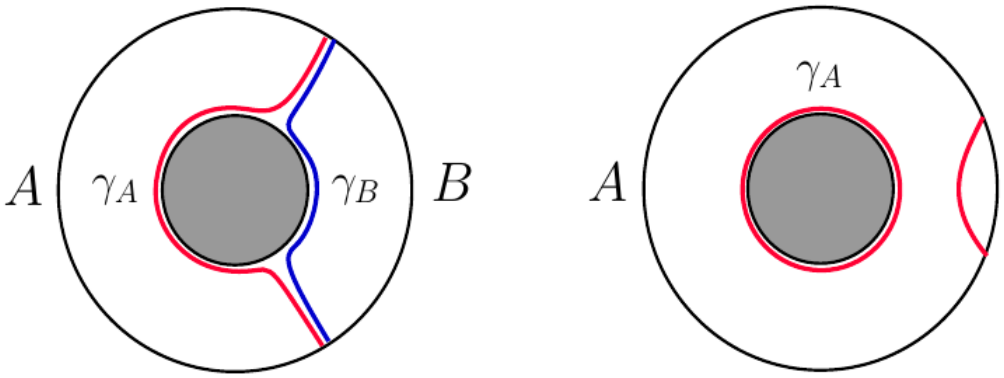

Source: [32]

The minimal surfaces for the region γ_A and the region γ_B wrap different parts of the horizon of the black hole. In the limit that A becomes very large, γ_A becomes separated into the horizon circle and a small half circle localized on the boundary, which corresponds to the reminiscent minimal surface γ_B.

In order to demonstrate the benefits of (3.3.13), let's consider two specific situations. Firstly, it is useful to try to reproduce the result (3.2.16) using the AdS_3/CFT_2 correspondence. The metric of the Euclidean AdS_3 in Poncaré coordinates is given by

$$ds^2 = \frac{L^2}{z^2}\left(dz^2 + dt^2 + dx^2\right). \tag{3.3.14}$$

In order to use (3.3.13), we need to build the area functional between the two points $(x,z) = (-\ell/2, 0)$ and $(x,z) = (\ell/2, 0)$,

$$Area = \int_{-\ell/2+\delta}^{\ell/2-\delta} \frac{L}{z}\sqrt{1+\left(\frac{dz}{dx}\right)^2}\,dx, \tag{3.3.15}$$

where we introduced the UV cut-off δ in order to avoid divergences at $z = 0$. The minimal surface γ_A is the solution of the following equation

$$z\frac{d^2z}{dx^2} + \left(\frac{dz}{dx}\right)^2 + 1 = 0. \tag{3.3.16}$$

The solution of this equation is given by

$$z\left(x\right) = \sqrt{a^2 - x^2}, \tag{3.3.17}$$

where a is a constant that assumes the value $a = \ell/2$ once $z = 0$ at the boundary ∂A. As consequence, the area of the minimal surface γ_A can be computed placing $z\left(x\right)$ inside

(3.3.15). As a result we have that

$$\begin{aligned} Area\left(\gamma_A\right) &= 2L\int_0^{a-\delta}\frac{a}{a^2-x^2}dx \\ &= -2L\log\left(\frac{\cos\theta+1}{\sin\theta}\right)\Big|_{\delta/a}^{\pi/2} \\ &= 2L\log\left(\frac{\ell}{\delta}\right). \end{aligned} \tag{3.3.18}$$

Finally from (3.3.13), the entanglement entropy for the CFT_2 at zero temperature is

$$S_A = \frac{c}{3}\log\left(\frac{\ell}{\delta}\right), \delta \ll \ell \tag{3.3.19}$$

where the holographic value for the central charge is

$$c = \frac{3L}{2G}, \tag{3.3.20}$$

which is obtained by the match between the trace anomalies [44]. This holographic computation of S_A agrees to the result (3.2.16) that is obtained from the CFT side.

The second example that we are going to consider is the entanglement entropy of a sphere S^{d-2} of radius R in a d-dimensional CFT. The Euclidean Poincaré AdS_{d+1} space is given by the metric

$$ds^2 = \frac{L^2}{z^2}\left(dt^2+dz^2+d\rho^2+\rho^2 d\Omega_{d-2}^2\right), \tag{3.3.21}$$

where $z = z\left(\rho\right)$ to respect the spherical symmetry of γ_A. The minimal surface γ_A is obtained by extremizing the area functional

$$Area = L^{d-1}\Omega_{d-2}\int_0^{R-\delta}\frac{\rho^{d-2}}{z^{d-1}}\sqrt{1+\left(\frac{dz}{d\rho}\right)^2}d\rho. \tag{3.3.22}$$

The equation of motion for $z\left(\rho\right)$ is given by

$$\left(d-1\right)\rho\left(1+\left(\frac{dz}{d\rho}\right)^2\right)+z\left(\left(d-2\right)\left(\frac{dz}{d\rho}\right)^3+\left(d-2\right)\frac{dz}{d\rho}+\rho\frac{d^2z}{d\rho^2}\right)=0. \tag{3.3.23}$$

Notice that the above equation of motion reduces to (3.3.16) for $d=2$. This fact provides the insight to consider a solution to the above equation of motion similar to (3.3.17),

$$z\left(\rho\right) = \sqrt{R^2-\rho^2}, \tag{3.3.24}$$

where we impose the boundary condition $\rho = R$ at the boundary $z = 0$. Substituting $z\left(\rho\right)$ inside the area functional (3.3.22) and using the holographic formula (3.3.13), we obtain

the entanglement entropy of a sphere of radius R . For odd d we have that

$$S_A = \frac{L^{d-1}\Omega_{d-2}}{4G}\left[\frac{1}{d-2}\left(\frac{R}{\delta}\right)^{d-2} - \frac{d-3}{2\,(d-4)}\left(\frac{R}{\delta}\right)^{d-4} + \cdots \right.$$
$$\left. + (-1)^{(d-3)/2}\frac{R}{\delta} + (-1)^{(d-2)/2}\sqrt{\pi}\Gamma\left(\frac{d-1}{2}\right)/2\Gamma\left(\frac{d}{2}\right) + O\left(\delta\right)\right] \tag{3.3.25}$$

while for even d,

$$S_A = \frac{L^{d-1}\Omega_{d-2}}{4G}\left[\frac{1}{d-2}\left(\frac{R}{\delta}\right)^{d-2} - \frac{d-3}{2\,(d-4)}\left(\frac{R}{\delta}\right)^{d-4} + \cdots \right.$$
$$\left. + \frac{1}{d-2}\left(\frac{R}{\delta}\right)^{2} + (-1)^{(d-2)/2}\frac{(d-3)!!}{(d-2)!!}\log\left(\frac{R}{\delta}\right)\right]. \tag{3.3.26}$$

The holographic entanglement entropy is consistent with the expected UV behavior (3.2.17). The leading divergent part is proportional to the area of the entangling surface $Area(\partial A) = R^{d-2}\Omega_{d-2}$, which is known to be the area law. Also, there are the logarithmic divergence when d is even and the universal constant term for odd d.

3.3.3 Thermofield double formalism

Once the basics statements of the AdS/CFT correspondence are established, we are in the position to demonstrate the important duality between eternal black holes in AdS_{d+1} and the thermofield double state describing some CFT_d. In order to demonstrate this, we will follow the same approach as [40]. Additional information can be found in [31].

For any QFT that has an Hamiltonian description, consider the complete set $\{|n\rangle\}$ of eigenstates of H, such that

$$H\,|n\rangle = E_n\,|n\rangle\,. \tag{3.3.27}$$

The thermofield double formalism is a trick to handle a thermal mixed state $\rho_{thermal} = e^{-\beta H}/Z\left(\beta\right)$ as a pure state in a bigger system. The idea is to double the degrees of freedom, considering a new QFT which is two copies of the original QFT, which we are going to denote by left and right QFT. If the theory is defined by a Lagrangian, for every field $\phi\left(x\right)$ in the original QFT, there are two fields $\phi_L\left(x_L\right)$ and $\phi_R\left(x_R\right)$ in the doubled QFT. These two theories live in different space-times with coordinates x_L and x_R. We also consider that there is no coupling between the QFTs. The states of the doubled QFT are $|n\rangle_L\,|n\rangle_R$, where $|n\rangle_R$ is the CPT conjugate of the state $|n\rangle_L$. If the doubled system is described by the thermofield double state

$$|TFD\rangle = \frac{1}{\sqrt{Z\left(\beta\right)}}\sum_n e^{-\beta E_n/2}\,|n\rangle_L\,|n\rangle_R\,, \tag{3.3.28}$$

the density matrix

$$\rho_{tot} = |TFD\rangle \langle TFD| \tag{3.3.29}$$

is similar to (3.2.2), which describes a pure state. We can compute the reduced density matrix of the left system, which is

$$\rho_L = \frac{e^{-\beta H}}{tr_L e^{-\beta H}}. \tag{3.3.30}$$

The reduced density matrix ρ_L is equal to the thermal density matrix ρ_{themal}. As consequence, if we restrict our attention to the left system, this pure state in the doubled system is indistinguishable from a thermal state. Another example is the 2-point function of local operators at equal time defined on the left system. Such correlation function has the form

$$\langle TFD| \phi(\vec{x}_L) \chi(\vec{y}_L) |TFD\rangle = \frac{1}{Z(\beta)} tr_L e^{-\beta H} \phi(\overrightarrow{x}_L) \chi(\overrightarrow{y}_L), \tag{3.3.31}$$

which is the 2-point at finite temperature

$$\langle \phi(x) \phi(y) \rangle_\beta = \frac{1}{Z(\beta)} Tr e^{-\beta H} \phi(x) \phi(y). \tag{3.3.32}$$

This entire procedure is called purifying the thermal state. In fact, any mixed state can be purified by adding enough auxiliary states and tracing them out.

There are two convenient choices of a total Hamiltonian H_{tot} acting on the doubled system, which are

$$H_{tot} = H_R - H_L \qquad \text{and} \qquad H'_{tot} = H_R + H_L. \tag{3.3.33}$$

The choice of H_{tot} is interesting because the TFD state is time-independent, since the phases cancel

$$|TFD(t)\rangle = e^{-iH_{tot}t} |TFD\rangle = e^{-i(H_R - H_L)t} |TFD\rangle = |TFD\rangle. \tag{3.3.34}$$

The Hamiltonian H_{tot} has a natural bulk interpretation. It is dual to the bulk Hamiltonian that generates time evolution for the usual Schwarzschild coordinate t.

3.3.4 The duality for eternal black holes

To justify the claim that the eternal black hole is dual to the TFD state, we will apply the AdS/CFT dictionary (3.3.7), in the form

$$Z_{grav}[\partial \mathcal{M} = M] = Z_{CFT}[M], \tag{3.3.35}$$

where $\mathcal{M}$ is the bulk manifold. The gravity path integral is performed with the boundary condition $\partial\mathcal{M} = M$. From the side of the CFT, the Euclidean path integral that prepares the TFD state is a path integral on an interval of length $\beta/2$ times a circle, in other words

$$M = I_{\beta/2} \times S^{d-1}. \tag{3.3.36}$$

The path integral for the TFD has two open cuts at the ends of the interval. It is possible to see the left cut as defining a state in the left system and the right cut as defining a state in the right system. This picture should be interpreted as a rule for computing the transition amplitude with field data ϕ_L and ϕ_R specified at the ends of the interval. To confirm that this path integral really prepares the TFD state, all we need to do is to check that it computes the correct transition amplitudes. The path integral with these boundary conditions is

$$\begin{aligned} {}_L\langle\phi_L|_R\langle\phi'|TFD\rangle &= \sum_n e^{-\beta E_n/2}\, {}_R\langle\phi'|n\rangle_R\, {}_L\langle\phi|n\rangle_L \\ &= \sum_n e^{-\beta E_n/2}\, {}_R\langle\phi'|n\rangle_R\, {}_R\langle n|\phi\rangle_R \\ &= \langle\phi'|\, e^{-\beta H/2}\,|\phi\rangle\,. \end{aligned} \tag{3.3.37}$$

Once we've produced the TFD state from an Euclidean path integral on the manifold M, we can apply (3.3.36) in order to find a Euclidean gravity solution with conformal boundary condition $\partial\mathcal{M} = I_{\beta/2} \times S^{d-1}$. In fact, half of the Euclidean black hole has precisely this boundary condition. That is, we consider the Euclidean Scharzschild-AdS solution and restrict the Euclidean time τ to $\tau \in [0, \beta/2]$ instead of the usual full range $\tau \in [0, \beta]$. The (τ, r) portion of this Euclidean space-time makes a half-disk. The boundary of the half-disk is $I_{\beta/2} \times S^{d-1}$. The half-disk has a cut in the middle. This cut is interpreted as the time $t = 0$ surface of the Lorentzian space-time. Figure 12 shows such arrangement. Pictorially, the bulk space-time has an Euclidean piece that prepares the state, then a Lorentzian piece describing the time evolution in Minkowski signature.

Figure 12 – Euclidean black hole half-disk.

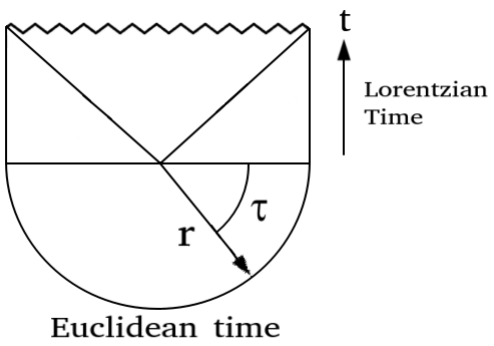

From $t = 0$, the time evolution of the black hole is dual to the time evolution of the TFD state.

4 Complexity in holography

We spent some time talking about complexity, black holes, entanglement, AdS/CFT, etc. It's time to put these concepts developed so far together . The objective of this chapter is to present how complexity started to play a relevant role in holography, as well as its relation with geometric objects that are defined in the bulk AdS geometry. In the context of the AdS/CFT correspondence, complexity is a quantity belonging to the CFT. It is associated with states in the Hibert space of such theory.

We are going to consider two alternatives to computing complexity holographically, instead of calculating it using some quantum circuit arguments. They are conjectures, which means that there is no proof yet that such alternatives always holds, however, since the formulation of the first one in [45], called complexity=volume conjecture, a large number of people started to pay attention to this subject and also interesting results have been appearing, in special for the two-sided AdS black hole, which is the standard object of study for holographic proposals of the complexity. Posteriorly, it was also proposed the second conjecture [22], called complexity=action conjecture.

Summarizing, both conjectures will be studied in more detail, where some holographic calculations for the two-sided AdS black hole case will be done. In order to convince the reader about the duality, we also will compare the holographic results with what we would expect from the quantum circuit approach for complexity.

4.1 Black holes, states and qubits

In order to formulate a holographic dual for complexity, it is necessary first to know how to compute the complexity of the states on the boundary CFT using quantum mechanical methods. Actually, what we are going to do is to describe the CFT using qubits. As a consequence, it will be possible to use the entire formalism of 2-level systems that is crucial for the study of quantum information. The details of such construction will be formulated in the next section. For now, the relevant discussion is about the necessary conditions that will allow us to describe the CFT of interest using a string of qubits. First, the string of qubits must have the sufficient number of degrees of freedom necessary to describe the boundary CFT. Consequently, our string will be also able to describe the dual theory of this CFT. As already stated, complexity plays an important role as a quantity associated to the long-time behavior of black holes. Then, the bulk geometry of interest is the AdS black hole, in special, the two-sided black hole that is

dual to the thermofield double state.

Following [46], we can assume that a black hole has

$$\frac{A_h}{4G} \tag{4.1.1}$$

degrees of freedom [47]. Entropy is a good quantity to count degrees of freedom. For example, consider a string of K qubits. There are 2^K possible distinct states. Following the Boltzmann's entropy formula

$$S = k_B \log W, \tag{4.1.2}$$

where k_B is the Boltzmann's constant and W is the number of microstates of a given macrostate. For the present case, $W = 2^K$. It is easy to see that

$$S \sim K. \tag{4.1.3}$$

The entropy is proportional to the number of qubits. Such fact is a good indication that it is possible to describe the black hole's degree of freedom by using a string of qubits. Additionally, we will assume that these degrees of freedom are a system of qubits that interact in a way that makes the black hole a *fast scrambler*. For a system with N degrees of freedom, the scrambling time t_* is a measure of how much time is necessary for the information, which is initially concentrated in a single degree of freedom, spreads over the all the system's degrees of freedom. It was conjectured in [48] that fast scramblers take a time t_* logarithmic in the number of degrees of freedom, namely

$$t_* \sim \log N, \tag{4.1.4}$$

and that black holes are the fastest scramblers in Nature because they have the smallest possible coefficient in front of the logarithm. More precisely, black holes scramble in a time

$$t_* = \frac{1}{\lambda_L} \log N. \tag{4.1.5}$$

The quantity λ_L is the so-called Lyapunov exponent. This quantity characterizes the rate of separation of infinitesimally close trajectories in the phase space. Positive values ofλ_L are considered as an indication that the system is chaotic. From the point of view of the dual CFT, a useful indication of chaos is provided by the out of time order four-point function $\langle W(t) VW(t) V\rangle_\beta$, where W and V are local operators with $W(t) = e^{iHt} W e^{-iHt}$, the same for $V(t)$ [49]. For chaotic systems, this correlation function has the form

$$\langle W(t) VW(t) V\rangle_\beta = A + Be^{\lambda_L (t - t_*)} + \mathcal{O}\left(N^{-2}\right), \tag{4.1.6}$$

which grows exponentially with time, which justify the chaotic behavior of the system. For black holes [48, 49]

$$\lambda_L = \frac{2\pi k_B T}{\hbar}. \tag{4.1.7}$$

The lesson here is that if we want to describe the boundary CFT using qubits and also to compute the complexity of the states using the formalism of quantum information, two conditions are necessary: the number of qubits in the string needs to be equal the entropy of the black hole and they also need to interact in such way that makes the string scrambles as a black hole.

4.1.1 Quantum circuit model for complexity

We already discussed a little bit about complexity and its relation with quantum circuits. The idea of this section is to review some concepts and also formalize them. Complexity is not something absolute. Analogously to other quantities in physics, like energy or entropy, what makes sense is the variation of complexity. We can define a reference state $|\psi_0\rangle$ and impose that such state has zero complexity. We also need to assume that any state of the theory can be obtained from $|\psi_0\rangle$ by the application of an operator U of interest. If such operator is not something trivial, like the identity for example, the final state

$$|\psi\rangle = U\,|\psi_0\rangle \tag{4.1.8}$$

is more complex that $|\psi_0\rangle$. The symbol U is a compact notation for a sequence of n operations

$$U = g_n g_{n-1} ... g_1 \tag{4.1.9}$$

that are necessary to produce the state $|\psi\rangle$. In this sense, we can also think about U as a time evolution operator. This claim makes sense specially in the situation where the operations g_i are quantum gates. In fact, what we are going to do is to consider that it is possible to build $|\psi\rangle$ using a quantum circuit equivalent to U. In order to avoid ambiguities, let's consider the smallest quantum circuits that implement U. Such assumption is reasonable if we don't want to throw out the initial definition of complexity that is the minimum number of simple operations needed to implement some task.

The quantum circuit model that we are going to consider in order to compute complexity is the so called Hayden-Preskill circuit model [23, 17]. Let us consider a system with K qubits. Two reasonable and equivalent choices of simplest state $|\psi_0\rangle$ are the states $|000...0\rangle$ or $|111...1\rangle$. Only to be in parallel with the convention of the literature, let us choose $|000...0\rangle$ as the zero complexity state. The evolution of the system will be implemented by a quantum circuit of width K that allows only two-qubit gates to act on

the qubits. Defining a dimensionless time

$$\omega = \frac{t}{\ell}, \tag{4.1.10}$$

where ℓ is some length scale and t is the time, it is possible to configure a circuit that applies a determined number of gates on the qubits at each time interval $\Delta\omega = \ell$. The time ω now assumes positive integers values after the circuit starts to run. The variable ω is the depth of the circuit. It measures how large is the circuit. The system at $\omega = 0$ is represented by the state $|\psi_0\rangle$. Successive application of gates will implement the operator U and in the end the result will be the state $|\psi\rangle$. As a consequence, the complexity $\mathcal{C}$ of the state $|\psi\rangle$ is the number of gates needed to implement U.

There are two ways to run a quantum circuit: series or parallel. In a series circuit, at each step ω a unique gate is allowed to act on some pair of qubits. The pair of qubits may be chosen according to some rule or can be chosen randomly. However, this is not a really good way to model the evolution of systems of many qubits because they can interact at the same time in small groups. A better model is the parallel circuit, where $K/2$ gates are allowed to simultaneously act at each discrete time ω. An interesting example is how to implement the process of scrambling on a string of qubits, see Figure 13, using a quantum circuit.

Figure 13 – Spreading of some perturbation on a string of qubits.

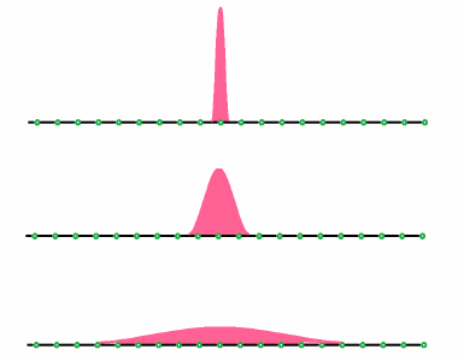

Source: [46]

Initially, the disturbance is highly concentrated on a specific qubit. After some time, it spreads over some other qubits and finally, after some time, all the qubits were disturbed. Such process can be implement by a quantum circuit assuming that at $\omega = 0$ there is a random disturbed qubit. After one step, this disturbed qubit interacts with some other by the action of a two-qubit gate on them, resulting in two disturbed qubits at $\omega = 1$. Then, these two qubits at $\omega = 2$ will interact with other two, resulting in four disturbed qubits. At $\omega = 3$ there will be eight disturbed qubits, as well as sixteen at $\omega = 4$.

So, the rule is that the number of disturbed qubits is 2^{ω}. The scrambling time ω_* will be reached when the number of perturbed qubits becomes equal K, in other words

$$\omega_* = \log K. \tag{4.1.11}$$

The conclusion is that a parallel circuit with depth $\log K$ can implement the process of scrambling satisfactorily.

From now on, we are going to consider parallel circuits in order to compute the complexity of the states. Despite the fact that complexity was defined as the number of quantum gates in the circuit, it isn't necessary mandatory. The strategy is to define a rule to compute complexity and follow it until the end. Complexity as the number of gates is a good rule, however, another good quantity to quantify the hardness of some quantum circuit is it depth ω. Given that, we are going to define our rule. The complexity of a state $|\psi\rangle$ that was built from the simplest state $|\psi_0\rangle$ by the application of the operator U is the product of the width and the depth of the quantum circuit that implement U, namely

$$\mathcal{C} = K\omega. \tag{4.1.12}$$

This definition is good because it depends only of geometric quantities of the quantum circuit. If we know the number of qubits of the system and the time necessary to implement U, we know the complexity of the process. In this scenario, the complexity of scrambling is

$$\mathcal{C}_* = K \log K. \tag{4.1.13}$$

The result shown in (4.1.11) and the convention for complexity (4.1.12) adopted so far match very well with was discussed previously about the conditions that are necessary to describe a black hole using a string of qubits. First, the number of qubits must be equal the entropy of the black hole. Second, the string needs to be a fast scrambler. With these two condition in mind and choosing $\ell = \beta = T^{-1}$ in (4.1.12), it is possible to rewrite (4.1.11), (4.1.12) and (4.1.13) as

$$t_* \sim \frac{1}{T} \log S, \tag{4.1.14}$$

$$\mathcal{C} \sim TSt, \tag{4.1.15}$$

$$\mathcal{C}_* \sim S \log S, \tag{4.1.16}$$

respectively. The string of qubits has the same scrambling time than a black hole. The above results also provide an interesting formula for the time derivative of the complexity, which is

$$\frac{d\mathcal{C}}{dt} \sim TS. \tag{4.1.17}$$

We abandoned the symbol of equal in the above expressions as a precaution. The temperature appeared in this expression because a specific choice $\ell = \beta$. The problem is that there is no special reason for this choice, it could be $\ell = L$. However, it is possible to relate the AdS radius, as well as any parameter of the system that has length dimension, with the temperature of the black hole.

The expression (4.1.16) doesn't mean that the maximum complexity was reached. If the circuit continues to run, the complexity will continue to increase until it reaches a maximum. The existence of a maximum follows from the fact that any unitary transformation can be implemented by a circuit with no more than an exponential number of gates in K [50]. Thus, complexity grows until it reaches a maximum that is

$$\mathcal{C}_{max} \sim e^K. \tag{4.1.18}$$

The expected behavior of complexity along the time is shown in the Figure 14.

Figure 14 – The increase of complexity along time.

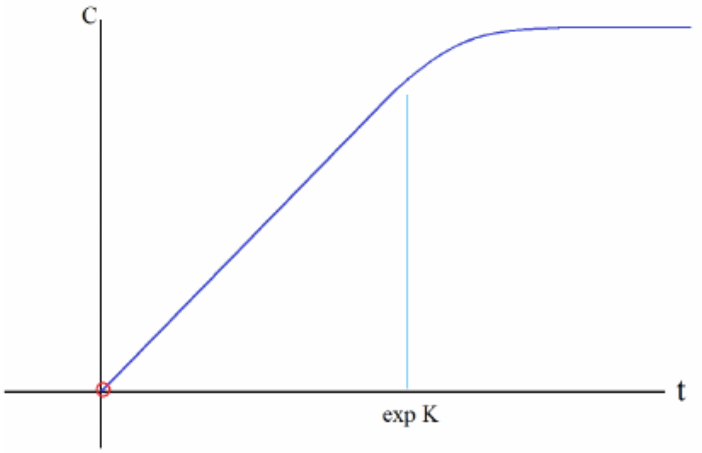

Source: [18]

On the same graph, the history leading up to thermal equilibrium would occupy a tiny region shown schematically in the red circle. After the saturation time, complexity is expected to fluctuate and eventually decrease at times of order the quantum recurrence time. Because of this, we will consider our computations for times less than $\mathcal{O}\left(e^K\right)$.

4.1.2 A model for the TFD state

We are specially interested in the qubit description of the TFD state. Since the Hilbert space of this system is $\mathcal{H}_L \times \mathcal{H}_R$, it is reasonable to assume that each

Hilbert space can be described by a string of K qubits, which implies that the total system is modeled by $2K$ qubits. Each space has dimension 2^K. Again, we assume that $K = S$. Considering as example the left space, any unitary operator U_L has a computational complexity $\mathcal{C}$ as was defined in (4.1.12). For the case where $U_L(t)$ and $U_R(t)$ are the time evolution operators for the two sides, the complexity of the states on both sides will increase linearly with t, with the proportionality factor being the entropy S times the temperature T. In our model for complexity, it is necessary to set a reference state that has zero complexity. The application of operators on this state will produce more complex states. It is already known that at $t = 0$ the two-sided AdS black hole is dually described by the TFD state. Then, we can choose this state to have zero complexity. Applying the time evolution operator in both sides will result in a more complex state

$$|\Psi(t_L, t_R)\rangle = U(t_L)\, U(t_R)\, |TFD\rangle\,, \tag{4.1.19}$$

which has complexity

$$\mathcal{C}(t_L, t_R) = TS(t_L + t_R)\,. \tag{4.1.20}$$

There is a important comment to be done about the qubit model for the TFD state. First, a state is said to be maximally entangled if the reduced density operator of the system is a multiple of the identity operator. For example, consider two qubits in an entangled state of the form

$$|\psi\rangle = \frac{1}{\sqrt{2}} \left(|0\rangle_L |0\rangle_R + |1\rangle_L |1\rangle_R\right). \tag{4.1.21}$$

Then, if we compute the reduced density matrix trancing out the left degrees of freedom, the result is

$$\rho_R = \frac{1}{2} \left(|0\rangle \langle 0| + |1\rangle \langle 1|\right), \tag{4.1.22}$$

which is essentially the identity matrix in the $\{|0\rangle, |1\rangle\}$ basis. On the other hand, the reduced density matrix for the TFD state is the thermal density matrix

$$\rho_{thermal} = \frac{1}{Z(\beta)} e^{-\beta H} = \frac{1}{Z(\beta)} \sum_n e^{-\beta E_n} |n\rangle \langle n|\,. \tag{4.1.23}$$

The above expression isn't a multiple of the identity, however, it is diagonal with coefficients $\exp(-\beta E_n)$. In this sense, it is possible to say that the TFD state is almost maximally entangled. Such parallel is important because the TFD state can be identified as a product of Bell pairs in which each pair is shared between the left and right systems. This arrangement is shown in Figure 15. Thus, the TFD state can be thought of as

$$|TFD\rangle \sim \frac{1}{\sqrt{2^K}} \bigotimes_{i=1}^{K} \left(|0\rangle_L |0\rangle_R + |1\rangle_L |1\rangle_R\right)_i. \tag{4.1.24}$$

There is an interesting fact with this construction. In order to create the entanglement between the pairs, it is necessary to act with one gate on each pair of qubits. Thus, it is required K gates[1] are required to create K Bell's pairs, implying then that the complexity of the TFD is K, which is the complexity necessary to construct the state. It isn't a problem for our above definition of zero complex state, because we are interested in the complexity of the time evolution of the TFD state.

Figure 15 – Product of Bell's pairs.

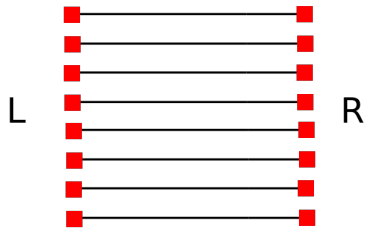

Source: [45]

With this comment, we finish the discussion about complexity of the states from the point of view of quantum circuits and qubit models. The next step is to present the results that can be obtained holographically by the CV duality and the CA-duality.

4.2 Complexity=Volume

The first conjecture about holographic complexity that we are going to discuss was proposed in [17, 45]. The complexity=volume conjecture, or CV duality, relates the complexity of the boundary states with the volume of geometrical objects connected to these states. Let's consider two-sided AdS_{d+1} black hole. The dual theory for such black hole is described by the time evolution of thermofield double state

$$|TFD\rangle = \frac{1}{\sqrt{Z(\beta)}} \sum_{n=0}^{\infty} e^{-\beta E_n/2} |n\rangle_L \otimes |n\rangle_R , \tag{4.2.1}$$

where $Z(\beta)$ is the partition function of the boundary theory. The black hole is holographically described by two identical uncoupled $CFTs$, the left and right sectors, defined on disconnected boundary spheres. Following the ER=EPR proposal, since the $|TFD\rangle$ describes two entangled CFTs, there is an ERB connecting the entangled CFTs.

[1] In the discussion about quantum gates, we saw that it is possible to entangle two qubits applying the Hadamard plus the CNOT gate. It could mean that are necessary two gates to entangle two qubits, implying then that the complexity of the TFD state is $2K$. It is true, however, for this discussion, what is important is that the complexity is proportional to K.

Figure 16 – ERB connecting two entangled $CFTs$.

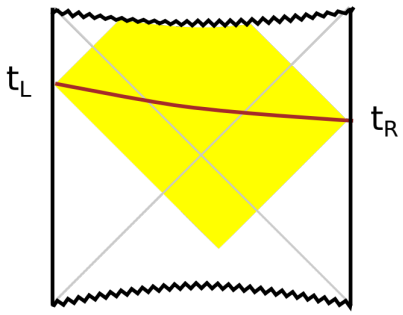

Source: [45]

The ERB is a geometric object that lives in the bulk theory, anchored at boundary times t_L and t_R, how is shown in the Figure 16. The ERBs should be Cauchy surfaces. Technically all complete time-like and light-like curves must intersect each slice exactly once. The yellow region is called Wheeler De-Witt patch, which is the domain of dependence of a Cauchy slice anchored at the boundary states. Such region contains all the spacelike surfaces which are anchored on the boundaries at times t_L and t_R. We are going to denote the volume of the ERB as $V\left(t_L, t_R\right)$. There is a $d-2$ sphere on each point of the brown curve in Figure 16. This means that the volume of the ERB is a functional of the coordinates of space-time. The time was included because the ERB is a dynamical object, its volume grows in time. The relation between complexity and volume is given by

$$\mathcal{C}_V\left(t_L, t_R\right) = \frac{V\left(t_L, t_R\right)}{G\ell}, \tag{4.2.2}$$

where G is Newton's constant and ℓ is some length scale associated with the geometry of the space-time, that will be for us the AdS radius. The volume $V\left(t_L, t_R\right)$ refers to the extremal/maximal volume of the time slice anchored at boundary times t_L and t_R.

There is also another relation between complexity and volume that is connected with the ideas of holographic entanglement entropy that was proposed in [19]. For a subsystem A on the boundary theory, we are able to compute holographically the entanglement entropy of A by finding the minimal co-dimension two hyper-surface in the bulk γ_A, whose boundary $\partial\gamma_A$ coincides with the boundary ∂A of the subsystem A. Let us call $V\left(\gamma_A\right)$ the volume in the bulk geometry enclosed by the minimal surface γ_A appearing in the computation of entanglement entropy. Then, the complexity of the subsystem A is related with the volume $V\left(\gamma_A\right)$ by

$$\mathcal{C}_A = \frac{V\left(\gamma_A\right)}{8\pi GL}. \tag{4.2.3}$$

What we are going to do next is to study with more details these conjectures and also do some checks of them.

4.2.1 Complexity of the two-sided AdS black hole

Let's consider an eternal black hole in AdS_{d+1}. The dual CFT_d is described by the time evolution of the TFD state. Its complexity grows linearly in time. As a consequence, it is reasonable that the rate of growing of complexity matches with the rate of growing of the ERB. So, instead of computing the volume of the ERB, it is more instructive first to compute the time derivative of V. Another argument to prefer such approach is the fact that holographic computations of complexity have UV divergences similar to those which appear in holographic entanglement entropy. In both cases, the bulk calculations evaluate the volume of an extremal surface extending to the asymptotic boundary. We will see that the rate of growing of the ERB isn't divergent. The approach where the volume is directly computed can be found in [51].

The technical details about the derivation of the expression for the time derivative of the complexity can be found in the Appendix B. The result is

$$\frac{d\mathcal{C}_V}{dt} = \frac{\Omega_{d-1}}{GL} r_{min}^{d-1} \sqrt{-f\left(r_{min}\right)}, \tag{4.2.4}$$

where r_{min} is determined by $\dot{r} = 0$, being interpreted as the radius of the throat of the ERB that connects the asymptotic AdS space-times.

4.2.1.1 The late time behavior

At late times, which means $t \to \infty$, the maximal surface starts to become almost tangent to a special slice of constant $r = \widetilde{r}_{min}$ inside the black hole, as illustrated in Figure 17.

Figure 17 – Different time slices for the two-sided ADS black

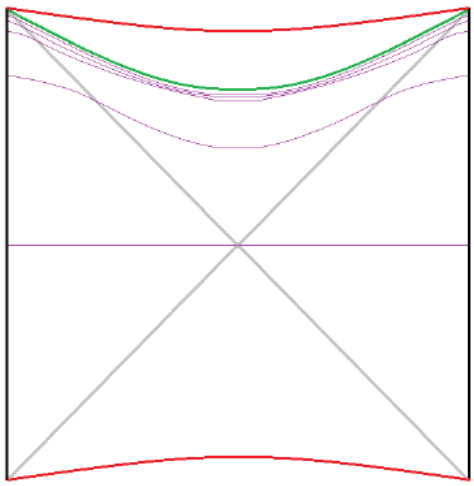

Source: [18]

As the time at which the surfaces are anchored increases the maximal surface moves toward the final slice shown as the green curve. Let us define the function

$$W\left(r\right)=r^{d-1}\sqrt{-f\left(r\right)}, \tag{4.2.5}$$

that appears in (4.2.4). In the limit $t\rightarrow\infty$, the green time slice is a constant curve of $r=\widetilde{r}_{min}$, which also corresponds to an extremum of $W\left(r\right)$. Such fact allows us to expand $W\left(r\right)$ around $\widetilde{r}_{min}$, providing a good description for the late time behavior of $d\mathcal{C}_V/dt$. As a consequence, (4.2.4) becomes

$$\frac{d\mathcal{C}_V}{dt}=\frac{\Omega_{d-1}}{GL}\left[W\left(\widetilde{r}_{min}\right)+\frac{1}{2}W''\left(\widetilde{r}_{min}\right)\left(r_{min}-\widetilde{r}_{min}\right)^2+\mathcal{O}\left(\left(r_{min}-\widetilde{r}_{min}\right)^3\right)\right]. \tag{4.2.6}$$

Asymptotically, $d\mathcal{C}_V/dt$ reaches the constant value

$$\lim_{t\rightarrow\infty}\frac{d\mathcal{C}_V}{dt}=\frac{\Omega_{d-1}}{GL}W\left(\widetilde{r}_{min}\right). \tag{4.2.7}$$

So, the next step is to determine $\widetilde{r}_{min}$ and then to compute $d\mathcal{C}_V/dt$ at least in the asymptotic limit. We will be also able to compute $d\mathcal{C}_V/dt$ for late times by considering higher order corrections in the expression (4.2.6). We already know that $W\left(r\right)$ has a extremum at $\widetilde{r}_{min}$, which implies that

$$2\left(1-d\right)\widetilde{r}_{min}^{d-2}f\left(\widetilde{r}_{min}\right)=\widetilde{r}_{min}^{d-1}f'\left(\widetilde{r}_{min}\right). \tag{4.2.8}$$

For the two-sided AdS black hole, considering the generalized case (3.1.39), the function $f\left(r\right)$ is

$$f\left(r\right)=k-\frac{2\mu}{r^{d-2}}+\frac{r^2}{L^2},\qquad\mu=\frac{8\pi GM}{\left(d-1\right)\Sigma_{k,d-1}}. \tag{4.2.9}$$

The mass parameter μ can be written in terms of r_h using the condition $f\left(r_h\right)=0$, which provides

$$\mu=\frac{r_h^{d-2}}{2}\left(1+\frac{r_h^2}{L^2}\right). \tag{4.2.10}$$

As a consequence

$$f\left(r\right)=k-\frac{r_h^{d-2}}{r^{d-2}}\left(1+\frac{r_h^2}{L^2}\right)+\frac{r^2}{L^2}. \tag{4.2.11}$$

It is possible to manipulate (4.2.8) in order to get some relation between $\widetilde{r}_{min}$ and r_h. The result is

$$d\widetilde{r}_{min}^{d}+\left(d-1\right)L^2\widetilde{r}_{min}^{d-2}k=d\frac{r_h^d}{2}\left(1+\frac{L^2}{r_h^2}\right), \tag{4.2.12}$$

$$d\widetilde{r}_{min}^{d}+\left(d-1\right)L^2\widetilde{r}_{min}^{d-2}k=dL^2\mu. \tag{4.2.13}$$

The first situation that we are going to consider are planar black holes in AdS, which means $k = 0$. This is the simplest case where (4.2.13) can be solved for any dimension of the space-time, namely

$$\widetilde{r}_{min}^{d} = L^2 \mu. \tag{4.2.14}$$

Placing the result inside of a generalized form of (4.2.7), we get that

$$\begin{aligned} \lim_{t\to\infty} \frac{d\mathcal{C}_V}{dt} &= \frac{\Sigma_{0,d-1}}{GL} L\mu = \frac{\Sigma_{k,d-1}}{G} \frac{8\pi G M}{(d-1)\,\Sigma_{k,d-1}} \\ \lim_{t\to\infty} \frac{d\mathcal{C}_V}{dt} &= \frac{8\pi M}{(d-1)}, \end{aligned} \tag{4.2.15}$$

or in terms of the radius of the horizon

$$\lim_{t\to\infty} \frac{d\mathcal{C}_V}{dt} = \frac{\Sigma_{k,d-1} r_h^{d-2}}{2G} \left(1 + \frac{r_h^2}{L^2}\right). \tag{4.2.16}$$

If we remember that for a black hole in AdS

$$T = \frac{(d-2)\,L^2 + d r_h^2}{4\pi L^2 r_h}, \qquad S = \frac{A_h}{4G} = \frac{\Sigma_{k,d-1} r_h^{d-1}}{4G}, \tag{4.2.17}$$

the expression in (4.2.16) becomes

$$\lim_{t\to\infty} \frac{d\mathcal{C}_V}{dt} = 2S \left(\frac{L^2 + r_h^2}{r_h L^2}\right). \tag{4.2.18}$$

The term that multiplies the entropy in the above expression is quite similar to the temperature of the black hole. If we consider small and large black holes, it is possible to make the temperature appears explicitly, namely

$$\lim_{t\to\infty} \frac{d\mathcal{C}_V}{dt} = \frac{8\pi}{(d-2)} ST, \qquad \text{small black holes,} \tag{4.2.19}$$

$$\lim_{t\to\infty} \frac{d\mathcal{C}_V}{dt} = \frac{8\pi}{d} ST, \qquad \text{large black holes.} \tag{4.2.20}$$

The above expressions are an important result because they match with what we got using the quantum circuit model: the time derivative of the complexity is proportional to the product of the entropy and the temperature.

It is possible to handle to the case where we have spherical horizons, which means $k = 1$,[2] for large black holes, i.e., large temperatures. Let's rewrite (4.2.12) as

$$\widetilde{r}_{min} = \frac{r_h}{2^{1/d}} \left[1 + \left(1 - \frac{2\,(d-1)}{d r_h^{d-2}} \widetilde{r}_{min}^{d-2}\right) \frac{L^2}{r_h^2}\right]^{1/d}. \tag{4.2.21}$$

[2] The same treatment for hyperbolic black holes can be find in [52].

For large black holes $r_h \gg L$, which implies that $L/r_h \ll 1$. Such fact allows us to solve (4.2.21) recursively, grouping powers of L/r_h in order to obtain a power series in such variables. This is tedious work, but it is possible to show that

$$\widetilde{r}_{min} = \frac{r_h}{2^{1/d}}\left[1 - \frac{\left(2^{2/d}\,(d-1) - d\right)}{d^2}\frac{L^2}{r_h^2} + \cdots\right]. \tag{4.2.22}$$

Plugging this inside (4.2.7) results in

$$\begin{aligned}\lim_{t\to\infty}\frac{d\mathcal{C}_V}{dt} &= \frac{8\pi M}{(d-1)}\left[1 - 2^{\frac{2}{d}-1}\frac{L^2}{r_h^2} + \frac{2^{2/d}\,(\gamma+d)}{d^2}\frac{L^4}{r_h^4} + \cdots\right]\\ \lim_{t\to\infty}\frac{d\mathcal{C}_V}{dt} &= \frac{8\pi}{d}ST\left[1 - \left(2^{\frac{2}{d}-1} - 1\right)\frac{L^2}{r_h^2} + \cdots\right],\end{aligned} \tag{4.2.23}$$

where γ is a numerical constant that is relevant for forth order corrections. The time derivative of the complexity for large spherical black hole is essentially what we obtained for the planar case plus higher order corrections. If we consider only second order corrections, it is possible to see that $d\mathcal{C}_V/dt$ is upper bounded, namely

$$\lim_{t\to\infty}\frac{d\mathcal{C}_V}{dt} \leq \frac{8\pi}{d}ST. \tag{4.2.24}$$

Such result is in agreement with one of the assumptions of the CA-duality as we are going to see soon.

4.2.1.2 Finite time behavior

It is time to discuss how the time derivative of the complexity behaves for general times. We are going to consider the case of planar black holes because they are simple to treat if we compared to black holes with curved horizons. Then, for $k = 0$ and $d \geq 3$, it is possible to rewrite (4.2.4) in term of two new variables

$$a = \frac{(d-1)}{8\pi M}\frac{d\mathcal{C}_V}{dt} \tag{4.2.25}$$

and

$$s_{min} = \frac{r_{min}}{r_h}. \tag{4.2.26}$$

It is also necessary to use (4.2.9) and (4.2.10). Then, the result is

$$a = 2s_{min}^{d/2}\sqrt{1 - s_{min}^d}. \tag{4.2.27}$$

Is is possible to invert the above relation in order to obtain s_{min} as a function of a, which means that

$$s_{min} = \left(\frac{1+\sqrt{1-a^2}}{2}\right)^{1/d}. \tag{4.2.28}$$

We can also rewrite (B.0.12) in terms of a, $s = r/r_h$, s_{min} and t/β, where $\beta = T^{-1}$. The computation is a change o variables in the integral. What we get is

$$\frac{t}{\beta} = \frac{da}{4\pi}\int_{s_{min}}^{\infty}\left[\frac{s^{d-2}}{(1-s^d)\sqrt{s_{min}^d\left(1-s_{min}^d\right)-s^d\left(1-s^d\right)}}\right]ds. \tag{4.2.29}$$

Once that the above integral is solved, it is possible write s_{min} in terms t/β. Such result can be put inside (4.2.27), providing then the behavior of the $d\mathcal{C}_V/dt$ as a function of the time. In [52] there is a plot of $a \sim d\mathcal{C}_V/dt$ as a function of t/β for some specific space-time dimensions.

Figure 18 – $d\mathcal{C}_V/dt$ as a function of τ/β for the finite time case.

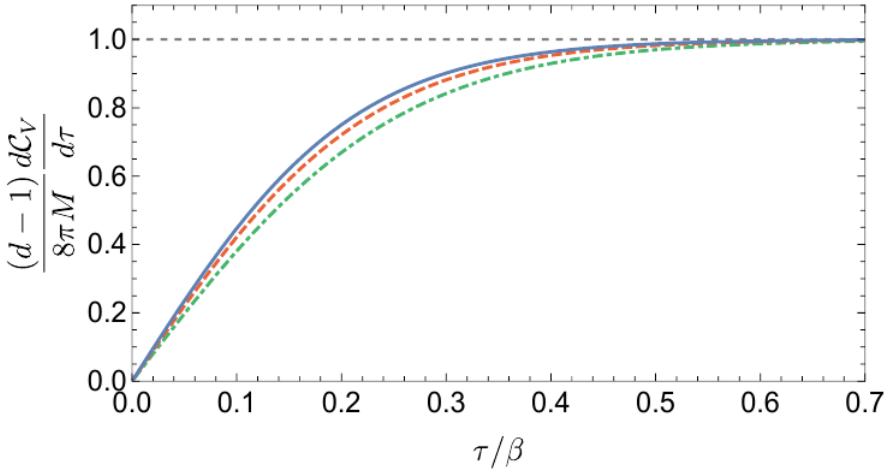

Source: [52]

Figure 18 shows the behavior for the planar $d = 4$ (blue), planar $d = 3$ (dashed-red) and $d = 2$ (dot-dashed green) black holes. All three curves are independent of r_h/L and converge to one at late times, which is in agreement with (4.2.15).

4.2.2 Subregion complexity

Consider a gravitational theory on an Euclidean AdS_{d+1} geometry in Poincaré coordinates

$$ds^2 = \frac{L^2}{z^2}\left(dt^2 + dz^2 + d\rho^2 + \rho^2 d\Omega_{d-2}^2\right), \tag{4.2.30}$$

which could provide a holographic dual for a strongly coupled CFT_d in its ground state. Using the RT prescription [9], it was possible to compute the holographic entanglement entropy for a sphere with radius R (see (3.3.25) and (3.3.26)). Before we got the above

result, it was also found that the minimal surface is given by

$$z = \sqrt{R^2 - \rho^2}. \tag{4.2.31}$$

Following the holographic subregion complexity proposal (4.2.3), we need to evaluate the volume enclosed by the above minimal surface, which means to compute

$$\begin{aligned} V &= \Omega_{d-2} L^d \int_\delta^R dz \int_0^{\sqrt{R^2-z^2}} d\rho \frac{\rho^{d-2}}{z^d}, \\ V &= \frac{\Omega_{d-2} L^d}{(d-1)} \int_\delta^R dz \frac{\left(R^2 - z^2\right)^{(d-1)/2}}{z^d}, \end{aligned} \tag{4.2.32}$$

implying then that

$$\mathcal{C}_A = \frac{\Omega_{d-2} L^{d-1}}{8\pi G\,(d-1)} \int_\delta^R dz \frac{\left(R^2 - z^2\right)^{(d-1)/2}}{z^d}. \tag{4.2.33}$$

For an even dimensional CFT, the result of the integral in (4.2.33) has the closed form

$$\mathcal{C}_A = \frac{\Omega_{d-2} L^{d-1}}{8\pi G\,(d-1)} \left[\frac{1}{(d-1)} \frac{R^{d-1}}{\delta^{d-1}} - \frac{(d-1)}{2\,(d-3)} \frac{R^{d-3}}{\delta^{d-3}} + \cdots + (-1)^{d/2} \frac{\pi}{2} \right]. \tag{4.2.34}$$

For odd dimensional CFTs we have

$$\mathcal{C}_A = \frac{\Omega_{d-2} L^{d-1}}{8\pi G\,(d-1)} \left[\frac{1}{(d-1)} \frac{R^{d-1}}{\delta^{d-1}} - \frac{(d-1)}{2\,(d-3)} \frac{R^{d-3}}{\delta^{d-3}} + \cdots + C_d + (-1)^{(d-1)/2} \log\left(\frac{R}{\delta}\right) \right], \tag{4.2.35}$$

where C_d is a constant that depends on the dimension d. It is interesting to note that for odd dimensions the holographic complexity contains a logarithmically divergent term.

The expressions for $\mathcal{C}_A$ above are divergent. However, notice that the most divergent term in the expression of holographic subregion complexity is proportional to the volume of the subsystem $V(A)$, providing the volume law behavior

$$\mathcal{C}_A = \frac{L^{d-1}}{8\pi G\,(d-1)} \frac{V\,(A)}{\delta^{d-1}} + \cdots, \tag{4.2.36}$$

which can be thought of as something analogous to the area law of the entanglement entropy. Additionally, the holographic subregion complexity contains a universal term $\mathcal{C}_V^{uni}$ in the sense that it is independent of the UV cut-off δ. For even d, the universal term can be identified with the finite term, while for odd d, it is given by the coefficient of the log divergence term. Explicitly,

$$\mathcal{C}_A^{uni} = \begin{cases} (-1)^{d/2} \frac{\Omega_{d-2} L^{d-1}}{16 G(d-1)} & \text{even } d \\ (-1)^{(d-1)/2} \frac{\Omega_{d-2} L^{d-1}}{8\pi G(d-1)} & \text{odd } d \end{cases}. \tag{4.2.37}$$

The universal terms are independent of the size of the subsystem R, indicating that it could reflect certain intrinsic properties of the theory under consideration.

4.2.2.1 The QIM in CFTs

The QIM is defined on an infinite dimensional space of all the deformations induced by all possible operators away from the unperturbed theory. In special, deformations induced by a single marginal operator acquires a interesting role because, besides the fact that marginal operators don't break conformal invariance, such deformation at a time $\tau = 0$ can be identified with a d dimensional defect brane with a given tension T, which extends from the time slice on the AdS boundary to the bulk.

The idea is to compute the QIM between the ground state of two d dimensional CFTs that are related by the insertion of term of the form $\delta\lambda\mathcal{O}(x)$, where $\mathcal{O}(x)$ corresponds to a conformal primary operator of the original theory with conformal (scaling) dimension Δ and $\delta\lambda$ is the coupling constant. It was computed in [53] (also in [54]). The result is

$$G_{\lambda\lambda} = \frac{1}{2}\int d^{d-1}x_1 \int d^{d-1}x_2 \int_{-\infty}^{-\delta} d\tau_1 \int_{\delta}^{\infty} d\tau_2 \left\langle \mathcal{O}(\tau_1, x_1)\, \mathcal{O}(\tau_2, x_2)\right\rangle , \tag{4.2.38}$$

where δ is a UV cut-off that was introduced in order to avoid UV divergences at $\tau = 0$. For primary operators we have that

$$\left\langle \mathcal{O}(\tau_1, x_1)\, \mathcal{O}(\tau_2, x_2)\right\rangle = \frac{1}{\left((\tau_1 - \tau_2)^2 + (x_1 - x_2)^2\right)^{\Delta}}. \tag{4.2.39}$$

We can put the above two point function inside (4.2.38). If $d + 1 - 2\Delta < 0$, we have that

$$G_{\lambda\lambda} = N_d V_{d-1} \delta^{d+1-2\Delta}, \tag{4.2.40}$$

where V_{d-1} is the infinity volume of $\mathbb{R}^{d-1}$ while the constant N_d is given by

$$N_d = \frac{2^{d-1-2\Delta}\pi^{(d-1)/2}\Gamma(\Delta - d/2 - 1/2)}{(2\Delta - d)\,\Gamma(\Delta)}. \tag{4.2.41}$$

In the case where $\mathcal{O}(x)$ is a marginal operator, which means that $\Delta = d$, allowing us to rewrite (4.2.40) as

$$G_{\lambda\lambda} = \frac{\pi^{(d-1)/2}\Gamma((d-1)/2)}{2^{d+1} d\,(d-1)!}\frac{V_{d-1}}{\delta^{d-1}}. \tag{4.2.42}$$

4.2.2.2 Complexity and QIM

It was proposed in [53] (see also [54]) an holographic estimate for the QIM of a CFT deformed by an exactly marginal perturbation parametrized by λ. Such proposal says that

$$G_{\lambda\lambda} = n_d \frac{V(\Sigma_{max})}{L^d}, \tag{4.2.43}$$

where n_d is a constant and L is the AdS radius. The d-dimensional spacelike surface Σ_{max} is the time slice that delimits the maximal volume in AdS which ends on the time slice at the AdS boundary. The gravity dual of the QIM follows the same idea than holographic subregion complexity.

As an example, let's consider the computation of the QIM for a specific case, which is AdS_3/CFT_2 where the boundary theory with $\mathcal{L}_1$ was perturbed by an exactly marginal operator, providing a resulting theory described by $\mathcal{L}_2$. The gravity dual which interpolates between two AdS spaces is called Janus solution [55, 56]. The massless bulk scalar field dual to the exactly marginal operator $\mathcal{O}$ is denoted by ϕ. The AdS_3 Janus solution is defined by the action

$$\mathcal{A} = -\frac{1}{16\pi G}\int d^3x\sqrt{g}\left(R - g^{\mu\nu}\partial_\mu\phi\partial_\nu\phi + \frac{2}{L^2}\right). \tag{4.2.44}$$

The equations of motion provided by the above action are

$$\begin{aligned} R_{\mu\nu} - \frac{1}{2}g_{\mu\nu}R - g_{\mu\nu}\frac{1}{L^2} &= 8\pi G\left(\partial_\mu\phi\partial_\nu\phi - \frac{1}{2}g_{\mu\nu}g^{\alpha\beta}\partial_\alpha\phi\partial_\beta\phi\right), \\ \partial_\mu\left(\sqrt{g}g^{\mu\nu}\partial_\nu\phi\right) &= 0, \end{aligned} \tag{4.2.45}$$

which have the following solutions

$$\begin{aligned} ds^2 = L^2\left[dy^2 + f(y)\frac{(dz^2+dx^2)}{z^2}\right], \qquad f(y) = \frac{1}{2}\left(1+\sqrt{1-2\lambda^2}\cosh(2y)\right), \\ \phi(y) = \lambda\int_{-\infty}^{y}\frac{dy}{f(y)} + \phi_1, \end{aligned} \tag{4.2.46}$$

where λ is the parameter deformation. The constant $\phi_1 = \phi(-\infty)$ is dual to the coupling constant of the exactly marginal deformation for the ground state of the unperturbed CFT $|\Omega_1\rangle$. On the other hand, the value $\phi_2 = \phi(\infty)$ for the ground state $|\Omega_2\rangle$ can be obtained by the integral (4.2.46). The fidelity between the vacuum states is given by

$$|\langle\Omega_2|\,\Omega_1\rangle| \simeq 1 - \frac{RV_1}{8\pi G\delta}\lambda^2, \tag{4.2.47}$$

implying that the QIM is

$$G_{\lambda\lambda} = \frac{cV_1}{12\pi\delta}, \tag{4.2.48}$$

where we used the holographic expression for the central charge (3.3.20).

Now we are in the position to argue about the connection between the idea of holographic subregion complexity and QIM. From (4.2.34), for the 2-dimensional case, the complexity of the subsystem A has the form

$$\mathcal{C}_A = \frac{LR}{8\pi G\delta} - \frac{L}{16G}. \tag{4.2.49}$$

Using again the holographic expression for the central charge, we have that

$$\mathcal{C}_A = \frac{cR}{12\pi\delta} - \frac{c}{24}. \tag{4.2.50}$$

In the large R limit, besides the fact that R becomes V_1, the factor $c/24$ can be ignored. This limit provides a match between the subregion complexity $\mathcal{C}_A$, obtained holographically, and the QIM (4.2.48). Furthermore, in [19] the authors also proposed a d-dimensional generalization for this match, namely

$$\mathcal{C}_A = \frac{V_{d-1}L^{d-1}}{8\pi G\,(d-1)\,\delta^{d-1}},$$

where V_d is the volume of the subsystem A in the large R limit, which is essentially the infinity volume of $\mathbb{R}^{d-1}$. The above expression is equal the QIM obtained from an AdS background with a defect brane, which is the general d-dimensional holographic model for marginal deformations considered by [53].

4.3 Complexity=Action

The second holographic proposal for the computation of complexity was proposed in [21, 22]. The complexity $\mathcal{C}_\mathcal{A}$ of the boundary state is equal to the classical action of a space-time region that extends along the bulk. Such region is shown in Figure 19. The so called Wheeler-DeWitt (WDW) patch is defined as the bulk domain of dependence of a bulk Cauchy slice anchored at the boundary state.

Figure 19 – Wheeler-De Witt patch for the two-sided geometry.

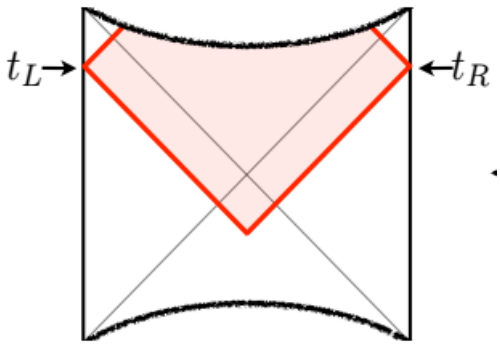

Source: [22]

Such region already appeared in the discussion about CV duality. All the co-dimension one surfaces anchored at the times (t_L, t_R) are contained inside the WDW patch (see again Figure 16). The CA duality may be considered a better version of the CV duality. It doesn't mean that complexity=volume is useless or something wrong, however,

the CV duality has a couple of unsatisfactory characteristics. First, it is necessary to chose a length scale ℓ depending of the situation. Second, it is not completely clear why the co-dimension one surface connecting the boundaries must have maximal volume. Why does this kind of surface play a preferred role? The CA duality will exhibits all the nice properties of the CV duality without these unsatisfactory elements presented above.

We are again interested in the time evolution of the TFD state's complexity, which means that the dual bulk geometry is the two-sided AdS black hole geometry at chosen times t_L and t_R. The WDW patch $\mathcal{W}(t_L, t_R)$ is the union of all spacelike surfaces anchored at t_L and t_R. It is equivalent to the space-time region inside the intersection between forward and backward light rays sent from the boundary at t_L and t_R. Let's define $\mathcal{A}_\mathcal{W}$ to be the action obtained by integrating the bulk action over $\mathcal{W}$ and including suitable boundary terms on $\partial\mathcal{W}$. The complexity $\mathcal{C}_\mathcal{A}$ is related to the action computed over the WDW patch by

$$\mathcal{C}_\mathcal{A}(t_L, t_R) = \frac{\mathcal{A}_\mathcal{W}(t_L, t_R)}{\pi\hbar}. \tag{4.3.1}$$

Additionally, it was also proposed a bound for the growth of the complexity. From our qubit model, we already know that the time derivative of complexity is proportional to the entropy times the temperature. Together with the CA proposal, a refinement for what we expect from the growth of the complexity was proposed. Using arguments of bounds for the storage of information and quantum evolution, it was conjectured that the growth of the complexity is bounded by

$$\frac{d\mathcal{C}_\mathcal{A}}{dt} \leq \frac{2E_\psi}{\pi\hbar}, \tag{4.3.2}$$

where E_ψ is the average energy of $|\psi\rangle$ relative to the ground state, which means pure AdS space-time in the bulk.

For uncharged black holes, E_ψ is the mass M of the black hole, which implies that

$$\frac{d\mathcal{C}_\mathcal{A}}{dt} \leq \frac{2M}{\pi\hbar}. \tag{4.3.3}$$

It is possible to generalize (4.3.3) for black holes that carry conserved charges, for example, charge Q or angular momentum J. In these cases, it is necessary to define a charged version of the TFD state. It can be done by the introduction of a chemical potential μ, which is positive on one side (left) and negative on the other side (right). Then, the charged TFD state has the form

$$|TFD_\mu\rangle = \frac{1}{Z^{1/2}} \sum_n e^{-\beta(E_n+\mu Q_n)/2} |E_n, Q_n\rangle_L |E_n, -Q_n\rangle_R, \tag{4.3.4}$$

where the time evolution of the state is changed by the introduction of the chemical potential, namely

$$|TFD_\mu(t)\rangle = e^{-i(H_L+\mu Q_L)} e^{-i(H_R-\mu Q_R)} |TFD_\mu\rangle. \tag{4.3.5}$$

For the charged TFD state, the equation (4.3.3) is also changed by the insertion of the μ. As result

$$\frac{d\mathcal{C}_{\mathcal{A}}}{dt} \leq \frac{2}{\pi\hbar}\left[(M-\mu Q)-(M-\mu Q)_{gs}\right], \tag{4.3.6}$$

where the subscript gs refers to the contribution of the state of the ground state. For rotating black holes, the above expression becomes

$$\frac{d\mathcal{C}_{\mathcal{A}}}{dt} \leq \frac{2}{\pi\hbar}\left[(M-\omega J)-(M-\omega J)_{gs}\right], \tag{4.3.7}$$

where J is the angular momentum and ω is the angular velocity. In order to clarify more the introduction of the parameters μ, Q, ω and J, let's consider the first law of thermodynamics for black holes

$$dM = TdS + \omega dJ + \mu dQ. \tag{4.3.8}$$

The charges Q and J in the black hole change the relation between its mass and entropy. For charged black holes (the same for rotating), it is possible to integrate (4.3.8) in order to obtain

$$\left[(M-\mu Q)-(M-\mu Q)_{gs}\right] = \int_{gs}^{S} TdS. \tag{4.3.9}$$

From the thermodynamics point of view, the quantity $\left[(M-\mu Q)-(M-\mu Q)_{gs}\right]$ is the internal energy relative to the ground state at a fixed μ. Such result allows us to rewrite (4.3.3), (4.3.6) and (4.3.7) in a unique expression, namely

$$\frac{d\mathcal{C}_{\mathcal{A}}}{dt} \leq \int_{gs}^{S} TdS, \tag{4.3.10}$$

which is a result similar to what we expect from the quantum circuit model of complexity and also to what was found in the computations using CV duality for the case o planar black holes (see Eq. (4.2.24)). The next step is to use the CA proposal and compute complexity holographicaly for some three specific cases: the uncharged black hole, the small charged black hole and the rotating BTZ. The details about the computations can be found in Appendix C.

4.3.1 Uncharged black hole

The action for an uncharged black black hole in AdS in given by

$$\mathcal{A} = \frac{1}{16\pi G}\int_{\mathcal{M}} d^{d+1}x\sqrt{-g}\,(R-2\Lambda) + \frac{1}{8\pi G}\int_{\partial\mathcal{M}}\sqrt{-h}K, \tag{4.3.11}$$

where the first term is the Einstein-Hilbert action with cosmological constant Λ and the second one is the Gibbons-Hawking-York term. The idea is to compute semi-classically the time derivative of the action $\mathcal{A}$ on the WDW patch, which is shown in Figure 20, using

the AdS black hole metric. In order to avoid the UV divergences that will appear because the WDW patch touches the boundaries, we are going to consider again the computation at the late times limit $(t_L + t_R \gg \beta)$.

Figure 20 – WDW patch for the uncharged AdS black hole.

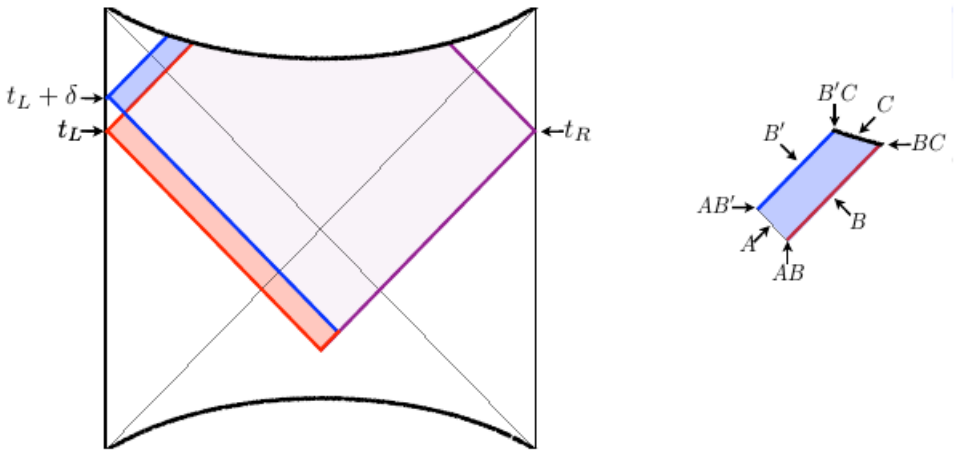

Source: [22]

For this situation, the right time t_R remains constant while the left time t_L changes by a small factor δ. As consequence, the WDW patch grows in some places (blue regions) and shrinks in others (red regions).

The contribution of the WDW patch outside the horizon, despite infinite, doesn't change with time because of the time translation symmetry outside of the horizon, while, similarly to what happens for late times computations in the CV duality, the WDW patch in the limit $t \to \infty$ acquires a final shape, which corresponds to the the situation where the entire WDW patch is inside the horizon. As a consequence, the contribution of the WDW patch inside the past horizon becomes irrelevant at late times.[3] The conclusion is that only the blue region inside the future horizon contributes to the computation at late times. This blue region is shown on the right hand side of Figure 20, where we are going to see that not all boundary elements of this region really contribute to the computation. For example, the boundary contribution at the light sheet B' replaces the old contribution at B. Since B' and B are related by the time translation symmetry, this change doesn't contributes to the total action. Similarly, the new corner contribution AB' cancels the old corner contribution AB as well as BC' cancels BC. This leaves us with two surface contributions, A at $r = r_h$ and C at $r = 0$, and the bulk contribution.

[3] In [22] the authors argument that it is possible to use the Gauss-Bonnet theorem to consider the contribution of the WDW patch inside the past horizon topological, so that it must be time independent at late times.

Now we are in the position to compute the time derivative of the action on the WDW patch, where for simplicity we are going to choose $t_L = t_R = t$. The bulk contribution is

$$\frac{d\mathcal{A}_{bulk}}{dt} = -\frac{\Omega_{d-1} r_h^d}{8\pi G L^2}, \tag{4.3.12}$$

while the boundary contribution that comes from the Gibbons-Hawking-York term is

$$\frac{d\mathcal{A}_{bdy}}{dt} = \left[-\frac{d}{d-1} M + \frac{\Omega_{d-1} r^{d-2}}{8\pi G} \left((d-1) + d\frac{r^2}{L^2} \right) \right] \Bigg|_0^{r_h}. \tag{4.3.13}$$

The sum of both contributions result in the simple expression

$$\frac{d\mathcal{A}}{dt} = 2M, \tag{4.3.14}$$

which is valid for any dimension and black hole size. Then, following the complexity=action proposal (4.3.1), the time derivative of the complexity is

$$\frac{d\mathcal{C}_{\mathcal{A}}}{dt} = \frac{2M}{\pi\hbar}. \tag{4.3.15}$$

Uncharged black holes precisely saturate the bound of the rate of change of complexity (4.3.3), independently of their size and number of space-time dimensions. In the original CV duality, the answer for $d\mathcal{C}/dt$ is not universal. For example, there are dimension dependent factors that cannot be absorbed into a universal coefficient (see equations (4.2.19) and (4.2.20)). Also, the rate of change of complexity has some dependence on whether the black hole is small or large compared to the AdS length.

4.3.2 Small charged black hole

In Figure 21 the WDW patch for the charged black hole in AdS is shown. Differently from what we have for the uncharged black hole, the ingoing light rays that delimit the WDW patch terminate when they meet each other at $t = 0$. Nevertheless, it is possible to reuse the same arguments above to find the late time growth of the enclosed action.

Figure 21 – WDW patch for the charged AdS black hole.

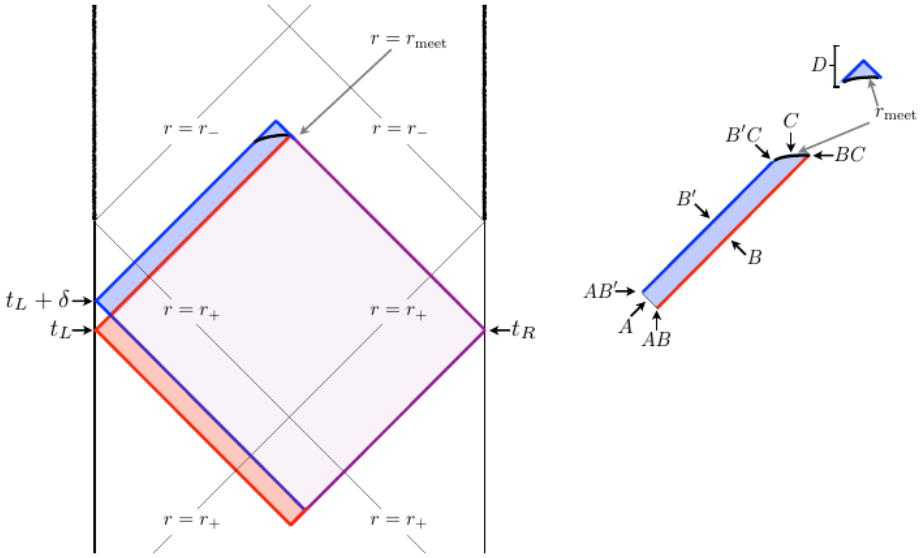

Source: [22]

The entire WDW patch is located outside of the inner horizon at r_-. As in the uncharged case, the part of the WDW patch that is located outside of the outer horizon is independent of time and the contribution of the part that lies behind the past horizon has an irrelevant contribution at late times. Then, the late time rate of change of action comes from the part of the patch behind the future horizon.

On the right side of Figure 21 it is possible to see, analogously to what was done for the uncharged case, that the contribution from B will cancel that from B', the corners at AB and AB' will cancel each other as well as the corners at BC and BC'. The contribution from D can be considered irrelevant since the size of the two-sphere is stationary at D. This leaves only the contribution of A, C and the bulk term.

The simplest situation that is possible to consider is the $(3+1)$-dimensional case where the electromagnetic energy-momentum tensor is traceless and the field strength is

$$F_{rt} = -F_{tr} = \frac{Q}{r^2}. \tag{4.3.16}$$

The time derivative of the action on the WDW is given by

$$\begin{aligned}\frac{d\mathcal{A}}{dt} &= \frac{1}{16\pi G}\int d\Omega_2 \int_{r_-}^{r_+} dr\sqrt{-g}\,(R - 2\Lambda) \\ &+ \frac{1}{8\pi G}\int d\Omega_2\sqrt{-h}K\Big|_{r_-}^{r_+} - \frac{1}{16\pi}\int d\Omega_2 \int_{r_-}^{r_+} dr\sqrt{-g}F_{\mu\nu}F^{\mu\nu}.\end{aligned} \tag{4.3.17}$$

The bulk contribution is

$$\frac{d\mathcal{A}_{bukl}}{dt} = \frac{r_+ - r_-}{2}\left(\frac{Q^2}{r_+ r_-} - \frac{r_-^2 + r_+ r_- + r_+^2}{GL^2}\right), \tag{4.3.18}$$

while the Gibbons-Hawking-York term at $r = r_+$ and $r = r_-$ provide

$$\frac{d\mathcal{A}_{bdy}}{dt} = \left(-\frac{3M}{2} + \frac{Q^2}{2r} + \frac{r}{G} + \frac{3}{2G}\frac{r^3}{L^2}\right)\Bigg|_{r_-}^{r_+}. \tag{4.3.19}$$

Then, the final result is

$$\frac{d\mathcal{A}}{dt} = \frac{Q^2}{r_-} - \frac{Q^2}{r_+}. \tag{4.3.20}$$

Taking the limit of small black holes, which means $r_\pm \ll L$, it is possible to obtain that

$$\frac{d\mathcal{A}}{dt} = 2\sqrt{M^2 - \frac{Q^2}{G}}. \tag{4.3.21}$$

In order to compare the result obtained in the gravity side to the prescription presented in (4.3.6), it is necessary to calculate the quantity $M - \mu Q$. In the limit of small black holes, the inner and outer horizons have the following form (see Appendix C)

$$r_\pm = GM \pm \sqrt{(GM)^2 - \left(\sqrt{G}Q\right)^2}. \tag{4.3.22}$$

The above expression can provide us with the following relation

$$r_+ + r_- = 2GM, \qquad r_+ r_- = GQ^2. \tag{4.3.23}$$

The outer horizon r_+ is essentially the entropy of the black hole. This way, from the first law of thermodynamics for charged black holes (4.3.8), the chemical potential μ can be determined by

$$\mu = \left.\frac{\partial M}{\partial Q}\right|_S. \tag{4.3.24}$$

Using (4.3.23), we have that

$$2GdM = dr_-, \qquad 2GQdQ = r_+ dr_-, \tag{4.3.25}$$

implying then the following result

$$\mu = \frac{Q}{r_+}. \tag{4.3.26}$$

Once we know μ, it is possible to compute the quantity $M - \mu Q$. As a result, we have that

$$\begin{aligned} M - \mu Q = M - \frac{Q^2}{r_+} &= \frac{r_+ + r_-}{2G} - \frac{r_+ r_-}{G r_+} \\ &= \sqrt{M^2 - \frac{Q^2}{G}}. \end{aligned} \tag{4.3.27}$$

For the ground state (AdS without the black hole), which means $M = Q = 0$, the above quantity is zero. Finally, the time derivative of the complexity, following (4.3.6), has the bound

$$\frac{d\mathcal{C}_{\mathcal{A}}}{dt} \leq \frac{2}{\pi\hbar}\sqrt{M^2 - \frac{Q^2}{G}}. \tag{4.3.28}$$

The above result is in agreement with (4.3.21). The small charged black hole precisely saturates the bound for the change of complexity proposed in (4.3.6).

4.3.3 Rotating BTZ black hole

The action for the rotating BTZ is the same that was considered for the uncharged black hole, while the Penrose diagram is similar to that for the charged case (see Figure 21). As a consequence, the bulk contribution for the time derivative of the action on the WDW patch is

$$\frac{d\mathcal{A}_{bulk}}{dt} = -\frac{\left(r_+^2 - r_-^2\right)}{4GL^2}, \tag{4.3.29}$$

while the boundary contribution is

$$\frac{d\mathcal{A}_{bdy}}{dt} = \left[\frac{2r^2}{4GL^2} - 2M\right]\Bigg|_{r_-}^{r_+}. \tag{4.3.30}$$

Then, the total rate of change of the action is

$$\frac{d\mathcal{A}}{dt} = 2\sqrt{M^2 - \frac{J^2}{L^2}}. \tag{4.3.31}$$

This way, using the complexity=action proposal (4.3.1), the time derivative of the complexity is

$$\frac{d\mathcal{C}_{\mathcal{A}}}{dt} = \frac{2}{\pi\hbar}\sqrt{M^2 - \frac{J^2}{L^2}}. \tag{4.3.32}$$

Using (4.3.7), it is possible to compute the bound of the change of the complexity. For the rotating BTZ, we have the following relations between the mass, angular momentum, inner and outer horizons

$$r_+^2 + r_-^2 = 8GML^2, \qquad r_+ r_- = 4GLJ, \qquad r_+^2 - r_-^2 = 8GL^2\sqrt{M^2 - \frac{J^2}{L^2}}. \tag{4.3.33}$$

The entropy of the black hole is proportional to the outer horizon r_+, implying that at constant S

$$dM = \frac{2r_-}{8GL^2}dr_-, \qquad dJ = \frac{r_+}{4GL}dr_-. \tag{4.3.34}$$

Using the first law of thermodynamics for rotating black holes (4.3.8), the angular velocity can be determined by

$$\omega = \left.\frac{\partial M}{\partial J}\right|_S, \tag{4.3.35}$$

which implies from (4.3.34) that

$$\omega = \frac{r_-}{r_+ L}. \tag{4.3.36}$$

As a consequence

$$\begin{aligned} M - \omega J = M - \frac{r_-}{r_+ L} J &= \frac{r_+^2 + r_-^2}{8GL^2} - \frac{r_-}{r_+ L}\left(\frac{r_+ r_-}{4GL}\right) \\ &= \sqrt{M^2 - \frac{J^2}{L^2}}. \end{aligned} \tag{4.3.37}$$

For the ground state, which correspond to a pure AdS space-time, the quantity $M - \omega J$ is computed assuming that $M = 0$ and $J = 0$, implying that $(M - \omega J)_{gs} = 0$. Finally, the bound for the change of complexity is

$$\frac{d\mathcal{C}_{\mathcal{A}}}{dt} \leq \frac{2}{\pi\hbar}\sqrt{M^2 - \frac{J^2}{L^2}}. \tag{4.3.38}$$

Comparing the above result with (4.3.32), the rotating BTZ black hole, as well as the uncharged black hole, precisely saturates the complexification bound proposed in (4.3.7).

5 Conclusion

The holographic entanglement entropy provided an easier alternative to compute entanglement entropy in CFTs. Instead of using replica trick, we are allowed to calculate the area of the minimal surface γ_A and then to obtain the entropy. This is a remarkable example of how holography can be a useful tool to compute complicated quantities in QFTs and vice-versa. In the case of complexity, the Hayden-Preskill circuit model provides a simple way to estimate the complexity of a given quantum state. In particular, we focused our attention to the specific case where we have the duality between the two sided AdS black hole and the TFD state. We obtained that the complexity grows linearly with t, while its time derivative is proportional to the entropy times the temperature of the black hole (or the thermal CFT). These estimates, specially the one about the time derivative, provided a match for the holographic proposals of complexity.

For certain limits, both CV and CA provided results that agree to what was obtained from the quantum circuit model. In order to avoid UV divergences, we restricted ourselves to calculations of complexity at late times. From the CV duality, there is an agreement for small and large planar black holes that the change of complexity is proportional to TS. The same was obtained for large spherical black holes. Furthermore, it was discussed a bit about the finite time case for planar black holes. As a result, it was found that $d\mathcal{C}_V/dt$ reaches the same constant behavior (4.2.15) in the limit $t/\beta \gg 1$, matching the late time's prediction. The CV proposal reproduced the TS behavior for the change of complexity, at least qualitatively.

Following the same philosophy of holographic entanglement entropy, the holographic subregion complexity is a bit different formulation of the CV. The computation of the volume enclosed minimal surface γ_A provided the complexity of a state of interest belonging to $\mathcal{H}_A$. Analogously to the area law for the entanglement entropy, the holographic subregion complexity provided the volume law (4.2.36), where $V(A)$ is the volume of the region A. In the limit where $V(A)$ approaches the volume of $\mathbb{R}^{d-1}$, there is a match between the subregion complexity $\mathcal{C}_A$ and the holographic QIM. This is a indicative that there is a relation between complexity and QIM. Actually, one of the conclusion of [53] is that the QIM for different TFD, which means slight different Hamiltonians, is the same formula used in the CV proposal.

The CA duality provided a more detailed relation between the rate of change of complexity, entropy and temperature. From CA, we obtained that an exact match between the computations in the gravity side and the bound for $d\mathcal{C}_A/dt$ conjectured in

(4.3.10). In the case of charged black holes, we restricted ourselves to the case of small black holes in order to obtain a result that agrees exactly to the bound (4.3.6). Intermediate and large black holes apparently violate this complexification bound. The reason is shortly discussed in [22]. The authors suspect that it has to do with the black hole's hair. Despite this issue with charged black holes, the CA-duality provides a degree of universality that is absent in the CV duality. The same universal constant connects action and complexity in the three considered cases, where in each one the computed complexity saturates the appropriate bound.

As a last comment, let us mention that the relevant papers about complexity in the context of the study of black holes and holography began to be published in 2013, which makes complexity a very recent subject. As was said by the authors of [57], where they argues about the existence of a thermodynamics description for the quantum complexity that includes a second law, "...Complexity theory, particularly its quantum version, is a new and relatively unknown mathematical subject to most physicists, including the authors of this paper...". It is necessary to comment that complexity is still being thoroughly studied by the community because some of the results presented in this thesis were improved in more recent papers [51, 52, 58]. Furthermore, it is not well understood how to compute complexity for QFTs. What we have so far is the Hayden-Preskill circuit model. However, this open questions is being studied by the community. For example, it was proposed in [59] a quantum circuit model for the preparation of Gaussian states, in particular the ground state, in a free scalar field theory for general dimensions.

Appendices

Appendix A – Schwarzschild black hole

The study of the Schwazschild solution in Minkowski space-time is important in order to have a better understanding of black holes in AdS. Many interesting computations can be done explicitly for this black hole, a task that is more difficult in AdS space-time.

A.1 Schwarzschild solution

Real-world black holes come from the gravitational collapse of massive objects, stars for example. It is possible to idealize stars that will collapse to black holes, for example, by a spherically symmetric ball of dust. After the collapse, the geometry of the region outside the collapsed star, which is a vacuum solution, is described by the Schwazschild metric. According to the Birkhoff's theorem, the Schwarzschild solution is the unique time independent spherically symmetric vacuum solution of Einstein's equations (3.1.2) with $\Lambda = 0$:

$$R_{\mu\nu} - \frac{1}{2} R g_{\mu\nu} = 0. \tag{A.1.1}$$

In d dimensions, it is given by

$$ds^2 = -f\left(r\right) dt^2 + \frac{dr^2}{f\left(r\right)} + r^2 d\Omega_{d-2}^2, \qquad f\left(r\right) = 1 - \frac{2\mu}{r^{d-3}}, \tag{A.1.2}$$

that is known as Schwarschild metric. The parameter μ is related to the mass M of the black hole and Newton's constant G by

$$\mu = \frac{8\pi G M}{\left(d-2\right) \Omega_{d-2}}, \qquad \Omega_{d-2} = \frac{2\pi^{(d-1)/2}}{\Gamma\left(\frac{d-1}{2}\right)}, \tag{A.1.3}$$

where Ω_{d-2} denotes the volume of the sphere S^{d-2}. Let us study in details the case $d = 4$, that was the first non-trivial solution of Einstein's equations. The metric for the four-dimensional case becomes

$$ds^2 = -\left(1 - \frac{2GM}{r}\right) dt^2 + \frac{dr^2}{\left(1 - \frac{2GM}{r}\right)} + r^2 d\Omega_2^2. \tag{A.1.4}$$

Taking the trace of equation (A.1.1), we obtain that

$$\left(2 - d\right) R = 0, \tag{A.1.5}$$

which implies that $R = 0$ for the cases $d \geq 3$. As a consequence, $R_{\mu\nu}$ is also zero (see (A.1.1)) and the Schawarschild metric is Ricci flat. Such fact is relevant in the

discussion about the singularities of the metric. There are two apparent singularities in the Scharzschild metric: $r = 0$ and $r = 2GM$. In order to verify if both singularities are physical, we need to compute some diffeomorphism invariant quantity and verify if it is divergent in these special points. A natural candidate is some invariant built from the Riemann tensor with itself, namely

$$R_{\mu\nu\rho\sigma}R^{\mu\nu\rho\sigma} = \frac{48G^2M^2}{r^6}. \tag{A.1.6}$$

Such quantity is known as Kretschmann's scalar. It becomes clear that only $r = 0$ is a physical singularity. The case $r = 2GM$ refers to a singularity of the coordinate system. More than that, for $r = 2GM$, known as Scharwschild radius[1] r_s of the black hole, $f(r_s) = 0$. For spherically symmetric metrics of the type (A.1.2), the larger root r_h of the equation $f(r_h) = 0$ is the event horizon of the black hole. In the specific case of Schwarzchild's geometry, there is an event horizon at $r = r_s$.

The coordinates (t, r, Ω) aren't global in the sense that they don't cover all the points of the space-time. We can fix this problem by introducing the tortoise coordinate $r^*(r)$ such that

$$dr^* = \frac{dr}{1 - \frac{2GM}{r}}, \qquad r^*(r) = r + 2GM \ln\left(\frac{r}{2GM} - 1\right). \tag{A.1.7}$$

The coordinate r^* is defined in the region $r \geq 2GM$. Its range is from $-\infty$ to ∞. The Schwarzschild metric becomes

$$ds^2 = \left(1 - \frac{2GM}{r}\right)\left(-dt^2 + dr^{*2}\right) + r^2 d\Omega_2^2. \tag{A.1.8}$$

The divergence in the metric disappeared, however, the components g_{tt} and $g_{r^*r^*}$ vanish for $r \to 2GM$. As a further step, let's define the light-cone tortoise coordinates (u, v),

$$v = t + r^*, \qquad u = t - r^*, \tag{A.1.9}$$

such that

$$ds^2 = -\left(1 - \frac{2GM}{r}\right) du dv + r^2 d\Omega_2^2. \tag{A.1.10}$$

Finally, we introduce the Kruskal-Szekeres coordinates U and V,

$$U = -4GM \exp\left(-\frac{u}{4GM}\right), \qquad V = 4GM \exp\left(\frac{v}{4GM}\right), \tag{A.1.11}$$

where the coordinates (t, r) are related with (U, V) by

$$\begin{aligned} UV &= -(4GM)^2 \left(\frac{r}{2GM} - 1\right) \exp\left(\frac{r}{2GM}\right), \\ \frac{U}{V} &= -\exp\left(-\frac{t}{2GM}\right). \end{aligned} \tag{A.1.12}$$

[1] For the d-dimensional case, $r_h = (2\mu)^{1/(d-3)}$.

The metric in Kruskal-Szekeres coordinates has the form

$$ds^2 = -\frac{2GM}{r\,(U,V)}\exp\left(-\frac{r}{2GM}\right)dUdV + r^2 d\Omega_2^2. \tag{A.1.13}$$

The range for the coordinates is $-\infty < U < 0$ and $0 < V < \infty$. In this way, they cover the exterior of the black hole $r > 2GM$. If we look at the metric (A.1.13), there isn't a divergence for $r = 2GM$. As consequence, it is possible to extend the Kruskal-Szekeres coordinates to $U, V \in (-\infty, \infty)$. The coordinates (U, V, Ω) are global coordinates. Actually, the Kruskal–Szekeres coordinates are the maximal analytic extension of the Schwarzschild solution once no more regions can be found by analytic continuation. Figure 22 is a sketch that shows lines of constant U and V as well as lines of constant r.

Figure 22 – Kruskal-Szekeres space-time.

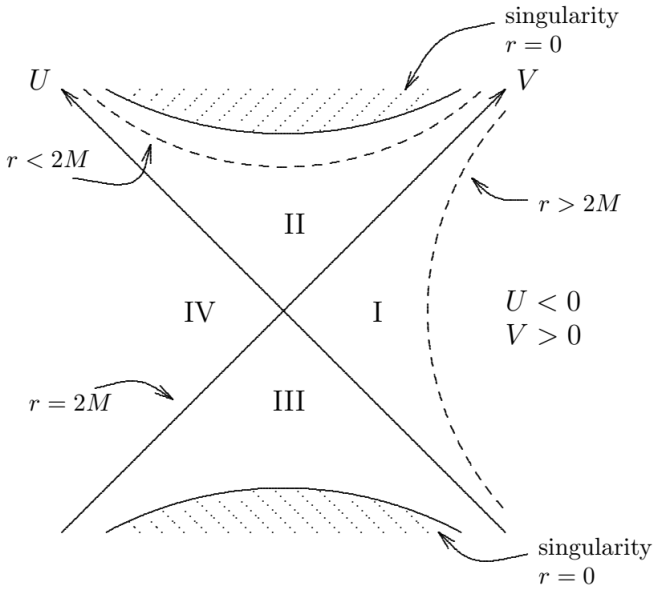

Source: [30]

The curve $r = 0$ gives the relation $UV = (-U)\,(-V) = 4GM$, which explains the two singularities in the diagram. In the same way, the event horizon $r_h = 2GM$ is located at $UV = 0$, consequently, along lines of either U or V equal zero.

It is possible to construct the conformal diagram for the Schwarschild black hole in Kruskal-Szekeres coordinates. Consider the metric (A.1.10). Introducing

$$\begin{aligned} u &= \tan\widetilde{U}, \qquad -\pi/2 < \widetilde{U} < \pi/2, \\ v &= \tan\widetilde{V}, \qquad -\pi/2 < \widetilde{V} < \pi/2, \end{aligned} \tag{A.1.14}$$

the result is

$$ds^2 = \frac{1}{4\cos^2\widetilde{U}\cos^2\widetilde{V}}\left[-4\left(1-\frac{2GM}{r}\right)d\widetilde{U}d\widetilde{V} + \left(\frac{r}{r^*}\right)^2\sin^2\left(\widetilde{V}-\widetilde{U}\right)d\Omega_2^2\right], \tag{A.1.15}$$

where we used the fact that r^* has the form

$$r^* = \frac{v-u}{2} = \frac{\sin\left(\widetilde{V}-\widetilde{U}\right)}{2\cos\widetilde{U}\cos\widetilde{V}}. \tag{A.1.16}$$

Analogously to the case of Minkowski space-time, defining $\Lambda = 2\cos\widetilde{U}\cos\widetilde{V}$, the compactified metric is

$$d\widetilde{s}^2 = -4\left(1-\frac{2GM}{r}\right)d\widetilde{U}d\widetilde{V} + \left(\frac{r}{r^*}\right)^2 \sin^2\left(\widetilde{V}-\widetilde{U}\right)d\Omega_2^2. \tag{A.1.17}$$

In the limit $r \to \infty$, the above metric has the same form of the compactified Minkowski metric (3.1.27) in four dimensions. Kruskal is an example of asymptotically flat space-time. The conformal diagram for Kruskal-Szekeres coordinates is shown in Figure 23.

Figure 23 – Conformal diagram for Kruskal-Szekers coordinates.

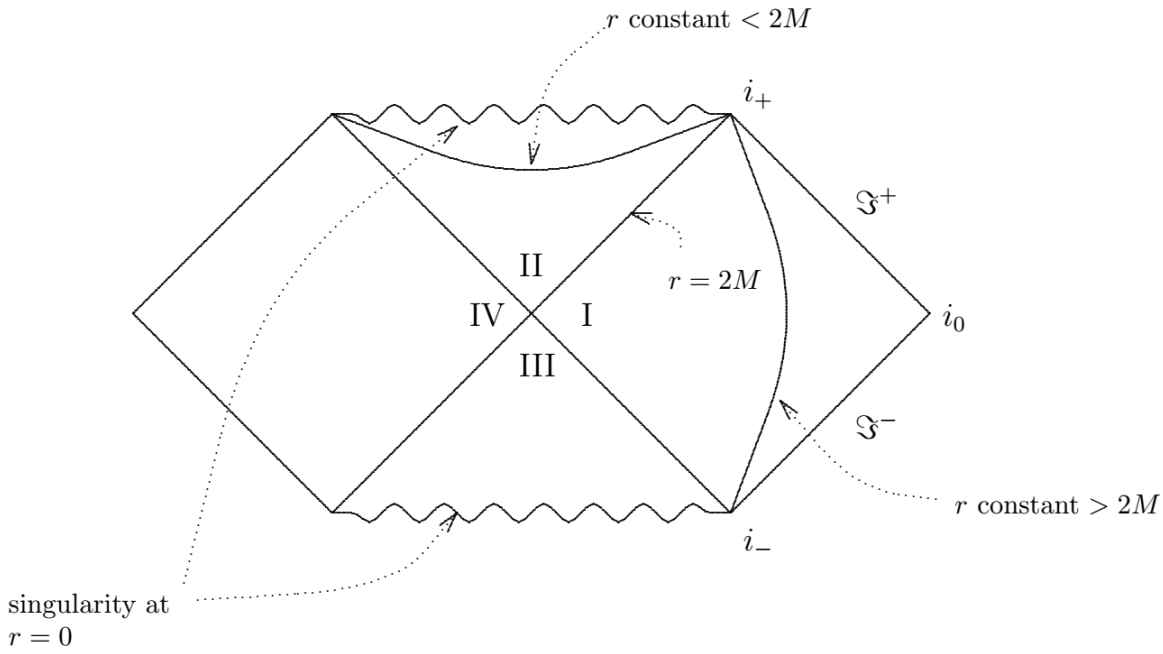

Source: [30]

A.1.1 Eternal black holes

The Schwarzschild metric is a static solution of Einstein's equations. Because of this, it can't describe the formation of a black hole. The Schwarzschild metric describes a black hole that has always existed. Such kind of black holes are known as eternal black holes. They are time symmetric and carry a past singularity, differently than what we expect of a black hole that come from of a gravitational collapse.

We already know that the Kruskal-Szekeres coordinates is the maximal analytic extension of the Schwarzschild solution, however, there is more to say about this. The full Schwarzschild geometry, also known as two-sided Schwarzschild black hole, describes two separated regions connected by an Einstein-Rosen bridge (ERB) [60], popularly known as wormhole, where each region is asymptotically flat. It isn't obvious to realize such fact, however, it's possible! Consider the metric in Kruskal-Szekeres coordinates (A.1.13). This metric is written in terms of light-cone Kruskal-Szekeres coordinates. For the current purpose, it is useful to perform the coordinate change

$$U = T - X, \qquad V = T + X, \tag{A.1.18}$$

in order to rewrite (A.1.13) as

$$ds^2 = -\frac{2GM}{r\left(U,V\right)} \exp\left(-\frac{r}{2GM}\right)\left(dT^2 - dX^2\right) + r^2 d\Omega_2^2. \tag{A.1.19}$$

For these coordinates, T is the timelike variable. Let's consider constant slices $T_0 \geq 0$ of the Kruskal space-time

$$ds^2 = \frac{2GM}{r\left(U,V\right)} \exp\left(-\frac{r}{2GM}\right) dX^2 + r^2 d\Omega_2^2. \tag{A.1.20}$$

From (A.1.12) we have that

$$dX^2 = \frac{r}{2GM\left[1 - \frac{2GM}{r} + \frac{T_0^2}{8GMr}\exp\left(-\frac{r}{2GM}\right)\right]} \exp\left(\frac{r}{2GM}\right) dr^2. \tag{A.1.21}$$

Inserting (A.1.21) inside of (A.1.20), we obtain

$$ds^2 = \frac{dr^2}{1 - \frac{2GM}{r}\left(1 - \frac{T_0^2}{(4GM)^2}\exp\left(-\frac{r}{2GM}\right)\right)} + r^2 d\Omega_2^2. \tag{A.1.22}$$

The metric above is quite similar to some time constant slice of the usual Schwarzschild metric, which are the same in the case $T_0 = 0$. Another similarity is the singularity in g_{rr}, given by the equation

$$\frac{r}{2GM} = 1 - \frac{T_0^2}{(4GM)^2}\exp\left(-\frac{r}{2GM}\right). \tag{A.1.23}$$

For the simplest case $T_0 = 0$, the space described by the metric (A.1.22) can be embedded into a four-dimensional space if we define a convenient new coordinate $z^2 = 4r_s\left(r - r_s\right)$, where r_s is the Schwarzschild radius. It is possible to check that the metric (A.1.22) in the coordinates (z, r, Ω) acquires the form of flat space in cylindrical coordinates

$$ds^2 = dz^2 + dr^2 + r^2 d\Omega_2^2. \tag{A.1.24}$$

Notice that the radius of the cylinder shrinks as z approaches to zero, until a minimum value $r = r_s$, which means that the circumference of the cylinder varies with z. The Figure 24 shows the ERB provided by (A.1.24). In the large z limit (or large r), the contribution of the z direction in the metric goes to zero,

$$\lim_{r\to\infty} dz^2 = \lim_{r\to\infty} \frac{r_s dr^2}{(r - r_s)} = 0. \tag{A.1.25}$$

In such limit, the space becomes a three dimensional flat space $\mathbb{R} \times S^2$, as expected.

Figure 24 – Einstein-Rosen Bridge connecting to flat spaces.

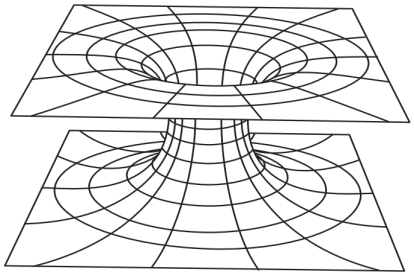

Source: [61]

Despite the case $T_0 = 0$ be very illustrative, there is a last point to clarify. Maybe looking at Figure 24, it is possible to complain about the fact that the metric (A.1.24) cover all the space because $r \in [r_s, \infty)$ and as a consequence the z coordinate should only cover the upper half of the space. Such complaining is solved if we notice that $z = \pm 2\sqrt{r_s\,(r - r_s)}$, which means that negative values of z cover the lower half of the space.

It isn't easy to do the same analysis for the cases $T_0 > 0$. For such situation, there isn't an obvious definition of a z coordinate in order to write the general metric (A.1.22) in such a way that it acquires the form of flat space in cylindrical coordinates. However, the difference is the size of the throat of the ERB, which is determined by the value of r where $g_{rr} \to \infty$, see (A.1.23). It decreases from r_s at $T_0 = 0$, approaching 0 as $T_0 \to 4GM$. The ERB closes up at the physical singularity. The behavior for $r \to \infty$ is the same as the case $T_0 = 0$, where the space becomes $\mathbb{R} \times S^2$.

A.1.2 Temperature and Entropy of Black Holes

In order to derive the temperature and the entropy for the Schwarzschild black hole, we will follow the same approach of [29, 40]. The path integral formulation of

quantum field theory has as central object the generating functional

$$Z[J] = \int D\phi e^{i\mathcal{A}[\phi]+\int d^dx\phi(x)J(x)}, \tag{A.1.26}$$

where $\mathcal{S}$ is the total action of the theory and $J(x)$ is the source of the field $\phi(x)$. The letter $\phi(x)$ usually refers to a scalar field, however the same formulation is also valid for vector fields $A^\mu(x)$ or spinoral fields $\psi(x)$. Such object is useful to compute time ordered n-point correlation functions

$$\langle\phi(x_1)\phi(x_2)...\phi(x_n)\rangle = (-i)^n \left.\frac{\delta^n Z[J]}{\delta J(x_1)\delta J(x_2)...\delta J(x_n)}\right|_{J=0}. \tag{A.1.27}$$

In terms of quantum states, the generating functional is also present in the computations of transition amplitudes. Consider an initial state $|\phi_i, t_i\rangle$ and a final state $|\phi_f, t_f\rangle$, where

$$\hat{\phi}(t_i,\vec{x})|\phi_i,t_i\rangle = \phi_i(\vec{x})|\phi_i,t_i\rangle, \qquad \hat{\phi}(t_f,\vec{x})|\phi_f,t_f\rangle = \phi_f(\vec{x})|\phi_f,t_f\rangle. \tag{A.1.28}$$

The transition amplitude between these states is given by

$$\langle\phi_f,t_f|\,\phi_i,t_i\rangle = \langle\phi_f|\,e^{-iH\left(t_f-t_i\right)}|\phi_i\rangle = \int_{\phi(t_i)=\phi_i}^{\phi\left(t_f\right)=\phi_f} D\phi e^{i\mathcal{A}[\phi]}. \tag{A.1.29}$$

There is an important connection between the generating functional $Z[J]$ and the partition function

$$Z(\beta) = Tre^{-\beta H}, \qquad \beta = \frac{1}{T}, \tag{A.1.30}$$

that appears in statistical mechanics. Performing a Wick rotation $t_E = it$ and also setting $t_i = 0$ and $t_f = t$, the amplitude transition in (A.1.29) becomes

$$\langle\phi_f|\,e^{-Ht_E}|\phi_i\rangle = \int_{\phi(0)=\phi_i}^{\phi(t)=\phi_f} D\phi e^{-\mathcal{A}_E[\phi]}. \tag{A.1.31}$$

If we set $t_E = \beta$ and $\phi_f = \phi_i$, which is equivalent to defining a periodic Euclidean time $t_E \sim t_E + \beta$ and also we impose periodic condition on time for the field, such that $\phi(t_E,\vec{x}) = \phi(t_E+\beta,\vec{x})$, the result will be

$$\langle\phi_i|\,e^{-\beta H}|\phi_i\rangle = \int_{\phi(0)=\phi_i}^{\phi(t)=\phi_f} D\phi e^{-\mathcal{A}_E[\phi]}. \tag{A.1.32}$$

It is possible to work out more with the left-hand side of this equation. The configuration of the field ϕ_i is one specific choice of initial conditions that respects the periodicity of the field. However, we can sum over all the possible initial configurations that satisfy the periodic conditions imposed on the field ϕ. This is equivalent to a periodic integral on the right-hand side of equation (A.1.32), which in other words means

$$\sum_{\phi_i}\langle\phi_i|\,e^{-\beta H}|\phi_i\rangle = \int_{periodic} D\phi e^{-\mathcal{S}_E[\phi]} = Tre^{-\beta H} = Z(\beta). \tag{A.1.33}$$

After of all these assumptions, we got that

$$Z(\beta) = \int_{periodic} D\phi e^{-\mathcal{A}_E[\phi]}. \tag{A.1.34}$$

The periodic Euclidean time will play an important role in the derivation of the Hawking temperature of black holes, while the partition function will be necessary to compute the entropy S of the black hole.

Let's consider a metric very similar to the well known Schwarzschild metric (A.1.2), where the only thing that we require is $f(r_h) = 0$, which means that there is an event horizon at $r = r_h$. The Euclidean version of such metric is

$$ds^2 = f(r)\, dt_E^2 + \frac{dr^2}{f(r)} + r^2 d\Omega_{d-2}^2. \tag{A.1.35}$$

Close to the event horizon, the function $f(r)$ can be expended as

$$f(r) = f'(r_h)(r - r_h) + \mathcal{O}\left(r^2\right), \tag{A.1.36}$$

where the prime denotes derivatives with respect to r. Inserting the expansion into the Euclidean metric (A.1.35) and keeping only the lowest order term of the expansion, we have that

$$ds^2 = f'(r_h)(r - r_h)\, dt_E^2 + \frac{dr^2}{f'(r_h)(r - r_h)} + r^2 d\Omega_{d-2}^2. \tag{A.1.37}$$

There is a smart change of coordinates

$$\rho^2 = \frac{4(r - r_h)}{f'(r_h)}, \qquad \theta = \frac{1}{2} f'(r_h)\, t_E, \tag{A.1.38}$$

such that the metric acquires a convenient form

$$ds^2 = \rho^2 d\theta^2 + d\rho^2 + r^2 d\Omega_{d-2}^2. \tag{A.1.39}$$

In order to interpret (ρ, θ) as polar coordinates, the variable θ must have periodicity equal to 2π, which implies that

$$t_E \sim t_E + \frac{4\pi}{f'(r_h)}. \tag{A.1.40}$$

As a consequence of the facts that $t_E \sim t_E + \beta$ and $\beta = 1/T$, we have the Hawking temperature T_H of the event horizon

$$T_H = \frac{f'(r_h)}{4\pi}. \tag{A.1.41}$$

Just as an example, consider the already known case where $f(r) = 1 - 2GM/r$, which corresponds to the Schwazschild black hole in $d = 4$. The Hawking temperature of the black hole is

$$T_H = \frac{\hbar c^3}{8\pi GM}. \tag{A.1.42}$$

The factors of $\hbar$ and c were reintroduced using dimensional analysis. The temperature of the black hole comes from quantum corrections of quantum gravity. In the classical limit $\hbar \to 0$, the temperature disappears, as expected classically.

It is possible to derive the black hole entropy using quantum gravity methods. The Euclidean path integral for quantum gravity is similar to what we have for scalar fields, namely

$$Z = \int D\phi Dg e^{-\mathcal{A}_E[\phi,g]}, \tag{A.1.43}$$

where in this case ϕ refers to all the matter fields. We need to specify the boundary conditions on the geometry, like we usually do for other fields. Because the fact that boundary terms containing derivatives of δg can appear, we need to introduce extra terms inside the action in order to cancel boundary terms like that. For example, let's consider an Euclidean version of the Einstein-Hilbert action. We need to introduce a new term called Gibbons-Hawking-York term. The full action then is

$$\mathcal{A}_E[g] = -\frac{1}{16\pi G}\int_{\mathcal{M}} d^d x\sqrt{g}R - \frac{1}{8\pi G}\int_{\partial\mathcal{M}} d^{d-1}x\sqrt{h}K, \tag{A.1.44}$$

where h is the determinant of the induced metric on ∂M

$$h_{ij} = g_{\mu\nu}\frac{\partial x^\mu}{\partial\sigma^i}\frac{\partial x^\mu}{\partial\sigma^j}, \tag{A.1.45}$$

where σ^i are the coordinates on ∂M. The quantity K is called extrinsic curvature,

$$K_{\mu\nu} = \nabla_\mu n_\nu, \qquad K = g^{\mu\nu}K_{\mu\nu}. \tag{A.1.46}$$

The unit vector n_μ is normal to the surface ∂M.

In order to compute the partition function for the action (A.1.44), we need to solve a path integral similar to (A.1.43). Except in special cases, it is not possible to do it exactly. What is done usually is to expand $\mathcal{S}_E$ around the saddle point

$$\begin{aligned}\mathcal{A}_E &= \mathcal{A}_E[g_{cl}] \\ &+ \frac{1}{2}\int d^d x_1 \int d^d x_2 \frac{\delta^2\mathcal{A}_E[g_{cl}]}{\delta g(x_1)\,\delta g(x_2)}\left(g(x_1) - g_{cl}(x_1)\right)\left(g(x_2) - g_{cl}(x_2)\right) + \mathcal{O}\left(g^3\right),\end{aligned} \tag{A.1.47}$$

where g_{cl} is the solution of the classical equations of motion. The zero-order term is the action computed for the classical solution while higher derivatives correspond to higher loop quantum contributions. The semi-classical approximation consists in keeping only the zero-order term, which implies that

$$Z(\beta) \simeq \exp\left(-\mathcal{A}_E[g_{cl}]\right). \tag{A.1.48}$$

Classical solutions of the form (A.1.35) are Ricci flat. As a consequence, the volume contribution in the action (A.1.44) disappears and only contributions from the Gibbons-Hawking-York term survive:

$$\mathcal{A}_E\left[g_{cl}\right] = -\frac{1}{8\pi G}\int_{\partial\mathcal{M}} d^{d-1}x\sqrt{h}K. \tag{A.1.49}$$

In order to avoid divergences, let us define our boundary $\partial\mathcal{M}$ at a constant $r = r_0$. In the end of the computation we need to impose that $r_0 \to \infty$. The normal vector to the surfaces at constant r is

$$n_\mu = \frac{\delta^r_\mu}{\sqrt{f\left(r\right)}}. \tag{A.1.50}$$

For Euclidean[2] spherically symmetric metrics, as the Schwarzschild metric for example, it is possible to find a quite simple expression for K. First, we compute the extrinsic curvature tensor for the $(d+1)$-dimensional case

$$\begin{aligned} K_{\mu\nu} &= \nabla_\mu n_\nu = \partial_\mu \frac{\delta^r_\mu}{\sqrt{f\left(r\right)}} - \Gamma^\lambda_{\mu\nu}\frac{\delta^r_\lambda}{\sqrt{f\left(r\right)}}, \\ K_{\mu\nu} &= -\frac{1}{\sqrt{f\left(r\right)}}\left[\frac{1}{2}\frac{1}{f\left(r\right)}f'\left(r\right)\delta^r_\mu\delta^r_\nu + \Gamma^r_{\mu\nu}\right]. \end{aligned} \tag{A.1.51}$$

Then, we can find the extrinsic curvature using the spherically symmetric metric

$$\begin{aligned} K &= g^{\mu\nu}K_{\mu\nu} = -\frac{1}{\sqrt{f\left(r\right)}}g^{\mu\nu}\left[\frac{1}{2}\frac{1}{f\left(r\right)}f'\left(r\right)\delta^r_\mu\delta^r_\nu + \Gamma^r_{\mu\nu}\right] \\ K &= -\frac{1}{\sqrt{f\left(r\right)}}\left[\frac{1}{2}f'\left(r\right) + g^{tt}\Gamma^r_{tt} + g^{rr}\Gamma^r_{rr} + g^{\Omega\Omega}\Gamma^r_{\Omega\Omega}\right], \end{aligned} \tag{A.1.52}$$

where the index Ω refers to the coordinates of the $(d-1)$-sphere. The Christoffel symbols of interest for spherically symmetric metrics are

$$\Gamma^r_{tt} = -\frac{1}{2}f\left(r\right)f'\left(r\right), \qquad \Gamma^r_{rr} = \frac{1}{2}f\left(r\right)\left(\frac{1}{f\left(r\right)}\right)', \qquad \Gamma^r_{\Omega\Omega} = -\frac{1}{2}f\left(r\right)\left(g_{\Omega\Omega}\right)'. \tag{A.1.53}$$

As a consequence

$$K = \frac{n^r}{2}\frac{\partial_r\left(f\left(r\right)r^{2(d-1)}\right)}{f\left(r\right)r^{2(d-1)}}. \tag{A.1.54}$$

The expression (A.1.54) is quite general. Considering $f\left(r\right)$ as the one that is in the Schwarzschild metric for $d+1=4$, the extrinsic curvature is

$$K = \frac{1}{\sqrt{f\left(r\right)}}\left(\frac{2}{r} - \frac{3GM}{r^2}\right). \tag{A.1.55}$$

[2] The result is also true for Lorentzian metrics.

Now we are in the position to compute the action for our classical solution

$$\begin{aligned}\mathcal{A}_E\left[g_{cl}\right] &= -\frac{1}{8\pi G}\int_{\partial\mathcal{M}} d^3x\sqrt{h}K \\ &= -\frac{\beta}{2G}\left(2r_0 - 3GM\right), \end{aligned} \tag{A.1.56}$$

where the induced metric for this case has the form

$$ds^2_{ind} = f\left(r_0\right)dt^2 + r_0^2\left(d\theta^2 + \sin^2\theta d\phi^2\right). \tag{A.1.57}$$

In the expression (A.1.56) there is a divergent contribution related to the piece that comes from the asymptotic behavior of the geometry. The way to handle such divergence is to insert a counter-term in the action (A.1.49),

$$\mathcal{A}_E\left[g_{cl}\right] = -\frac{1}{8\pi G}\int_{\partial\mathcal{M}} d^3x\left(\sqrt{h}K - \sqrt{h^{ct}}K^{ct}\right). \tag{A.1.58}$$

The metric $h^{ct}_{\mu\nu}$ describes the same boundary ∂M given by the metric (A.1.57) embedded into the asymptotic Euclidean geometry

$$ds^2_{ct} = dt^2 + dr^2 + r^2\left(d\theta^2 + \sin^2\theta d\phi^2\right). \tag{A.1.59}$$

The calculations are basically the same. The normal vector to the boundary is

$$n^{ct}_{\mu} = \delta^r_{\mu}, \tag{A.1.60}$$

which means from (A.1.54) that

$$K^{ct} = \frac{\left(n^{ct}\right)^r}{2}\frac{\partial_r\left(r^4\right)}{r^4} = \frac{1}{2}\frac{4r^3}{r^4} = \frac{2}{r}. \tag{A.1.61}$$

Then, the result for the counter-term contribution is

$$\begin{aligned}\mathcal{A}_{ct} &= -\frac{1}{8\pi G}\int_{\partial\mathcal{M}} d^3x\sqrt{h^{ct}}K^{ct} \\ &\simeq -\frac{1}{2G}\beta\left(2r_0 - 2GM\right). \end{aligned} \tag{A.1.62}$$

We already threw out in the above result all the terms of the form $1/r_0^n$. Inserting (A.1.62) in (A.1.58), the total action $\mathcal{A}_E\left[g_{cl}\right]$ becomes

$$\begin{aligned}\mathcal{A}_E\left[g_{cl}\right] &= -\frac{1}{2G}\beta\left(-3GM + 2r_0\right) + \frac{1}{2G}\beta\left(2r_0 - 2GM\right) \\ &= \frac{\beta}{2}M \end{aligned} \tag{A.1.63}$$

Then, the partition function (A.1.48) gets the form

$$Z\left(\beta\right) = \exp\left(-\frac{\beta M}{2}\right), \tag{A.1.64}$$

which allow us to compute the free energy of the theory

$$F = -\frac{1}{\beta} \ln Z = \frac{M}{2}. \tag{A.1.65}$$

From the formula for the Hawking temperature (A.1.42), it is possible to relate the black hole mass M and the inverse temperature β,

$$M = \frac{\beta}{8\pi G}. \tag{A.1.66}$$

Then, the energy of the black hole is

$$E = \frac{\partial}{\partial \beta} (\beta F) = \frac{\partial}{\partial \beta} \left(\frac{\beta^2}{16\pi G} \right) = M. \tag{A.1.67}$$

Finally, the entropy S can be computed by

$$\begin{aligned} S = \beta (E - F) = \beta \left(M - \frac{M}{2} \right) = 4\pi G M^2 \\ = \frac{A_h}{4G}. \end{aligned} \tag{A.1.68}$$

The entropy of the Schwarzschild black hole was obtained in $d = 4$, however, such result is true for higher dimensions and also for black holes in AdS.

Appendix B – Details about CV

In this Appendix, we will discuss some technical details about the computation of the volume of co-dimension-one bulk surface present in the CV proposal. Figure 25 shows the two-sided AdS black hole with co-dimension-one bulk surface anchored at symmetric boundary times t_L and t_R.

Figure 25 – Co-dimension-one bulk surface at $t_L = t_R$.

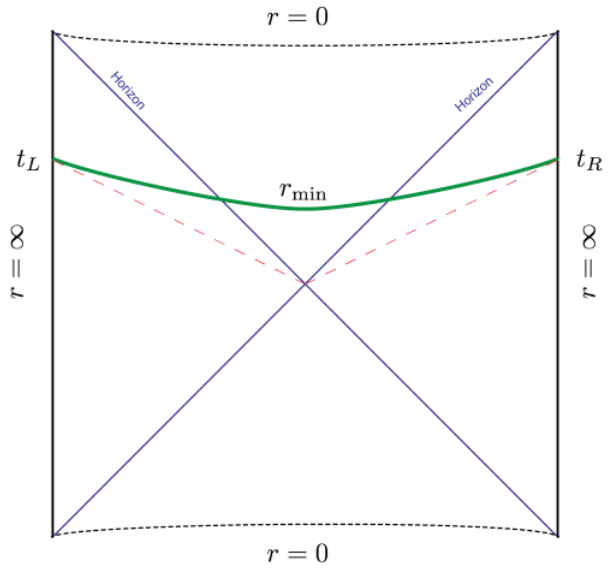

Source: [52]

The bridge reaches the minimum radius r_{min}, that is related to the size of the throat of the ERB, approaching each boundary tangentially to constant time slices. We are going to follow the same procedure proposed in [52]. The two-sided AdS black hole is the analytic extension of the Schwarzschild solution in AdS. In order to do the calculations, instead of the regular Schwarzschild metric or even of considering the Kruskal coordinates, let's consider the infalling Eddington-Finkelstein coordinates (r, v) given by

$$v = t + r^* (r) , \qquad ds^2 = -f (r) dv^2 + 2dvdr + r^2 d\Omega_{d-1}^2. \tag{B.0.1}$$

Such coordinates are an intermediate step between spherical coordinates (t, r, Ω) and the light-cone coordinates (u, v, Ω). The co-dimension-one bulk surface is spherically symmetric. Then, its shape will be determined by the coordinates $r(\lambda)$ and $v(\lambda)$, where λ is some parameter that parametrizes the (r, v) curve. With this is mind, the induced metric

that describes the shape of the ERB is given by

$$ds^2_{ERB} = \left(-f\left(r\right)\dot{v}^2 + 2\dot{v}\dot{r}\right)d\lambda^2 + r\left(\lambda\right)^2 d\Omega^2_{d-1}, \tag{B.0.2}$$

where the dots indicate derivatives with respect to λ. The volume of the ERB has the form

$$V\left[v,r\right] = \int \sqrt{h} = \Omega_{d-1}\int d\lambda r^{d-1}\sqrt{-f\left(r\right)\dot{v}^2 + 2\dot{v}\dot{r}}, \tag{B.0.3}$$

where h refers to the determinant of the induced metric (B.0.2). The next step is to maximize the volume V. In order to do this, we suppose to solve the Euler-Lagrange equations for the Lagrangian

$$\mathcal{L}\left(\dot{v},r,\dot{r}\right) = r^{d-1}\sqrt{-f\left(r\right)\dot{v}^2 + 2\dot{v}\dot{r}}. \tag{B.0.4}$$

Since the Lagrangian doesn't depend explicitly on v, there is a conserved quantity

$$E = \frac{\partial\mathcal{L}}{\partial\dot{v}} = -\frac{r^{d-1}\left(f\left(r\right)\dot{v} - \dot{r}\right)}{\sqrt{-f\left(r\right)\dot{v}^2 + 2\dot{v}\dot{r}}}. \tag{B.0.5}$$

The expression for the volume V is reparametrization invariant, which means that we can use this freedom to simplify the computations. Let's choose a λ such that the integrand in (B.0.3) remains constant, namely

$$r^{d-1}\sqrt{-f\left(r\right)\dot{v}^2 + 2\dot{v}\dot{r}} = 1. \tag{B.0.6}$$

With this choice, it is possible to work out on (B.0.5) and (B.0.6), getting then

$$E = -r^{2(d-1)}\left(f\left(r\right)\dot{v} - \dot{r}\right) \tag{B.0.7}$$

and

$$r^{4(d-1)}\dot{r}^2 = r^{2(d-1)}f\left(r\right) + E^2, \tag{B.0.8}$$

respectively. After the above considerations, the maximal volume can be written as

$$V = 2\Omega_{d-1}\int d\lambda = 2\Omega_{d-1}\int_{r_{min}}^{r_{max}}\frac{dr}{\dot{r}} = 2\Omega_{d-1}\int_{r_{min}}^{r_{max}}\frac{r^{2(d-1)}dr}{\sqrt{r^{2(d-1)}f\left(r\right) + E^2}}. \tag{B.0.9}$$

The factor of 2 appears in the expression of the volume because we are considering the symmetric configuration where $t_L = t_R$. Otherwise, the above expression would take into account only half of the ERB. The integral is defined over a minimum radius r_{min} to the cutoff surface at r_{max}. The minimal radius is determined by setting $\dot{r} = 0$ in (B.0.8), which means that the equation

$$f\left(r_{min}\right) + r_{min}^{-2(d-1)}E^2 = 0 \tag{B.0.10}$$

will provide the value of r_{min}.

In order to proceed in our calculations, let's do a smart trick. We can compute a finite variation of the coordinate v, that is

$$\Delta v = \int_{v_{min}}^{v_{max}} \dot{v} d\lambda. \tag{B.0.11}$$

Looking at (B.0.1), we see that it is possible to set $v_{max} = t_R + r^* (r_{max})$ and $v_{min} = r^* (r_{min})$. On the other hand, using (B.0.7),

$$t_R + r^* (r_{max}) - r^* (r_{min}) = \int_{r_{min}}^{r_{max}} \left[\frac{1}{f(r)} - \frac{E}{f(r) \sqrt{r^{2(d-1)} f(r) + E^2}} \right] dr. \tag{B.0.12}$$

It is useful to multiply the above expression by E, obtaining then

$$E \left(t_R + r^* (r_{max}) - r^* (r_{min}) \right) = \int_{r_{min}}^{r_{max}} \left[\frac{E}{f(r)} - \frac{E^2}{f(r) \sqrt{r^{2(d-1)} f(r) + E^2}} \right] dr. \tag{B.0.13}$$

From the above expression and also (B.0.9), we have that

$$\begin{aligned} \frac{V}{2\Omega_{d-1}} = & \int_{r_{min}}^{r_{max}} \frac{1}{f(r)} \left[\sqrt{r^{2(d-1)} f(r) + E^2} - E \right] dr \\ & + E \left(t_R + r^* (r_{max}) - r^* (r_{min}) \right). \end{aligned} \tag{B.0.14}$$

The above expression provides the time derivative of the volume dV/dt_R, which is

$$\frac{1}{2\Omega_{d-1}} \frac{dV}{dt_R} = E, \tag{B.0.15}$$

where we used (B.0.12) to perform the calculations. It is possible to define a total time $t = t_L + t_R$. Once $t_L = t_R$, we have that

$$\frac{dV}{dt} = \Omega_{d-1} E. \tag{B.0.16}$$

The time derivative of the volume is completely determined by computing either E or r_{min} with (B.0.10), which means that

$$E = \pm r_{min}^{d-1} \sqrt{-f(r_{min})}. \tag{B.0.17}$$

However, we will only keep the positive value of E. From (B.0.7), applying $r = r_{min}$, it is possible to see that

$$E = -r_{min}^{2(d-1)} f(r_{min}) \dot{t} > 0, \tag{B.0.18}$$

because of the fact that the turning point r_{min}, where $\dot{r} = 0$, is inside the horizon, implying also that $f(r_{min}) < 0$. Finally, using (4.2.2), the time derivative of complexity is

$$\frac{d\mathcal{C}_V}{dt} = \frac{\Omega_{d-1}}{GL} r_{min}^{d-1} \sqrt{-f(r_{min})}, \tag{B.0.19}$$

where L is the radius of the AdS space.

Appendix C – Computations of CA

In this Appendix, we will provide details about the computations involving CA duality for the cases of uncharged, small charged and rotating black holes.

C.1 Uncharged black hole

The time derivative of the action on the WDW patch shown in Figure 20 has the form

$$\frac{d\mathcal{A}}{dt} = \frac{1}{16\pi G}\int d\Omega_{d-1}\int_0^{r_h} dr\sqrt{-g}\,(R-2\Lambda) + \frac{1}{8\pi G}\int d\Omega_{d-1}\sqrt{-h}K\Big|_0^{r_h}. \tag{C.1.1}$$

The first term refers to the bulk contribution, which is

$$\frac{d\mathcal{A}_{bukl}}{dt} = -\frac{\Omega_{d-1}r_h^d}{8\pi GL^2}, \tag{C.1.2}$$

where we used that

$$R = \frac{2\,(d+1)}{(d-1)}\Lambda, \qquad \Lambda = -\frac{d\,(d-1)}{2L^2}. \tag{C.1.3}$$

The second term is the contribution from the Gibbons-Hawking-York term at $r = r_h$ and $r = 0$. Such term is necessary because the WDW patch has boundaries. For surfaces of constant $r = r_*$, the induced metric is

$$ds_{ind}^2 = -f\,(r_*)\,dt^2 + r^2 d\Omega_{d-1}^2, \qquad f\,(r_*) = 1 - \frac{2\mu}{r_*^{d-2}} + \frac{r_*^2}{L^2} \tag{C.1.4}$$

while the normal vector is

$$n_\mu = \frac{\delta_\mu^r}{\sqrt{f\,(r)}}. \tag{C.1.5}$$

For spherically symmetric metrics, the extrinsic curvature[1] has the form

$$K = \frac{1}{2}n^r\frac{\partial_r\left(r^{2(d-1)}f\,(r)\right)}{r^{2(d-1)}f\,(r)}. \tag{C.1.6}$$

For uncharged black holes, the function $f\,(r)$ is shown above, resulting in the following expression for the extrinsic curvature

$$K = \frac{1}{\sqrt{f\,(r)}}\left(\frac{(d-1)\,f\,(r)}{r} + (d-2)\,\frac{\mu}{r^{d-1}} + \frac{r}{L^2}\right). \tag{C.1.7}$$

[1] See equation (A.1.54) for more details about the derivation of the following expression for K.

Consequently, the boundary contribution is

$$\begin{aligned}\frac{d\mathcal{A}_{bdy}}{dt} &= \frac{1}{8\pi G}\int d\Omega_{d-1}\sqrt{-h}K\Big|_0^{r_h},\\ \frac{d\mathcal{A}_{bdy}}{dt} &= \left[\frac{\Omega_{d-1}}{8\pi G}r^{d-2}\left((d-1)+d\frac{r^2}{L^2}\right)-\frac{d}{(d-1)}M\right]\Bigg|_0^{r_h}.\end{aligned} \tag{C.1.8}$$

Finally, the sum between the bulk and boundaries contributions give rises to the total time derivative of the action

$$\begin{aligned}\frac{d\mathcal{A}}{dt} &= \frac{d\mathcal{A}_{bulk}}{dt}+\frac{d\mathcal{A}_{bdy}}{dt}\\ &= 2M,\end{aligned} \tag{C.1.9}$$

where it was necessary to use that

$$\mu = \frac{8\pi GM}{(d-1)\,\Omega_{d-1}}, \qquad \mu = \frac{r_h^{d-2}}{2}\left(1+\frac{r_h^2}{L^2}\right). \tag{C.1.10}$$

This second above expression for μ comes from the fact that $f\left(r_h\right)=0$. Using the time derivative version of the complexity=action proposal

$$\frac{d\mathcal{C}_{\mathcal{A}}}{dt} = \frac{1}{\pi\hbar}\frac{d\mathcal{A}_{\mathcal{W}}}{dt}, \tag{C.1.11}$$

it is possible to see from (C.1.9) that

$$\frac{d\mathcal{C}_{\mathcal{A}}}{dt} = \frac{2M}{\pi\hbar}, \tag{C.1.12}$$

which precisely saturates the bound for the rate of the change of the complexity conjectured in (4.3.3).

C.2 Small charged black hole

For the charged black hole in AdS, the time derivative of the action on the WDW patch is given by

$$\begin{aligned}\frac{d\mathcal{A}}{dt} &= \frac{1}{16\pi G}\int d\Omega_{d-1}\int_{r_-}^{r_+}dr\sqrt{-g}\left(R-2\Lambda\right)\\ &+\frac{1}{8\pi G}\int_{\partial\mathcal{M}}d^dx\sqrt{-h}K\Big|_{r_-}^{r_+}-\frac{1}{16\pi}\int d\Omega_{d-1}\int_{r_-}^{r_+}dr\sqrt{-g}F_{\mu\nu}F^{\mu\nu}\end{aligned} \tag{C.2.1}$$

where r_- and r_+ are the inner and outer horizon, respectively. Analogously to what we have for the uncharged case, there are contributions for the above expression from the bulk and boundary terms. In order to compute the bulk contribution, it is possible to use again

the same expression that were used for the uncharged case. The difference is the function $f(r)$, which for the charged case is

$$f(r) = 1 - \frac{2\mu}{r^{d-2}} + \frac{\alpha^2}{r^{2(d-2)}} + \frac{r^2}{L^2}, \qquad \alpha^2 = \frac{8\pi G}{(d-1)\,\Omega_{d-1}} Q^2. \tag{C.2.2}$$

Additionally, the Ricci scalar for charged black holes is given by

$$R = 2\frac{(d+1)}{(d-1)}\Lambda + \frac{d-3}{2\,(d-1)} G F_{\mu\nu} F^{\mu\nu}, \qquad \Lambda = -\frac{d\,(d-1)}{2L^2}. \tag{C.2.3}$$

Let's focus our attention to the case $(d+1) = 4$, where the electromagnetic energy-momentum tensor is traceless and the field strength is

$$F_{rt} = -F_{tr} = \frac{Q}{r^2}. \tag{C.2.4}$$

For this specific case, the bulk contribution is

$$\begin{aligned} \frac{d\mathcal{A}_{bulk}}{dt} &= \frac{1}{16\pi G} \int d\Omega_2 \int_{r_-}^{r_+} dr \sqrt{-g}\,(R - 2\Lambda) - \frac{1}{16\pi} \int d\Omega_2 \int_{r_-}^{r_+} dr \sqrt{-g} F_{\mu\nu} F^{\mu\nu} \\ &= \frac{r_+ - r_-}{2} \left(\frac{Q^2}{r_+ r_-} - \frac{r_+^2 + r_+ r_- + r_-^2}{GL^2} \right). \end{aligned} \tag{C.2.5}$$

In order to compute the boundary terms, it is necessary to obtain first the value of the extrinsic curvature for the surfaces at $r = r_+$ and $r = r_-$. It is possible again to use (C.1.6) to compute K. The result is

$$\begin{aligned} K &= \frac{1}{2} n^r \frac{\partial_r \left(r^4 f(r)\right)}{r^4 f(r)} \\ &= \frac{1}{\sqrt{f(r)}} \left(\frac{2f(r)}{r} + \frac{\mu}{r^2} - \frac{\alpha^2}{r^3} + \frac{r}{L^2} \right). \end{aligned} \tag{C.2.6}$$

Consequently,

$$\begin{aligned} \frac{d\mathcal{A}_{bdy}}{dt} &= \frac{1}{8\pi G} \int d\Omega_2 \sqrt{-h} K \Big|_{r_-}^{r_+} \\ &= \left(\frac{r}{G} - \frac{3M}{2} + \frac{Q^2}{2r} + \frac{3r^3}{2GL^2} \right) \Big|_{r_-}^{r_+}. \end{aligned} \tag{C.2.7}$$

Finally, putting both contributions together, the result for the total time derivative of the action is

$$\begin{aligned} \frac{d\mathcal{A}}{dt} &= \frac{r_+ - r_-}{2} \left(\frac{Q^2}{r_+ r_-} - \frac{r_+^2 + r_+ r_- + r_-^2}{GL^2} \right) + \left(\frac{r}{G} - \frac{3M}{2} + \frac{Q^2}{2r} + \frac{3r^3}{2GL^2} \right) \Big|_{r_-}^{r_+} \\ &= (r_+ - r_-) \left[\frac{1}{G} + \frac{r_+^2 + r_+ r_- + r_-^2}{GL^2} \right]. \end{aligned} \tag{C.2.8}$$

From the condition $f(r_+) = f(r_-) = 0$, we have that

$$\frac{d\mathcal{A}}{dt} = \frac{Q^2}{r_-} - \frac{Q^2}{r_+}. \tag{C.2.9}$$

Let's consider again the condition $f(r_+) = f(r_-) = 0$, but now as powers of $r_\pm/L$, namely

$$\left(\frac{r_\pm}{L}\right)^4 + \left(\frac{r_\pm}{L}\right)^2 - \frac{2GM}{L}\frac{r_\pm}{L} + \frac{GQ^2}{L^2} = 0. \tag{C.2.10}$$

Taking the limit of small black holes, which means $r_\pm \ll L$, it is possible to ignore the fourth-order contribution, implying that the above expression becomes

$$r_\pm^2 - 2GMr_\pm + GQ^2 = 0. \tag{C.2.11}$$

Then, the coordinates of the inner and outer horizon are

$$r_\pm = GM \pm \sqrt{(GM)^2 - \left(\sqrt{G}Q\right)^2}. \tag{C.2.12}$$

The explicit form of $r_\pm$ allows us to rewrite (C.2.9) as

$$\begin{aligned}\frac{d\mathcal{A}}{dt} &= \frac{Q^2}{r_-} - \frac{Q^2}{r_+} \\ &= 2Q^2\frac{\sqrt{(GM)^2 - \left(\sqrt{G}Q\right)^2}}{\left(\sqrt{G}Q\right)^2} \\ &= 2\sqrt{M^2 - \frac{Q^2}{G}}\end{aligned} \tag{C.2.13}$$

C.3 Rotating BTZ black hole

The $(2+1)$-dimensional rotating black hole in AdS [62] is described by the metric

$$ds^2 = -f(r)\,dt^2 + \frac{dr^2}{f(r)} + r^2\left(d\phi - \frac{8GJ}{2r^2}dt\right)^2, \tag{C.3.1}$$

where J is the angular momentum and the function $f(r)$ is given by

$$f(r) = \frac{r^2}{L^2} - 8GM + \frac{(8GJ)^2}{4r^2}. \tag{C.3.2}$$

Using that the $f(r)$ is zero at the horizon, we have that

$$r_\pm^2 = 4GML^2\left(1 \pm \sqrt{1 - \left(\frac{J}{ML}\right)^2}\right), \tag{C.3.3}$$

which allows us to write $f(r)$ in terms of the outer and inner horizons

$$f(r) = \frac{\left(r^2 - r_+^2\right)\left(r^2 - r_-^2\right)}{r^2 L^2}. \tag{C.3.4}$$

Additionally, it is possible to derive useful relations from (C.3.3), which are

$$r_+^2 + r_-^2 = 8GML^2, \qquad r_+ r_- = 4GLJ, \qquad r_+^2 - r_-^2 = 8GL^2\sqrt{M^2 - \frac{J^2}{L^2}}. \tag{C.3.5}$$

The metric (C.3.1) doesn't have the usual form of a spherically symmetric metric, it has out of diagonal elements. It is possible to work on (C.3.1) in order to see this fact explicitly

$$ds^2 = -\left(f(r) - \left(\frac{8GJ}{2r}\right)^2\right)dt^2 + \frac{dr^2}{f(r)} + r^2 d\phi^2 - 8GJ dt d\phi. \tag{C.3.6}$$

The metric $g_{\mu\nu}$ then has the following structure

$$g_{\mu\nu} = \begin{pmatrix} -\left(f(r) - \left(\frac{8GJ}{2r}\right)^2\right) & 0 & -4GJ \\ 0 & 1/f(r) & 0 \\ -4GJ & 0 & r^2 \end{pmatrix}, \tag{C.3.7}$$

which implies that

$$g = -r^2. \tag{C.3.8}$$

The metric determinant g is the same as for the uncharged case.

The action of rotating BTZ has the same form as for the the uncharged black hole, which means that

$$\frac{d\mathcal{A}}{dt} = \frac{1}{16\pi G}\int_0^{2\pi} d\phi \int_{r_-}^{r_+} dr\sqrt{-g}\,(R - 2\Lambda) + \frac{1}{8\pi G}\int_0^{2\pi} d\phi\sqrt{-h}K\Big|_{r_-}^{r_+}. \tag{C.3.9}$$

Using (C.1.3), it is possible to compute the bulk contribution as was done for the uncharged case. The result is

$$\begin{aligned} \frac{d\mathcal{A}_{bulk}}{dt} &= \frac{1}{16\pi G}\int_0^{2\pi} d\phi \int_{r_-}^{r_+} dr\sqrt{-g}\,(R - 2\Lambda) \\ &= -\frac{\left(r_+^2 - r_-^2\right)}{4GL^2}. \end{aligned} \tag{C.3.10}$$

The boundary term can be calculated using the following expression for the induced metric on the surface constant r:

$$h_{ij} = \begin{pmatrix} -\left(f(r) - \left(\frac{8GJ}{2r}\right)^2\right) & -4GJ \\ -4GJ & r^2 \end{pmatrix}, \tag{C.3.11}$$

whose the determinant is

$$h = -f\left(r\right) r^2. \tag{C.3.12}$$

The extrinsic curvature of such surface is

$$\begin{aligned} K &= \frac{1}{2} n^r \frac{\partial_r \left(r^2 f\left(r\right)\right)}{r^2 f\left(r\right)} \\ &= \frac{1}{\sqrt{f\left(r\right)}} \left[\frac{2r}{L^2} - \frac{8GM}{r}\right]. \end{aligned} \tag{C.3.13}$$

With the above results in hand, it is possible to compute the boundary contribution, namely

$$\begin{aligned} \frac{d\mathcal{A}_{bdy}}{dt} &= \frac{1}{8\pi G} \int_0^{2\pi} d\phi \sqrt{-h} K \Big|_{r_-}^{r_+} \\ &= \frac{1}{4G} \sqrt{f\left(r\right)} r \frac{1}{\sqrt{f\left(r\right)}} \left[\frac{2r}{L^2} - \frac{8GM}{r}\right] \Big|_{r_-}^{r_+} \\ &= \left[\frac{2r^2}{4GL^2} - 2M\right] \Big|_{r_-}^{r_+} \end{aligned} \tag{C.3.14}$$

Finally, the total time derivative of the action on the WDW patch is

$$\begin{aligned} \frac{d\mathcal{A}}{dt} &= -\frac{\left(r_+^2 - r_-^2\right)}{4GL^2} + \left[\frac{2r^2}{4GL^2} - 2M\right] \Big|_{r_-}^{r_+} \\ &= 2\sqrt{M^2 - \left(\frac{J}{L}\right)^2}. \end{aligned} \tag{C.3.15}$$

Using the complexity=action relation (C.1.11), the time derivative of the complexity for the rotating BTZ has the form

$$\frac{d\mathcal{C}_{\mathcal{A}}}{dt} = \frac{2}{\pi\hbar} \sqrt{M^2 - \left(\frac{J}{L}\right)^2}. \tag{C.3.16}$$

Bibliography

[1] HOOFT, G. 't. Dimensional reduction in quantum gravity. In: *Salamfest 1993:0284-296*. [S.l.: s.n.], 1993. p. 0284–296.

[2] SUSSKIND, L. The World as a hologram. *J. Math. Phys.*, v. 36, p. 6377–6396, 1995.

[3] BEKENSTEIN, J. D. Black holes and entropy. *Physical Review D*, APS, v. 7, n. 8, p. 2333, 1973.

[4] HAWKING, S. W. Particle creation by black holes. *Communications in mathematical physics*, Springer, v. 43, n. 3, p. 199–220, 1975.

[5] MALDACENA, J. M. The Large N limit of superconformal field theories and supergravity. *Int. J. Theor. Phys.*, v. 38, p. 1113–1133, 1999. [Adv. Theor. Math. Phys.2,231(1998)].

[6] EINSTEIN, A.; PODOLSKY, B.; ROSEN, N. Can quantum-mechanical description of physical reality be considered complete? *Physical review*, APS, v. 47, n. 10, p. 777, 1935.

[7] BELL, J. S. On the problem of hidden variables in quantum mechanics. *Reviews of Modern Physics*, APS, v. 38, n. 3, p. 447, 1966.

[8] CALABRESE, P.; CARDY, J. L. Entanglement entropy and quantum field theory. *J. Stat. Mech.*, v. 0406, p. P06002, 2004.

[9] RYU, S.; TAKAYANAGI, T. Holographic derivation of entanglement entropy from AdS/CFT. *Phys. Rev. Lett.*, v. 96, p. 181602, 2006.

[10] RYU, S.; TAKAYANAGI, T. Aspects of Holographic Entanglement Entropy. *JHEP*, v. 08, p. 045, 2006.

[11] SWINGLE, B. Entanglement Renormalization and Holography. *Phys. Rev.*, D86, p. 065007, 2012.

[12] RAAMSDONK, M. V. Comments on quantum gravity and entanglement. 2009.

[13] RAAMSDONK, M. V. Building up spacetime with quantum entanglement. *Gen. Rel. Grav.*, v. 42, p. 2323–2329, 2010. [Int. J. Mod. Phys.D19,2429(2010)].

[14] MALDACENA, J.; SUSSKIND, L. Cool horizons for entangled black holes. *Fortsch. Phys.*, v. 61, p. 781–811, 2013.

[15] ALMHEIRI, A. et al. Black Holes: Complementarity or Firewalls? *JHEP*, v. 02, p. 062, 2013.

[16] HARLOW, D.; HAYDEN, P. Quantum computation vs. firewalls. *Journal of High Energy Physics*, v. 6, p. 85, jun. 2013.

[17] SUSSKIND, L. Computational Complexity and Black Hole Horizons. *Fortsch. Phys.*, v. 64, p. 44–48, 2016. [Fortsch. Phys.64,24(2016)].

[18] SUSSKIND, L. Entanglement is not Enough. *ArXiv e-prints*, nov. 2014.

[19] ALISHAHIHA, M. Holographic Complexity. *Phys. Rev.*, D92, n. 12, p. 126009, 2015.

[20] ABT, R. et al. Topological Complexity in AdS3/CFT2. 2017.

[21] BROWN, A. R. et al. Holographic Complexity Equals Bulk Action? *Phys. Rev. Lett.*, v. 116, n. 19, p. 191301, 2016.

[22] BROWN, A. R. et al. Complexity, action, and black holes. *Phys. Rev.*, D93, n. 8, p. 086006, 2016.

[23] HAYDEN, P.; PRESKILL, J. Black holes as mirrors: Quantum information in random subsystems. *JHEP*, v. 09, p. 120, 2007.

[24] PRESKILL, J. Lecture notes for physics 229: Quantum information and computation. *California Institute of Technology*, v. 16, 1998.

[25] WATROUS, J. Quantum Computational Complexity. *ArXiv e-prints*, abr. 2008.

[26] DAWSON, C. M.; NIELSEN, M. A. The Solovay-Kitaev algorithm. *eprint arXiv:quant-ph/0505030*, maio 2005.

[27] AHARONY, O. et al. Large N field theories, string theory and gravity. *Phys. Rept.*, v. 323, p. 183–386, 2000.

[28] MALDACENA, J. M. Eternal black holes in anti-de Sitter. *JHEP*, v. 04, p. 021, 2003.

[29] AMMON, M.; ERDMENGER, J. *Gauge/gravity duality: foundations and applications*. [S.l.]: Cambridge University Press, 2015.

[30] TOWNSEND, P. K. Black holes: Lecture notes. 1997.

[31] HARLOW, D. Jerusalem lectures on black holes and quantum information. *Reviews of Modern Physics*, APS, v. 88, n. 1, p. 015002, 2016.

[32] NISHIOKA, T.; RYU, S.; TAKAYANAGI, T. Holographic Entanglement Entropy: An Overview. *J. Phys.*, A42, p. 504008, 2009.

[33] RANGAMANI, M.; TAKAYANAGI, T. Holographic entanglement entropy. In: *Holographic Entanglement Entropy*. [S.l.]: Springer, 2017. p. 35–47.

[34] LIEB, E. H.; RUSKAI, M. B. A fundamental property of quantum-mechanical entropy. *Physical Review Letters*, APS, v. 30, n. 10, p. 434, 1973.

[35] LIEB, E.; RUSKAI, M. Proof of the strong subadditivity of quantum-mechanical entropy. *J. Math. Phys.*, v. 14, p. 1938–1941, 1973.

[36] CASINI, H.; HUERTA, M. A Finite entanglement entropy and the c-theorem. *Phys. Lett.*, B600, p. 142–150, 2004.

[37] CASINI, H.; HUERTA, M. A c-theorem for the entanglement entropy. *J. Phys.*, A40, p. 7031–7036, 2007.

[38] HOLZHEY, C.; LARSEN, F.; WILCZEK, F. Geometric and renormalized entropy in conformal field theory. *Nucl. Phys.*, B424, p. 443–467, 1994.

[39] NASTASE, H. *Introduction to the ADS/CFT Correspondence*. [S.l.]: Cambridge University Press, 2015.

[40] HARTMAN, T. Lectures on quantum gravity and black holes. *Cornell physics*, v. 7661.

[41] FRANCESCO, P.; MATHIEU, P.; SÉNÉCHAL, D. *Conformal field theory*. [S.l.]: Springer Science & Business Media, 2012.

[42] GUBSER, S. S.; KLEBANOV, I. R.; POLYAKOV, A. M. Gauge theory correlators from noncritical string theory. *Phys. Lett.*, B428, p. 105–114, 1998.

[43] WITTEN, E. Anti-de Sitter space and holography. *Adv. Theor. Math. Phys.*, v. 2, p. 253–291, 1998.

[44] BALASUBRAMANIAN, V.; KRAUS, P. A Stress tensor for Anti-de Sitter gravity. *Commun. Math. Phys.*, v. 208, p. 413–428, 1999.

[45] STANFORD, D.; SUSSKIND, L. Complexity and Shock Wave Geometries. *Phys. Rev.*, D90, n. 12, p. 126007, 2014.

[46] SUSSKIND, L. Butterflies on the Stretched Horizon. 2013.

[47] SUSSKIND, L.; THORLACIUS, L.; UGLUM, J. The Stretched horizon and black hole complementarity. *Phys. Rev.*, D48, p. 3743–3761, 1993.

[48] SEKINO, Y.; SUSSKIND, L. Fast Scramblers. *JHEP*, v. 10, p. 065, 2008.

[49] MALDACENA, J.; SHENKER, S. H.; STANFORD, D. A bound on chaos. *JHEP*, v. 08, p. 106, 2016.

[50] KNILL, E. Approximation by quantum circuits. 1995.

[51] CARMI, D.; MYERS, R. C.; RATH, P. Comments on Holographic Complexity. *JHEP*, v. 03, p. 118, 2017.

[52] CARMI, D. et al. On the Time Dependence of Holographic Complexity. 2017.

[53] MIYAJI, M. et al. Distance between Quantum States and Gauge-Gravity Duality. *Phys. Rev. Lett.*, v. 115, n. 26, p. 261602, 2015.

[54] TRIVELLA, A. Holographic Computations of the Quantum Information Metric. *Class. Quant. Grav.*, v. 34, n. 10, p. 105003, 2017.

[55] BAK, D.; GUTPERLE, M.; HIRANO, S. A Dilatonic deformation of AdS(5) and its field theory dual. *JHEP*, v. 05, p. 072, 2003.

[56] BAK, D.; GUTPERLE, M.; HIRANO, S. Three dimensional Janus and time-dependent black holes. *JHEP*, v. 02, p. 068, 2007.

[57] BROWN, A. R.; SUSSKIND, L. The Second Law of Quantum Complexity. 2017.

[58] CHAPMAN, S.; MARROCHIO, H.; MYERS, R. C. Complexity of Formation in Holography. *JHEP*, v. 01, p. 062, 2017.

[59] JEFFERSON, R. A.; MYERS, R. C. Circuit complexity in quantum field theory. *JHEP*, v. 10, p. 107, 2017.

[60] EINSTEIN, A.; ROSEN, N. The particle problem in the general theory of relativity. *Physical Review*, APS, v. 48, n. 1, p. 73, 1935.

[61] ZEE, A. *Einstein gravity in a nutshell*. [S.l.]: Princeton University Press, 2013.

[62] BANADOS, M.; TEITELBOIM, C.; ZANELLI, J. The Black hole in three-dimensional space-time. *Phys. Rev. Lett.*, v. 69, p. 1849–1851, 1992.

[63] NAKAYAMA, Y. Scale invariance vs conformal invariance. *Phys. Rept.*, v. 569, p. 1–93, 2015.